2020

Effects of Gestational Ozone Exposure on Privileged Placental and Brain Barrier Integrity

Alexander I. Hamm
Virginia Commonwealth University

Effects of Gestational Ozone Exposure on Privileged Placental and Brain Barrier Integrity

A thesis submitted in partial fulfillment of the requirements for the degree of Master of Science, at Virginia Commonwealth University.

By
Alexander I. Hamm,
B.S. in Neuroscience, Susquehanna University, 2015

Director: Andrew K. Ottens, Ph.D.

Associate Professor, Department of Anatomy and Neurobiology

Virginia Commonwealth University

Richmond, Virginia

July, 2020

Acknowledgements

I would first like to extend my gratitude to Dr. Ottens, my advisor. Without you, I would not have ever conceived such a project. Your wisdom extends well beyond the lab and I wish you the best of luck in your future research. Thank you, Dr. Dupree and Dr. Koblinski, my committee members, who have been outstandingly supportive in accommodating changes to my project. A special thanks goes to Dr. Matthew Campen and his skilled team at New Mexico State University. Without their work in preparing dams for this project, I would not be here today. I would also like to thank Dr. Raymond Colello, Anatomy and Neurobiology Master's degree director, for being a tremendous source of equal parts wisdom and laughter. His guidance, dating back to my time in the CERT program, will be remembered.

I wish to thank current and former members of Andrew Ottens' laboratory - Dr. Ekaterina Mostovenko, Ambrine Chacko, Christopher Canal, and Ekaterina Stepanova. My gratitude is extended for your constant support and jovial lunches every day. A special thank you goes to Ambrine Chacko for teaching me my microscopy techniques.

I also wish to send a very special recognition to my mother, father, sister and loving girlfriend. Without your undying love and support, I would still be driving a box truck. My thanks also goes out to the team at Triple Crossing Brewing, whom have become lifelong friends and always were able to accommodate my special work requests for school.

Table of Contents

List of Tables

List of Figures

Abstract

Effects of Gestational Ozone Exposure on Privileged Placental and Brain Barrier Integrity

By Alexander Hamm, B.S.

A Thesis submitted in partial fulfillment of the requirements for the degree of Master of Science at Virginia Commonwealth University

Virginia Commonwealth University, 2020

Major Director: Andrew K. Ottens, Ph.D., Associate Professor, Department of Anatomy and Neurobiology

Ambient outdoor ozone, a common of component of photochemical smog and urban air pollution, is linked to various neurological and vascular pathologies. Its immediate reaction with lung surfactant after inhalation results in complete reactivity of the gas, with no active ozone passing into circulation. This indicates the presence of secondary and tertiary mediators in ozone-related systemic pathologies after pulmonary insult. In vasculature, ozone exposure is associated with an acute hypertensive phenotype apparent at least 24 hours after dose, such as experienced on a hot summer afternoon in a large metropolitan area like Los Angeles or Mexico City. However, the effects of ozone have been underexplored during gestation, when inducible teratogenesis during critical periods for development can result in catastrophic fetal outcomes, but also when more subtle impacts on placental supply can hamper sensitive developmental aspects such as in the brain. As the interface of maternal-fetal circulation, the placenta is a target organ of toxicological interest in hypertensive disorders of pregnancy such as preeclampsia. Moreover, the developing fetal blood-brain barrier (BBB) is underexplored, especially in relation to toxicological study. In the study at hand, proteomic analysis of amniotic fluid (AF) was assessed after exposure of pregnant Sprague-Dawley rats at two gestational timepoint representing critical periods during rat development. The AF proteome is an understudied window into

the privileged amniotic environment and its response to toxicological stressors. Pregnant dams experienced a single 4-h exposure to ozone at GD10, a critical period of placental and BBB development, or at GD20, a period just prior to term and one of anatomical significance in brain development. AF samples were then collected at term for detailed proteomic analysis. Studies assessed: AF proteomic impacts between GD10 and GD20 time points; the differential response to 0.3 ppm or 1.0 ppm ozone dosage at GD20; and the overlap between AF proteomic and maternal serum proteomic responses to 0.3 ppm or 1.0 ppm GD20 ozone exposures. Subsequently, a plan was devised for targeted immunofluorescence microscopy assessments on the pathological effects within the placental and blood-brain barriers linked with the toxicological ozone response observed within the AF proteome.

Overall, we identified 231 significant AF proteomic responses across all time points and ozone doses within the amniotic fluid. To our knowledge, this is the most comprehensive assessment of the AF proteome. Overlap was low between the AF proteomic responses to gestational exposure time or ozone dose, while considerably more consistent for maternal serum responses. The highly dynamic AF proteomic response to ozone, however, consistently related to extracellular matrix and vascular remodeling processes, many proteins with well-defined roles in the placenta and developing conceptus. Results with maternal serum indicated activation of the maternal compliment cascade system and systemic inflammation. Additionally, limited overlap between maternal serum and matched AF proteomes indicated the placenta or fetus as the primary contributors to the AF proteomic response to ozone. With placentation and cerebral angiogenesis just beginning in rat at GD10, we hypothesized a dramatic effect on these structures to be assessed with the devised immunofluorescence analysis. In placenta, we expect to observe conditions consistent with a hypertensive preeclamptic-like state. Our AF proteomic results showed significant fold changes in proteins associated with this disease such as galectin-1, MMP-2, TIMP-2, and osteopontin. In follow-up targeted analysis of these proteins in placenta, we expect to observe classic signs of preeclampsia and general placental dysfunction—shallow

invasion of the maternal endometrial decidualized tissue layer and inadequate remodeling of the maternal spiral arteries resulting in inadequate fetal circulation. AF proteomic data also showed shifts in proteins important for vascular development in the fetal brain such as TGFβ, PKM and neuropilin-1. Thus, we devised follow-up studies to test for ozone-induced BBB barrier dysfunction within the fetal brain to include augmented tight-junction proteins, albumin leakage and promoted astrocytic and microglial reactivity proximal to the cerebrovasculature. Overall, the outlined studies have potential to demonstrate stark effects of critical-period ambient ozone exposure on the placenta and developing fetus.

Chapter 1: Introduction

1.1. Air Pollution

Existing experimental data continues to link air pollution exposure with a myriad of pathological conditions. General air pollution is significantly higher in highly urbanized areas and those at a greater risk for air pollution are those generally given "high risk" health status such as the elderly, infants and those with a predisposition to respiratory dysfunction. In 2016, the World Health Organization (WHO) estimated 4.2 million premature deaths per year are directly attributable to general ambient air pollution (WHO, 2016). Additionally, the governing body estimated that 91% of the world's population currently lives in locale not meeting WHO guideline levels for air pollution (WHO, 2018).

Air pollution is highly correlated with a myriad of adverse health effects in a diverse set of tissues. Of the aforementioned premature deaths, 18% are estimated from lower respiratory infection and chronic obstructive pulmonary disease, 5% from trachea, bronchial and lung cancers, and 58% from ischemic heart disease and stroke (WHO, 2018). Given this data, respiratory and vascular tissues seem to be of particular vulnerability to inhaled pollutants. In respiratory tissue, this is manifested by an increased presence of COPD, acute lung inflammation and infections (Robertson et al., 2012). Mice exposed to nitrogen dioxide, a large component of diesel exhaust and precursor to ozone formation, exhibited emphysema-like lesions in the conduction airways. Such lesions were seen in conjunction with an influx of neutrophils and macrophages into the tissue, indicating an influx of inflammatory mediators (Wegmann et al., 2005). In humans, similar adverse effects have been demonstrated in youths placed in Mexico City who demonstrated an acute inflammatory response in nasal epithelium that persisted for approximately two weeks after removal from the area of high pollution (Calderón-Garcidueñas et al.,

1994). Particulate matter common to highly polluted areas is also proven to result in persistent inflammation of respiratory tissue (Tamagawa et al., 2008). Similarly stark effects are demonstrated in vascular tissues. Acute vasoconstriction and inflammation have been widely observed across a range of pollutants such as diesel exhaust, particulate matter and nitrogen oxides (Peretez et al., 2008; Mostovenko et al., 2019; Chuang et al., 2007; Aragon et al., 2017). Some 5-10% of global pregnancies experience hypertensive disorders, making the vasoconstrictive properties of also particular importance during gestation (Say et al., 2014).

Air pollution is also associated with adverse neurological effects across age groups. Elevated levels of air pollution seen in urban areas are associated with decreased cognitive function in the elderly (Power et al., 2013; Wellenius et al., 2012; Power et al., 2011), elevated risk of Alzheimer's and Parkinson's diseases and subsequent neuropathologies (Jung et al., 2015; Kirrane et al., 2015) and accelerated disease progression to the first hospital admission in neurodegenerative diseases (Kioumourtzoglou et al., 2016). In younger subjects, an increased incidence of autism has been associated with prenatal traffic-related ozone exposure in Los Angeles (Becerra, 2013), an association corroborated across multiple studies (Volk et al., 2013; Volk et al, 2011; Roberts et al., 2013). Gestational exposure to high levels of air pollution are also associated with: lower birth weight (Geer et al., 2012), increased microglial activation in rat offspring after birth (Bolton et al., 2012), impaired neurogenesis and vascular leakage in 5 month old offspring (Woodward et al., 2018) and an increased risk of pre-term birth and pre-eclampsia, with 1 in 20 cases of pre-eclampsia being associated with ozone exposure (Olsson et al., 2012). Exposure to ozone also drastically increases embryolethality across gestational exposure timepoints (Kavlock et al., 1979).

1.2. Ozone

Ozone is a photochemically generated air pollutant of high toxicological interest. Volatile organic compounds and nitric oxides produced in fossil fuel emissions react rapidly in the presence of ultraviolet light from the sun to produce ozone in the lower atmosphere (Stedman, 2004; Johnson, 2017) (**Figure 1.1).** Thus, ozone is a prevalent pollutant in urban and industrial areas with dense living and working conditions, implicating ozone as a risk for a high percentage of the human population. Ozone levels in and around urban areas are moreover expected to increase (Smith et al., 2014). Climate change presents confounding factors involving changing air movement, cloud cover, humidity along with overall increased emission rates that will enhance the presence of ozone. Ozone levels fluctuate throughout the day as morning traffic and factory emissions combined with increased ultraviolet light lead to a steady rise until peaking a few hours after midday (**Figure 1.2)**. Such fluctuation means many individuals may only be exposed to unsafe levels of ozone for a few hours daily. In congruence with this observation, the rats in our model were exposed to a single 3 hour ozone exposure similar to that a person living in a highly populated area like Los Angeles or Mexico City may experience on a hot summer day. The amplified effects seen in urban areas present potential to effect the most concentrated source of human inhabitation. In 2018, the United Nations estimated 55% of the world's population lives in urban areas. This estimate is projected to increase to 68% by 2050. Urbanization and an increased global population together will contribute to the incidence of ozone exposure, with another 2.5 billion populating urban areas by mid-century. Close to 90% of these increases are expected in Africa and Asia (United Nations, 2018). Such projections paint a picture of a larger portion of the world's population being exposed to higher ambient ozone levels in the future. **Figure 1.3** shows counties in the United States that did not meet daily standards for ozone (nonattainment areas) established by the Environmental Protection Agency in 2015. The most extreme concentration of these is in southern California.

Once inhaled, ozone reacts exclusively with the surfactant lining of the alveolar epithelium. The thickness of this lung lining fluid layer (LLFL) was originally thought to have a direct impact on the cellular effects of ozone. However, a complete lack of ozone transfer to other tissue compartments indicates the rapid reaction of ozone at the site of the surfactant interface (Pryor, 1992). The rapid reaction of ozone *in vivo* is concentrated to the conducting airways of the upper respiratory system where the highest concentration of LLFL exists, with little damage observed in the lower respirating airways (Postlethwait et al., 1994). Because of its immediate reactivity in the lung, ozone is a model pollutant for establishing an understanding of how pulmonary interactions with inhaled pollutants result in systemic health effects (Paffett et al., 2015).

As ozone is neutralized at the lung surfactant interface, the deleterious effects of ozone are carried out by secondary and tertiary reactants (Frampton et al., 1999; Kafoury et al., 1999; Postlethwait et al., 1998; Pryor et al., 1995). Given the relationship between respiratory and vascular tissues, endothelial cells would seem to be of particular target to these reactants. The increased presence of aldehyde products in BALF of ozone exposed animals indicates reactivity consistent with lipid peroxidation and oxidative stress conditions (Frampton et al., 1999). Such reactants have the potential to modify lipids or produce alternate protein adducts. These products are subsequently capable of binding as epitopes to pattern recognition receptors such as lectin-like oxidized low-density lipoprotein receptor-1, Toll-like receptor 4 (TLR4) and cluster of differentiation receptor 36 (CD36) (Garantziotis et al., 2010; Kampfrath et al., 2011; Kumano-Kuramochi et al., 2012; Li et al., 2011). Of note, impaired vasorelaxation with ozone exposure appears to follow a CD36-dependent signaling mechanism (Robertson et al., 2013). Such findings promise to shed light on the otherwise ill-researched mechanism of systemic ozone toxicity.

The functional relationship between the pulmonary and cardiovascular systems is direct. Because of this intimate relationship, induced pathologies in the lungs are likely to have additional effect

in the vasculature. Given the aforementioned reactions in the lung after ozone exposure, it comes as no surprise that similarly stark effects are seen in the vasculature. Generally, exposure to ground level ozone is associated with increased cardiovascular mortality (Samet et al., 2000). Mice and primates exposed acutely to ozone exhibit significantly increased formation of atherosclerotic lesions and endothelial mithochondrial damage (Chuang et al., 2009). Acute arterial vasoconstriction, a risk factor for catastrophic cardiovascular outcomes, is caused by ozone inhalation (Brook et al., 2002). When analyzing serum and bronchoalveolar lavage transcriptomes after ambient level ozone, differentially expressed genes were shared between ozone exposure and atherosclerosis studies (Tham et al., 2017).

The acute reactions observed in lung surfactant have demonstrated additional responses in the CNS. Increased microglial activation, a defining characteristic of neuroinflammation, is seen after acute ozone exposure (Gonzalez-Guevara et al., 2014). In adult rats, ozone induced oxidative stress resulted in loss of hippocampal brain repair and memory deficits (Rivas-Arancibia et al., 2010). Promotion of activity in stress responsive regions of the CNS after ozone exposure has been linked to activation of nucleus tractus solitarius neurons via vagus nerves upstream (Gackiere et al., 2011). Recently, significant increases in serum amyloid A were demonstrated after ozone exposure and the protein showed an ability to cross the BBB (Erickson et al., 2017). This demonstrates a possible mediator between ozone-related lung inflammation and CNS inflammatory response.

While vascular, pulmonary and neuronal dysfunctions are relatively well characterized, ozone effects during gestation are poorly investigated mechanistically. Multiple common air pollutants, including ozone, have recently been implicated in the development of gestational hypertension (Zhu et al., 2017). Given the hypertensive qualities shown in other ozone studies, these findings are consistent with ozone being a causative force behind maternal hypertension in pregnancy. Additionally, pollutant exposure has been consistently correlated with low term birth weight in human cohort and animal studies (Geer et al., 2012; Miller et al., 2017; Tu et al., 2016). Due to the vascular nature of the majority

of ozone related negative health outcomes, the placenta has emerged as a target organ, given its complex vascular bed and vascular barrier functionality, for future studies investigating gestational vascular effects of ozone. Moreover, abnormal placental function can have significant impacts on fetal development, particularly on hypoxia-sensitive organs such as the brain (Amiel-Tison et al., 1991; Baschat, 2011; Neerhof and Thaete, 2008).

1.3. Cardiovascular Complications in Pregnancy

Cardiovascular related health outcomes during pregnancy are generally hypertensive in nature, with approximately 1 in 10 pregnancies experiencing such complications worldwide (Say et al., 2014). Such effects are closely tied to both maternal and fetal morbidity and mortality (Endeshaw, G. et al., 2015). While such outcomes are well documented epidemiologically, critical periods for exposure and biochemical mechanisms of pathology remain underexplored. In investigating such complications as preeclampsia, the placenta has emerged as the leading target organ of interest for maternal vascular-related complications during pregnancy. The relationship between maternal hypertensive disorders and oxidative stress is well documented and presents a link between these and more general vascular abnormalities such as atherosclerosis (Hubel, 1999; Roberts and Cooper, 2001; Singh and Jialal, 2006). Given the established link between ozone exposure and oxidative stress, an association between ozone exposure and preeclampsia must be investigated (Valavanidis et al., 2013; Corradi et al., 2002).

Preeclampsia is the most common medical complication of pregnancy worldwide, occurring in 2-8% of pregnancies, and accounts for approximately 50,000 annual worldwide deaths (Duley, 2009; Ghulmiyyah and Sibai, 2012). The onset of the disease is marked by hypertension and significant proteinuria on or after gestational week 20 in a previously healthy woman (Eiland et al., 2012). In the placenta, the disorder is characterized by shallow invasion of the uterine endometrium and inadequate remodeling of the maternal spiral arteries after implantation. In addition to these basic diagnostic

parameters, preeclampsia can be viewed from a specific pathological state in the placenta similar to tissues under conditions of hypoxia and/or oxidative stress. Such a pathological state considers protein shifts indicative of an anti-angiogenic state in the placenta (Eiland et al., 2012). These specific protein expression patterns will be discussed later in this introduction. Despite extensive efforts to actively diagnose and treat gestational hypertensive disorders for decades, a lack of consistent biomarkers and *in vivo* experimentation have made such efforts less than fruitful (Chao et al., 2017).

1.4. Amniotic Fluid

The basis for our further exploration into placenta and fetal development is proteomic analysis of amniotic fluid (AF) from ozone exposed dams. Directly following implantation, AF volume increases faster than embryonic size. The liquid volume of AF is derived from maternal plasma which passes through the fetal membranes via hydrostatic and osmotic forces. As pregnancy continues, a large volume of AF in the embryonic cavity is displaced by the growing size of the fetus. At this stage, further contributions to AF volume are generally derived from fetal urine and other fluid secretions. Circulation of the amniotic fluid continues via intramembranous diffusion, fetal swallowing, and excretion until term. Thus, AF can serve as a viable diagnostic tool for both mother and fetus throughout pregnancy. High levels of inflammatory cytokines (such as IL-1, IL-6, and TNF-alpha) have been associated with premature rupture of membranes prior to term (Underwood et al., 2005). Proteomic comparison studies in rodent and human models of disease have shown differences in AF protein composition between normal fetuses and those with down syndrome and spina bifida (Tsangaris et al., 2006; Shan et al., 2012). Thus, proteomic analysis of AF from ozone exposed dams can provide insight into the state of the dam and the fetus. Little has been explored in the way of amniotic fluid toxicology in relation to air pollution exposure effects on the amnio-proteome.

1.5. Maternal-Fetal Circulation

A diagram of maternal-fetal blood circulation can been seen in **Figure 1.4**. Maternal blood supply begins from radial arteries that enter the uterus via the myometrium on the mesometrial side. Branches of these arteries either pass laterally through the myometrium or directly through to enter the metrial gland. At this point, the radial arteries branch into spiral-shaped arteries. Upon penetrating the decidua basalis, the spiral arteries converge to form a small number of centrally located arterial canals. These canals lead into the trophoblast-lined maternal sinusoid spaces in the labyrinth zone. It is at this location that gas and nutrient exchange between the dam and fetus occurs. Maternal blood drains from the labyrinth through venous sinuses back towards the decidua basalis, crossing the basal zone again. These venous sinuses then traverse the outer metrial gland to exit into radial veins outside the myometrium (Furukawa et al., 2011).

1.6. Placenta Models and structure

When considering the placenta as an organ of interest, one must consider its highly specialized anatomy (**Figure 1.5**), regulation, and structural difference amongst species. A key distinction between placenta types is in the location of the materno-fetal exchange site(s). Primates, rodents and rabbits possess a discoid or bidiscoid placenta. In these placentae, interaction between invading trophoblast cells and the uterine endometrium is confined to a single or two circular areas. Given these, discoid or bidiscoid placentae are optimal for building a study of function analogous to humans (Wooding and Burton, 2008). Additional distinctions are made regarding the invasiveness of the placenta. Primates, rabbits and rats all feature differing varieties of hemochrial placentae. These are the most invasive placenta. In such tissues, all maternal tissue layers disappear through erosion and direct connection between the chorion and maternal blood is established. A differentiation between species in the hemochorial subtype is made based on the number of trophoblast layers, with humans being

hemomonochorial (single layer) and rats and mice being hemotrichorial (three layers) (Takata et al., 1997). The high level of invasiveness of hemochorial placentae make them more permeable than other placenta phenotypes. For instance, amino acid contribution to fetal oxidative metabolism is observed to a much greater extent in rodents, rabbits and primates in comparison to rumants, pigs and horses (Pere, 2003).

Let's first consider the mammalian placental structure and function. A discussion on the development of the placenta, or placentation, will follow. The placenta supports the fetus as the exchange point for all respiratory gases, nutrients and waste (Reynolds et al., 1995). The human placenta consists of structures called villi, termed for their treelike structure. In rodents, a similarly branching network is formed by fetal capillaries surrounded by trophoblast cells. Floating villi are in direct contact with circulating maternal blood and mediate gas and nutrient exchange between mother and fetus. An outer, single layer of syncytiotrophoblast cells line each villous tree and is bathed in maternal blood, resulting in nutrient and gas exchange. Another class of villi, anchoring villi, contact both maternal blood and the decidualized uterine endometrium and anchor the placenta to the uterine wall. The ends of anchoring villi attach the placenta to the uterine wall, remodeling uterine blood vessels to enable blood flow to the fetus and facilitate histiotrophic nutrition for the embryo. Lastly, the villous stroma, which surrounds the villi in a network of connective tissues, houses fetal macrophages (Hofbauer cells) and other structural cells, including the massive vascular network required for fetal-maternal circulation (Bushway et al., 2014). In rat, this villous system is analogous to the labyrinth zone of gas and nutrient exchange.

The rat placenta consists of four distinct regions, two derived from the fetus and two derived from the dam. The fetal-derived portions, formed from the trophoectoderm of the embryo, are termed the labyrinth and the basal zone. The maternally-derived placenta is formed from the uterine endometrium and is termed the decidua and the metrial gland (Furukawa et al, 2011). The metrial gland

is composed of a mix of decidual cells and fibroblasts, uterine natural killer cells and the maternal arteries. The gland is formed early on and is fully developed by mid-gestation. After this point the gland regresses and is deeply invaded by trophoblasts. This is consistent with the highly invasive model of rat placentation (Fonseca et al., 2012; Charest et al., 2018).

The labyrinth zone is the principal location of maternal-fetal exchange as it is highly vascularized and contains the placental barrier. It is here that gas and nutrient exchange occurs through maternal sinusoids. Thus, this area of the interface is of specific interest in toxicological study of the placenta. In rat, this barrier is formed by three trophoblast layers, one of cytotrophoblast cells and two of synctiotrophoblast cells, consistent with the hemotrichorial placental phenotype (Wooding and Burton, 2008). These layers separate the maternal and fetal vascular tissues to form the barrier. The rat placenta is considered well vascularized by GD12, with the labyrinth of capillaries developing further over the next days before the placenta reaches its peak weight by GD19 (Jollie, 1964; Furukawa et al., 2019).

Between the decidua and labyrinth zones is the basal zone. This area serves as the primary endocrine cell layer of the placenta to maintain viability of the organ until term. Within the basal zone are three types of specifically differentiated trophoblast cells. These three distinct cell types are the trophoblast giant cells, spongiotrophoblast cells and glycogen cells. Trophoblast giant cells form the main separation between maternal and fetal placenta tissues. They serve as the major endocrine cells of the organ and serve diffuse purposes in protein secretion, cell adhesion and cytokine signaling to promote specific adaptations of the dam throughout pregnancy (Hu and Cross, 2010; Furukawa et al., 2011; Charest et al., 2018). The decidua composes a region of altered maternal endometrial stromal cells. These cells are altered via the process of decidualization from elongated, fibroblastic shaped stromal cells to densely packed decidual cells (Fonseca et al., 2012). The decidual region produces signaling factors unique to those of the basal zone. The decidua is observed at its largest size directly after implantation and degenerates progressively in the last half of the pregnancy as the placenta nears

term. At term, these cells form a single thin layer at the base of the placenta called the decidua basalis (Furukawa et al., 2011).

Instrumental to successful development of the conceptus is adequate implantation of the placenta in the uterine endometrium. Implantation in rat is established by pregnancy days 4-5, well past our first window for ozone exposure. However, the process of placentation is only just beginning with implantation. There are two key processes inherent to adequate placentation necessary for a successful pregnancy: spiral artery remodeling and controlled trophoblast invasion. The principle local blood supply to placentation sites are the uterine spiral arteries. These vessels are specifically modified to allow for high volume transfer free of maternal immunosurveillance (Whitely et al., 2009). Structurally, all components of the spiral arteries, including endothelium, basement membrane, and smooth muscle, are altered in this process deemed spiral artery remodeling. These changes are manifested by the change of the spiral arteries from high-resistance, low-flow vessels into large dilated vessels showing increased blood flow at a markedly decreased pressure (Burton et al., 2009). Control of this remodeling is critical to a successful pregnancy, as dysfunction in the process is linked to preeclampsia, intrauterine growth restriction, and premature pregnancy termination (Soares et al., 2011). While the importance of the process is known, mechanistically spiral artery remodeling is poorly understood. The process is thought to be controlled by highly complex interactions between specific invasive trophoblast cell lineages and the uterine endometrium in induced apoptotic events. Recently, induced inflammation between GD 13.5-16.5 has demonstrated causative impairment of spiral artery remodeling, resulting in fetal growth restriction and preeclamptic features at term (Cotechini et al., 2014).

Trophoblast invasion is either interstitial through the decidua or endovascular through the distal ends of spiral arteries where invasion is in the opposite direction of blood flow. While invasion and vascular remodeling are inherently related, research suggests the two are independently controlled, with invasion being controlled by signaling from the conceptus and remodeling being influenced by both

the invading trophoblast cells and maternal tissues, including immune cells. Inherent to our current study, histological landmarks can be used to assess normal placentation at specific timepoints. As our tissues were harvested at term, observations for normal placentation in the term placenta will be used for assessment of ozone mediated alteration to the organ. By day 14, endothelial cells of larger vessels within the myometrium are covered by trophoblasts (de Rijk et al., 2002). Given the period during which is observed and known effects on vasculature of ozone, a possible effect of ozone may be alteration of this trophoblast cover, effectively altering the functionality of the placental barrier. Additionally, by GD14, large rounded decidualized cells are completely replaced by smaller, multi-nucleated decidualized cells. The presence of larger decidualized cells at term can be a measure of abnormal placentation in rat. By GD12, a cell layer with many lacunae has formed, the largest of these lacunae being filled with maternal blood and smaller lacunae filled with embryofetal blood. As these smaller lacunae develop into capillaries, the layer is termed the labyrinth zone. The alteration of these lacunae and their connective tissue structure can have distinct effects on the maternal-fetal circulation. Given its timepoint during placental development, we hypothesize mid-term ozone exposure will have a distinct effect on the development of the labyrinth zone manifested by vessel expression and ECM organization at term.

1.7. Osteopontin

Osteopontin (OPN), or secreted phosphoprotein 1, is a soluble ECM protein in the small integrin-binding ligand N-linked glycoprotein (SIBLING) family with binding capabilities for multiple integrin receptors (Hynes, 1997; Brown et al., 1992; Sodek et al., 2000). The protein has been implicated in embryogenesis, wound healing/fibrosis and tumorigenesis (Weber et al., 2012). OPN can undergo extensive post-translational modification via phosphorylation, glycosylation and proteolytic cleavage. Such diverse modifications make for a diverse set of interactions across multiple isoforms of the protein (Johnson et al., 2003).

Documented ligands for OPN include ECM proteins fibronectin, fibrinogen, vitronectin, collagen, laminin and hyaluronic acid (Wai and Kuo, 2008). With abundant and diverse integrin interactions, OPN and its integrin substrates are more generally involved in adhesion cascades necessary for wound healing (Kling et al., 1992), and more specifically, of interest for its potential role in implantation across several animal models (Johnson et al., 2014). Early on in pregnancy, the invading trophoblast begins to secrete estrogen. While vital to the pregnancy state in many other ways, estrogen has been shown to regulate the expression of OPN in the uterine endometrium (Burghardt et al., 2002). Moreover, OPN has been shown in other tissues to upregulate MMP2, which can be influential during implantation (Zhang et al, 2011). Such data suggests the possibility of a feedback loop regulating the activity of both proteins through proteolytic cleavage of OPN by MMP2. OPN's cleavage by multiple MMPs, amongst other proteases, helps to make the protein a crossroads for inflammatory and tissue remodeling regulation. Overall, OPN is diversely expressed after initial implantation in the uterine endometrium, trophoblast and throughout the entire maternal-fetal interface (White et al., 2005). Such locale support the premise of OPN playing a fundamental role in invasive trophoblast activity. Numerous studies have implicated OPN as the most highly upregulated ECM molecule in the human uterus during the implantation period (Carson et al., 2002; Kao et al., 2002; Mirkin et al., 2005). However, as new invasive trophoblast activity has been observed as 5 days prior to term, the protein appears to continue to play a role well after implantation. The expression of the protein is upregulated in mouse tissues being actively decidualized. Given the process of decidualization progresses until term in rats, OPN appears to have influence throughout pregnancy (Herington and Bany, 2007).

Integrin receptors are integral membrane proteins consisting of alpha and beta subunits necessary in processes such as cell-cell adhesion and cytokine signal transduction. The A5B3 and A5B1 integrin receptor subtypes on trophoblast cells bind OPN to aid in mediation of implantation (Kim et al., 2010). The interaction between OPN and integrins is thus thought to facilitate trophoblast guidance

during uterine invasion and facilitate adherence to the uterine endometrium during the peri-implantation period. Integrin-based signaling with OPN is involved in the epithelial-mesenchymal transition (Weber et al., 2017).

1.8. Extracellular Matrix (ECM) and Matrix Metalloprotease Contributions

Between implantation and the beginning of true maternal-fetal circulation, an elaborate system of ECM formation and degradation is established (Chen and Aplin, 2003). The primary structural components of the placenta consist of differing collagen subtypes (Amenta et al., 1986). Collagen I is shown to be the major interstitial fibrillar species, whereas collagen IV is a major structural component of the basement membrane of both vessels and trophoblasts. Also prevalent are elastin (observed in vascular and muscle cell ECM), thrombospondin I and tenascin C. The latter of these is often observed at sights of tissue remodeling (Chen and Aplin, 2003). Little to no ECM reactivity is observed in the trophoblast layers bordering the amnion (Chen and Aplin, 2003). While relative normal distributions for such proteins have been established in healthy placenta, abnormal distributions have alternatively been demonstrated in disorders of abnormal placental function.

Real-time quantitative PCR and transcriptome assessment of healthy and preeclamptic human placentae has indicated an altered expression of ECM proteins between the two. Of particular relevance, the preeclamptic placenta exhibited up-regulated collagens and down-regulated expression of matrix metalloproteases (MMPs) involved in ECM remodeling at term (Kim et al., 2016). In accord with downregulated MMPs, tissue inhibitors of metalloproteases (TIMPs), such as TIMP1 and TIMP3, were upregulated. MMP regulation is largely overseen by TIMP expression and the balance between these two protein types is the main regulator of ECM degradation and subsequent deposition (Brew et al., 2000; Kim et al., 2008). The primary role of MMPs in the placenta, specifically MMP2 and MMP9, is trophoblast invasion and the level of such invasion has been directly correlated with MMP expression

and activity *in vitro* (Huisman et al., 2004). In altering the ECM of invaded tissue, MMPs allow for angiogenesis of spiral arteries necessary for fully developed maternal-fetal circulation. A shallow trophoblast invasion in term placenta caused by abnormal ECM remodeling has been readily demonstrated in pathology of dysfunctional placentae.

MMPs are a family of zinc-requiring enzymes whose activity is implicated in both normal and pathological tissue remodeling (Jiang and Bond, 1992; Stevenson et al., 1993; Huisman et al., 2004). These molecules have been identified in both human and rat placenta (Pustovrh et al., 2007). MMP2 is classified as a type I collagenase and MMP9 is classified as a Type IV collagenase or gelatinase, specifically gelatinase A (Klein & Bischoff, 2011). Their secretion in the placenta differs both temporally and anatomically. MMP2 protein and mRNA is expressed in both cytotrophoblastic anchoring villi and decidual cell lines during the first semester (Huisman et al., 2004; Huppertz et al., 1997). Immunohistochemical analysis of MMP9 has localized its expression to the syncytiotrophoblast and the extra-villous cytotrophoblast (de Jager et al., 2003; Isaka et al., 2003). In the third trimester, trophoblast secretes mainly MMP9, with minimal recorded amounts of MMP2 (Shimonovitz et al., 1994). While little data exists on temporal MMP expression past the implantation period in rats, the labyrinth zone, the area most analogous to human villi structure, exhibits invasive trophoblast activity continuing until approximately GD16 (Soares et al., 2016). Thus, mid-gestational teratogenic exposure will affect the placenta during a critical period of development for the placental circulation. Both MMP's are shown to be increased in the placentae of diabetic rats at mid-gestation, a condition often caused directly by the placenta (Pustovrh et al., 2005). Thus, regulation of MMP expression is altered in a pathological state.

Data from Kim *et al.* (2008) indicates higher expression of collagens and other structural ECM proteins in dysfunctional placentae in conjunction with decreased expression of MMP's. These results support a hypothesis of impaired ECM remodeling, specifically in areas of spiral artery angiogenesis, in placental dysfunction. Distribution of ECM proteins in preeclamptic placentae is of interest for pathological and

mechanistic understanding of the condition (Kim et al., 2016; Chen and Aplin, 2003). We hypothesize observing similar results when assessing the amniotic proteome and placental histology of rats exposed to ozone during gestation with upregulation of ECM structural proteins and downregulation of ECM remodeling proteins such as MMP2 and MMP9. In addition to structural proteins such as collagens, MMP's regulate other proteins of interest in placental implantation and stability.

1.9. Galectin-1

Yet another factor of importance in the placenta is galectin, a family of cytokine-like immuneregulatory proteins with an affinity for beta-galactosides present on cell surface glycoconjugates (Than et al., 2008). The diverse functions of these molecules include cell-matrix interactions, apoptosis and cell migration (Than et al., 2008). Its overexpression in a systemic inflammatory state has been demonstrated across cell types and pathologies, from cultured endothelial cells to rheumatoid arthritis to preeclampsia (Than et al., 2008).

The period of implantation and placentation is marked by an increase in galectin-1 levels during the first trimester. The molecule has been shown to be expressed on trophoblast cells of the blastocyst prior to implantation (Tirado-Gonzalez et al., 2013). Evidence also suggests that galectin-1 is vital in establishing the immunotolerance necessary for the placenta to implant into the uterus even while possessing paternal antigens (Balogh et al., 2019). Pathologically, the molecule has become a target in the tracking of preeclampsia (Than et al., 2008; Hirishima et al., 2018). Recent evidence suggests the presence of temporal indicators in the protein's association with the disease. Specifically, low expression levels in the second semester in conjunction with markedly increased expression in the third trimester with disease onset have been consistently demonstrated in disease progression (Than et al., 2008; Hirashima et al., 2018). Such timepoints in rodent models are analogous to the post-implantation period following GD12 once placental circulation has been fully established in these animals. Given the ability

of teratogens such as ozone to induce placental dysfunction, exposure at this critical timepoint may induce galectin-1 levels associated with pathologic conditions like preeclampsia. Such levels are measured in maternal serum, where they are associated with a hallmark of preeclampsia, gestational hypertension. Recent studies suggest measuring galectin-1 at different timepoints in pregnancy as a means of tracking possible progression of preeclampsia and gestational hypertension.

1.10. Neurological Effects of Air Pollution and BBB Development

Air pollution, specifically ozone, has been linked to several neurological pathologies, including Alzheimer's and Parkinson's diseases (Kirrane et al., 2015; Jung et al., 2015). Further, exposure to such substances has been associated with early ultrastructural changes in nasal mucosa and conditions of abnormal neurodevelopment during childhood. Exposure levels are inversely correlated with multiple measures of cognitive performance (Angiulli, 2018). Of particular note are deficits in executive function in childhood that are never recovered as the brain develops (Allen et al., 2017). Additionally, prescriptions for psychiatric conditions in children such as ADHD are increased in areas of high air pollution (Oudin et al., 2016). Given these associations, recent efforts have focused on better elucidating the underlying toxicological mechanisms along lung-brain axis of primary and secondary insult. As this axis is linked through vasculature, the blood-brain barrier (BBB) represents a fundamental point of intersection. Our understanding of the BBB has evolved through a greater appreciation of this privileged barrier's complexity. Much like any vascular interface, the anatomical foundation of the BBB are endothelial cells (ECs) of the cerebral blood vessels. However, these ECs are distinct from all other ECs by the continuous presence of intercellular tight junctions (TJs) and the lack of fenestration along the luminal surface (Obermeier et al., 2013). Functionally, these anatomical features are translated to extremely low rates of transcytosis, highly limiting paracellular and transcellular movement of molecules through the EC layer (Abbott et al., 2006). Specialized membrane-bound transporters facilitate nutrient

delivery and extrusion of toxins in an otherwise tightly controlled barrier at all levels of the cerebrovascular tree (Danem, 2012).

Development and maintenance of the healthy BBB is controlled by a network of cellular and non-cellular structures that work in conjunction with neural ECs. Structural and functional support for the BBB is provided by astrocytes, pericytes, and ECM components in what is termed the "neurovascular unit" (NVU) (Iadecola, 2017) (**Figure 1.6**). The abluminal surface of capillaries in the brain is enclosed by a basement membrane that separates ECs from pericytes, and pericytes from astrocytes (Obermeier et al., 2013; Hallmann et al., 2005). Such compartmentalization contributes to the structural integrity of the barrier, protecting the parenchyma from possible damage. Development of the BBB during the embryonic period involves complex series of steps, beginning with sprouting angiogenesis at the neuroepithelium (Risau, 1997). Invasion of neural tissue from the surrounding perineural vascular plexus is initiated by endothelial progenitor cells in a caudal to cranial direction. Molecular secretions from neural progenitor cells drive endothelial migration into neural tissue while ECs secrete signals to recruit pericytes (Hellstrom et al., 1999). Such activity is seen in early embryogenesis, prior to the development of astrocytes. In rodents, the first vessels invade the cerebral cortex starting around gestational day 10 when we plan to perform our first ozone exposure. This is also right at the start of when microglia are beginning to populate the developing brain, establishing the capacity for a neuroinflammatory response within the brain (Kaur et al., 2017). At this time, the rat BBB is more permeable to small molecules (Daneman et al., 2010). However, early tightening of the BBB is facilitated by pericyte interactions by around GD15 (Ben-Zvi et al., 2014; Sohet et al., 2015). This is generally demarcated as the BBB gaining functionality, although more subtle refinement continues perinatally, most particularly by the introduction of astroglial endfeet, which begins shortly before term when we plan to perform our second ozone exposure (Daneman et al., 2010; Yang et al., 2013). Our study time points would

correspond to similar BBB developmental events for initial vessel formation at 8 weeks of gestation and astrogliogenesis by around 15 weeks of gestation (Lippman et al., 2015) (Saili et al., 2017).

Rodent models of acute ozone exposure have demonstrated induced oxidative stress and inflammation within the brain (Gonzalez-Guevara et al., 2014). In rodent neurodevelopment, prominent critical periods have been identified in mid- and late gestation (Woodworth et al., 2012), matching our study design's use of GD10 and GD20 time points. This timing is differentiated as preceding and following establishment of the rudimentary BBB, subdivides the potential for teratogenic effects from ozone exposure. As acute ozone exposure has demonstrated BBB compromise, albumin leakage and neuroinflammation proximal to the vessels with astrocyte and microglial reactivity (Mumaw et al., 2016), we posit that these effects may be augmented based on the gestational period of exposure. Toxicological studies on BBB formation, however, are very limited. One study showed that exposure to pesticides at GD10 in rodents dramatically increased BBB permeability at birth (Gupta et al., 1999). In another study, gestational diesel exhaust exposure significantly altered microglial reactivity, suggesting an impact to the nascent BBB, and resulted in prolonged changes in microglial morphology and neuro-glial interactions well after birth (Bolton et al., 2017). The induced neuroinflammatory response was comorbid with decreased cortical volume at birth, a finding consistent with neurological models of autism (Courchesne et al., 1993).

While primarily a disease of maternal vasculature, preeclampsia and maternal hypertension have demonstrated marked and lasting effects on brain function in offspring, with little effect on maternal cognitive function (Liu et al., 2016). Importantly, the onset of preeclampsia is typically mid-gestation, coincident to BBB formation, with the condition continuing until birth (Steegers et al., 2012). Moreover, preeclampsic pathobiology is associated with oxidative stress and inflammation (Hubel, 1999), both hallmarks of the neurotoxicological response to ozone exposure. Studies linking preeclampsia with developmental and functional changes in the CNS of offspring are few (Liu et al.,

2016), and to our knowledge studies investigating xenobiotic-exposure induced placental abnormality in combination with fetal BBB deficits are nonexistent. Permeability of rodent cerebral vessels has been shown to increase after exposure to plasma from women with preeclampsia (Amburgey et al., 2010). Combining effects observed in maternal BBB and vasculature with the anti-angiogenic effects observed in the preeclamptic placenta, it is within reason to hypothesize a significant effect on the fetal BBB in the term pregnancy of rodents placed under conditions promoting oxidative stress and inflammation.

1.11. Conclusion and Hypothesis

The above content intends to reflect rationale for the project at hand. In earnest, our work seeks to explore three core aims. Aim 1 seeks to assess the effect of acute ozone inhalation on the amniotic environment during pregnancy. We will examine how moderate (0.3ppm) ozone exposure differentially influences the amniotic proteome at two critical periods – GD10, when the blood brain barrier has yet to be fully formed versus GD20, when astrocyte and microglial populations have established and synaptogenesis is prevalent. Also of interest is examining the proteome at GD20 for how ozone dose influences the amniotic proteome. The deleterious effects of ozone have been well established earlier in this paper yet underexplored on prenatal development. Given the vascular nature of many of these effects and amniotic fluid's origin from maternal serum, we expect marked differences in proteomic profile at different gestational timepoints and ozone dosages. We will analyze the amniotic fluid via liquid chromatography-gas spectrometry and analyze data using a conservative linear approach. We expect fold-changes in inflammatory mediators and ECM proteins similar to a preeclamptic state in ozone administered animals. GD20 exposed animals will demonstrate proteomic shifts after acute ozone exposure late in gestation, whereas GD10 exposed placenta will demonstrate an altered proteome after allowing development to finish.

Our second aim seeks to devise follow-up assessments to further inform on ozone-induced influences on the amniotic environment. We aim to devise a targeted immunohistological approach to assess placental abnormality corresponding with observed shifts in the amniotic proteome. These approaches will use markers for ECM and vascular proteins to assess effects of placental barrier integrity after ozone exposure. We plan to devise a targeted immunohistological approach to assess effects on the fetal blood brain barrier with ozone exposure at GD10 and GD20, assessing barrier integrity and glial reactivity. The approach will provide selected antigen targets, the study design and experimental methodology, and how the results would be analyzed. Rationale for many of the targets has been discussed in this introduction.

The final aim will evaluate how ozone-induced effects on the amniotic fluid proteome correspond to responses within the maternal serum proteome. In doing so, we will employ the same techniques used in LC/MS analysis of AF. We will assess correlating responses that would suggest a maternal source of responsive factors within the amniotic environment and their functional significance. Also, we plan to examine amniotic proteome responses that are distinctive from those in the maternal circulation as evidence for fetal effects. Given the origination of AF from maternal serum, a comparative analysis of each fluid's proteome will provide further insight to the true origin of AF findings. Additionally, serum data has potential to bolster an argument for an induced preeclamptic-like state, an outcome we expect given the effects of ozone on other vascular beds.

The effects of acute ozone exposure on the adult specimen are well established and diffuse in nature. The present work seeks to shed similar light onto ozone effects in the developing fetus, which have not been explored in earnest. Such work has potential to demonstrate effects on the transient placenta organ and developing fetal structures particularly sensitive to teratogenesis, such as the brain. In demonstrating effects on the fetal brain, the study presents an argument for continued research on all air pollutants and their relation to neurodevelopment.

Figure 1.1

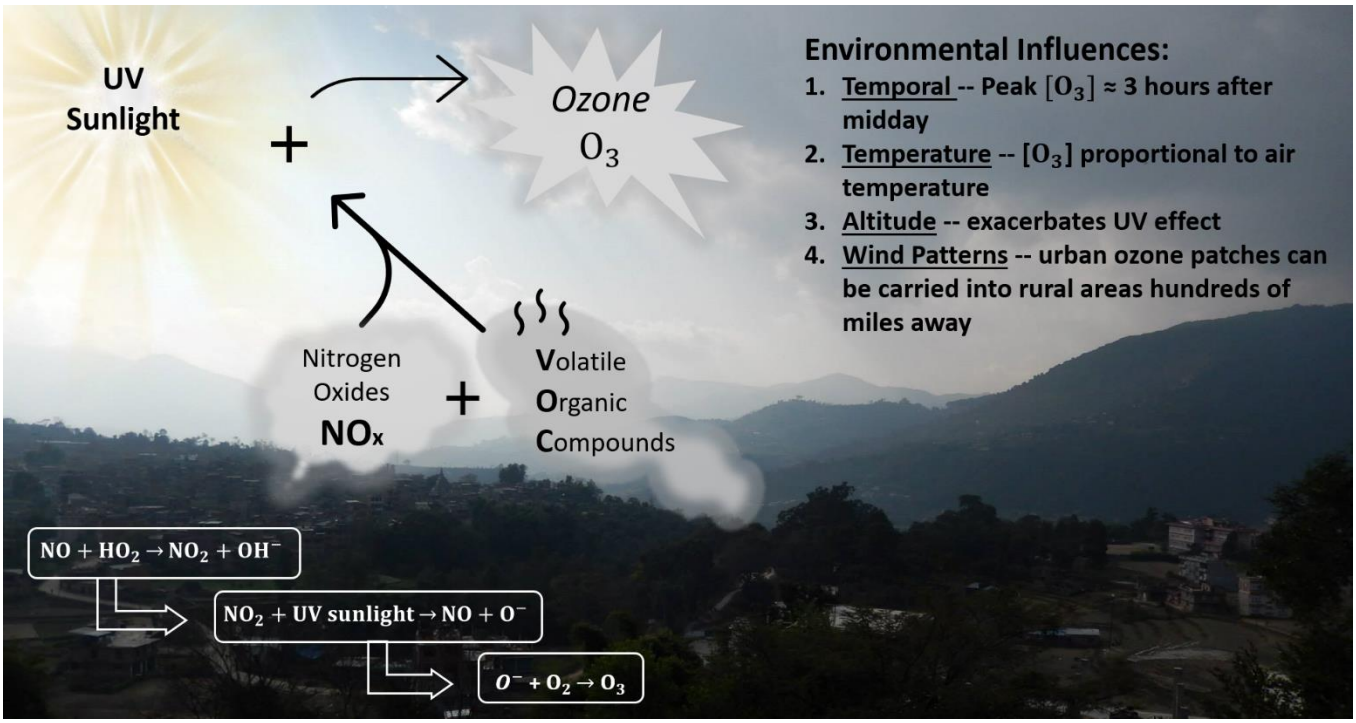

Figure 1.1 Ambient Tropospheric Ozone Pollution

The majority of ambient ozone formation stems from nitrogen oxides, common air pollutants, readily reacting with sunlight to produce nitric oxide and an oxygen free radical. This free radical reacts with molecular oxygen to form ozone. Similarly, hydrogen peroxide, an intermediate of volatile organic compound oxidation, reacts readily with nitric oxide to form nitrogen dioxide, producing more ozone precursors.

Figure 1.2

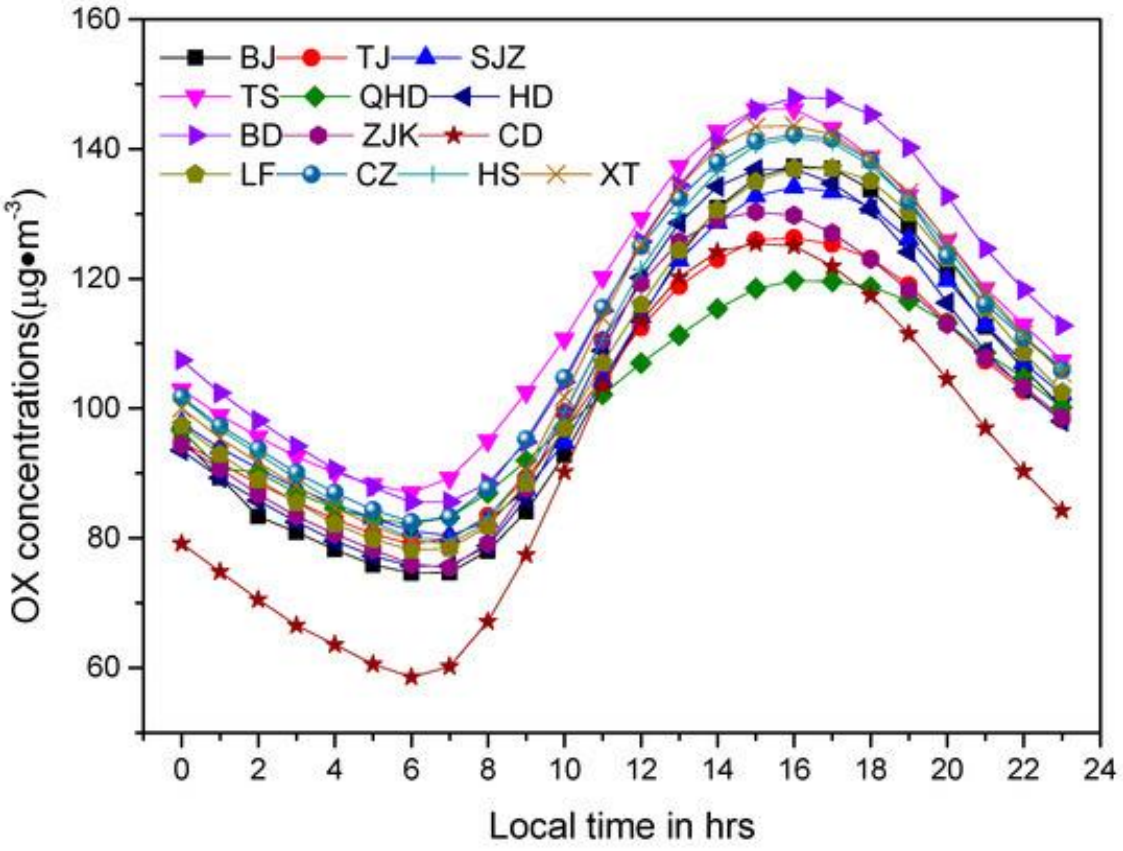

Figure 1.2 Daily Fluctuations in Ambient Ozone Concentrations in a Heavily Urbanized Area

Daily ozone concentration fluctuation in Beijing, China and surrounding areas. Courtesy of: Fang, X.; Xiao, H.; Sun, H.; Liu, C.; Zhang, Z.; Xie, Y.; Liang, Y.; Wang, F. Characteristics of Ground-Level Ozone from 2015 to 2018 in BTH Area, China. *Atmosphere* **2020**, *11*, 130.

DOI: https://doi.org/10.3390/atmos11020130

Figure 1.3

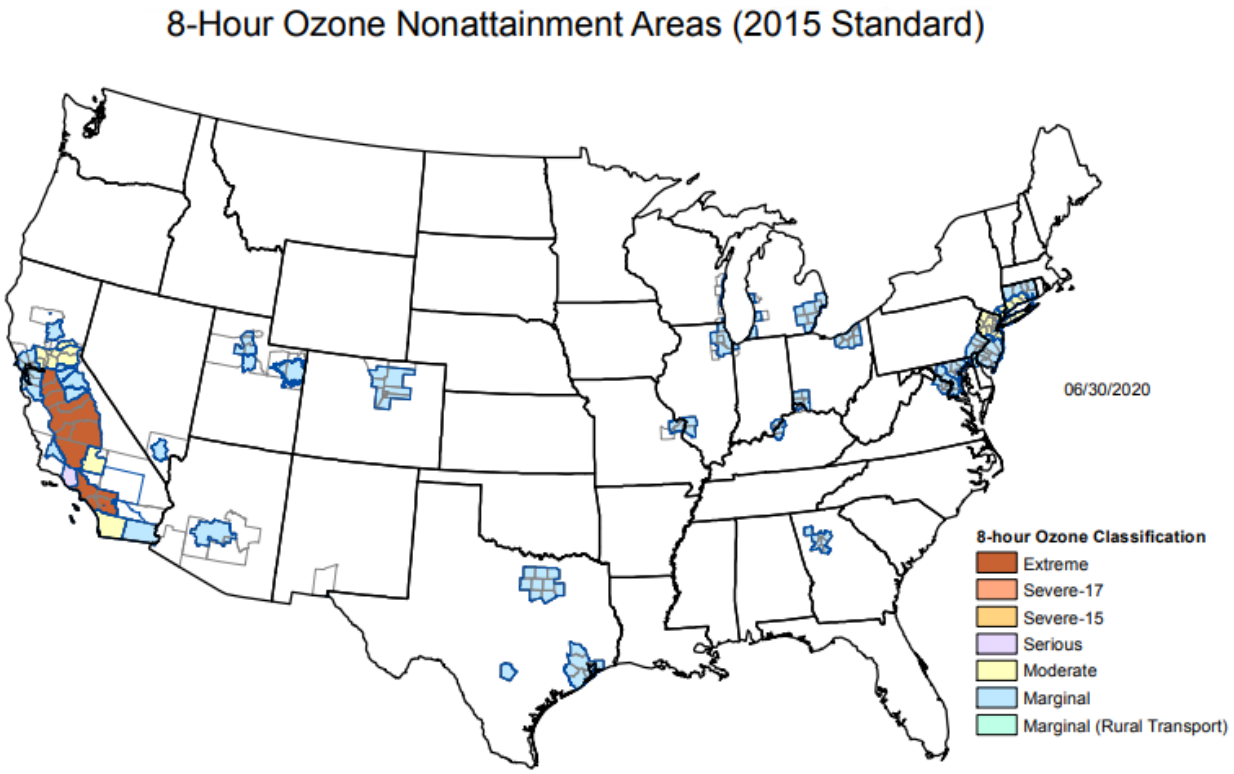

Figure 1.3 EPA Designated Ozone Nonattainment Areas in the United States

Map of US counties with 8-hour ozone concentrations falling outside of safe limits established by the 2015 EPA standard. Courtesy: United States Environmental Protection Agency "Green Book"

Link: https://www3.epa.gov/airquality/greenbook/map8hr_2015.html

Figure 1.4

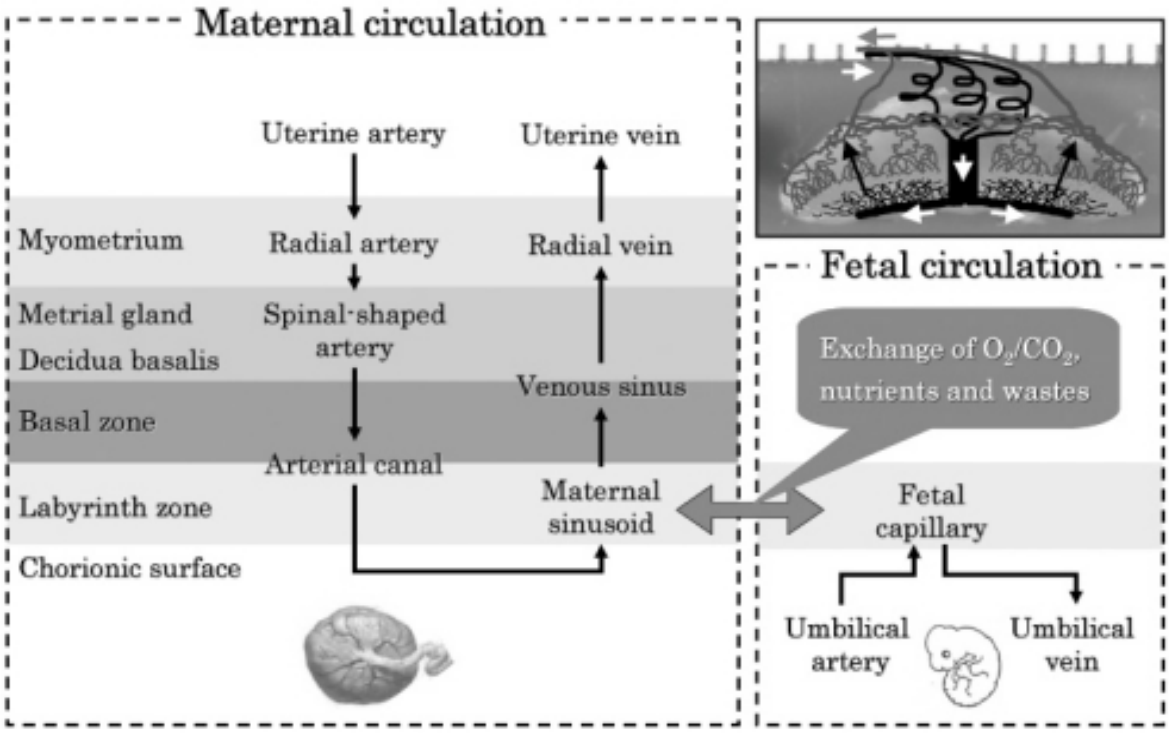

Figure 1.4 Spatial Relationship of Maternal-Fetal Circulation in Rat

Placental circulation in the rat. Courtesy of Furukawa et al., 2011. Copyright Japanese Society of Toxicologic Pathology. License. Original text available at: https://dx.doi.org/10.1293%2Ftox.24.95

Figure 1.5

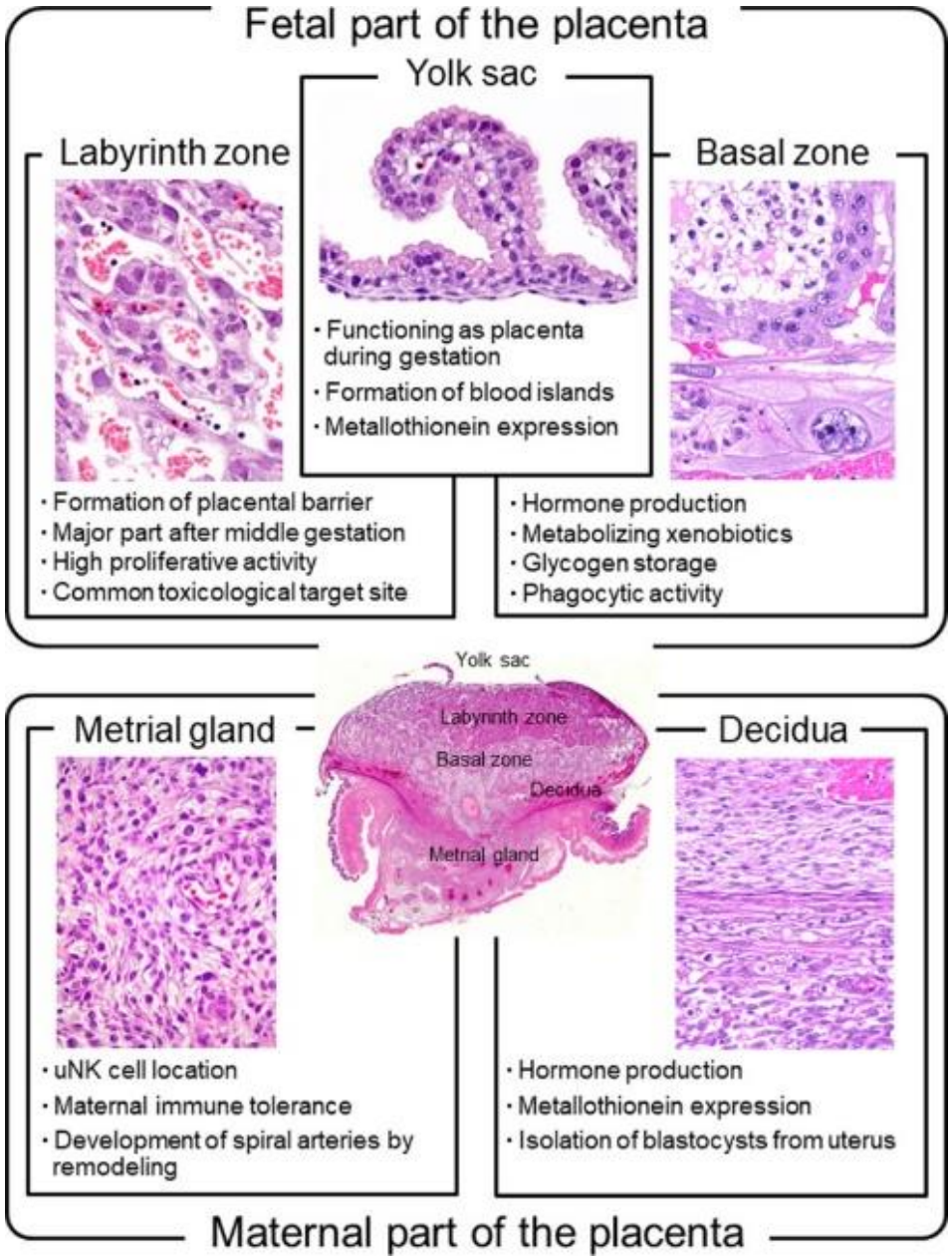

Figure 1.5 Histological Anatomy of Rat Placenta

Histological anatomy of rat placenta is shown. Courtesy of Furukawa et al., 2019. Copyright Japanese Society of Toxicologic Pathology. License. Original text available at:

https://dx.doi.org/10.1293%2Ftox.2018-0042

Figure 1.6

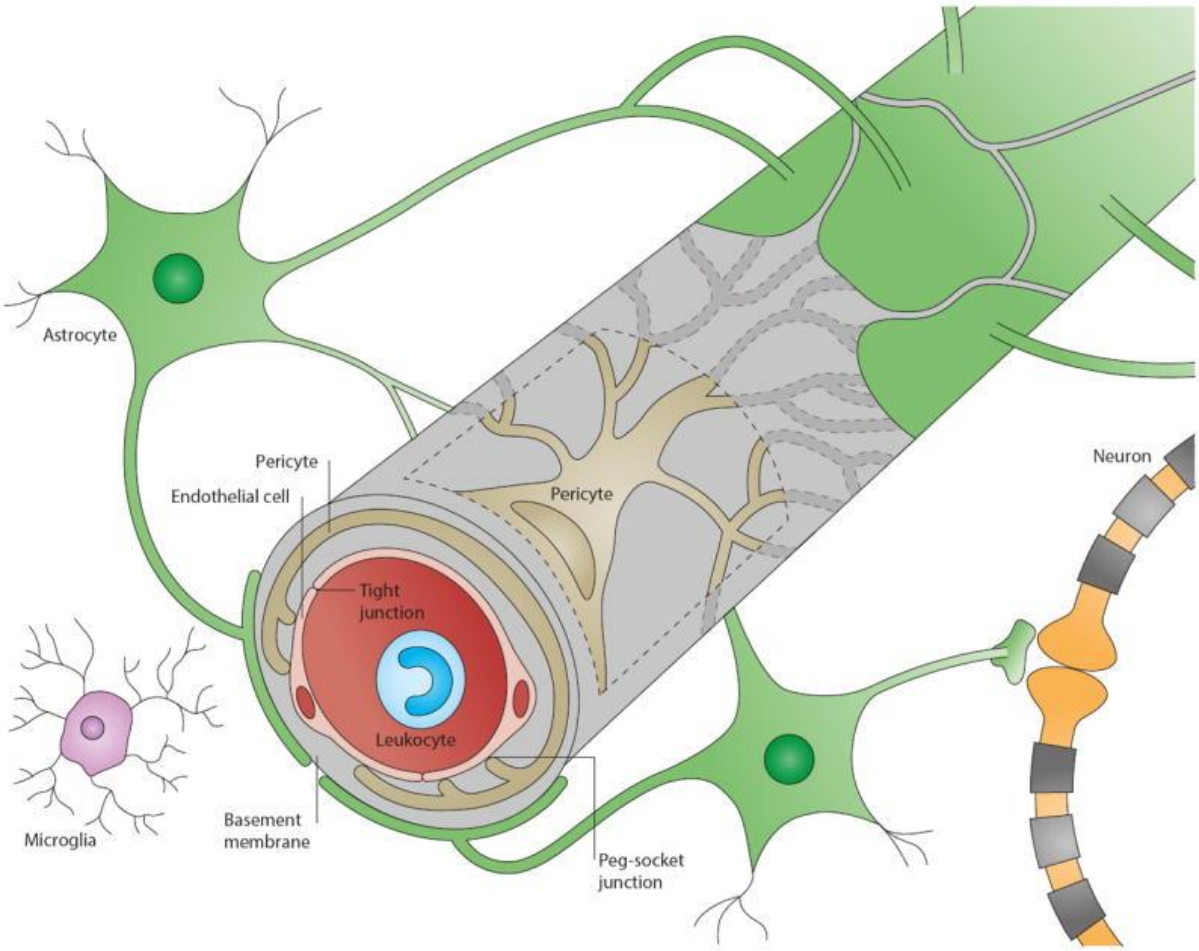

Figure 1.6 Anatomy of the Developed BBB

The blood-brain barrier (BBB) is part of the neurovascular unit (NVU), which represents an elaborate interplay of central and peripheral cells. Vascular endothelial cells sealed by tight junctions constitute the BBB. The endothelium's abluminal surface is coveredGH by a basement membrane in which pericytes and their processes are embedded. Direct intercellular crosstalk between endothelial cells and pericytes are implemented by peg-socket junctions. Astrocytes extend foot processes which encircle the abluminal side of the vessel to an extent of nearly 100%. Although at the capillary level the basement membrane is regarded as a composite basement membrane, it is separated into endothelial and parenchymal basement membranes at the level of the post-capillary venule, delimiting the perivascular space (not shown). Neurons and microglia are considered members of the NVU as they interact with core elements of the BBB and influence barrier functions. Peripheral blood cells including leukocytes also participate in this cellular interplay as they modulate BBB functions under pathological conditions such as inflammation.

Chapter 2: Design and Methodology

2.1. Animal Model

Pregnant Sprague-Dawley rats (10-12 weeks old) were used for the experiment (Taconic Biosciences, Rensselaer, NY). Rats were housed in an Association for Assessment and Accreditation of Laboratory Animal Care–accredited housing facility, maintained at 20–24°C and on a 12 h light–dark schedule. Animals were provided food and water *ad libitum* in their home cages. All animal modeling was conducted by our collaborators under International Care and Use Committee approval at the University of New Mexico, following the *Guidelines for the Care and Use of Laboratory Animals* (National Institutes of Health, Bethesda, MD, USA).

2.2. Ozone Exposure and Tissue Collection

O_3 was generated *via* an OREC silent arc discharge generator (Osmonics, Phoenix, AZ, USA). The O_3 concentration was continuously monitored with a photometric O_3 analyzer (TG-501, GrayWolf Sensing Solutions, Shelton, CT, USA) with temperature maintained at 21 ± 2°C. The rats were randomly assigned to a group and were exposed to either filtered air (FA), 0.3 part per million (ppm), or 1.0 ppm O_3 for 4 h. One cohort of rats was exposed at gestational day (GD) 10 (absent the 0.3 ppm exposure) and another at GD20 (**Figure 2.1**). Importantly, rodents are less sensitive to O_3 toxicity than humans, owing to their complex nasal turbinates, lung morphologic differences and high urate and ascorbate concentrations in the airway surfactant. Traditionally, modeled exposure involves an increase in ozone concentration by a factor of 3, which is the accepted practice for extrapolating concentrations from rodents to primates (Mumaw et al., 2016). Thus, our 1 ppm O_3 concentration in this rodent model is equivalent to a 0.2-0.3 ppm human exposure, which is frequent in areas of high urban air pollution at peak midday expression (Jerrett et al., 2009).

During exposures, the rat dams were singly placed in standard shoebox cage, inserted into a sealed chamber (Biospherix, Parish, NY, USA) without bedding to avoid decomposition of the O_3. Food, but not water, was withheld during the 4 h exposure period to preclude ingestion of ozonation products. The exposure chambers were also analyzed for oxides of nitrogen contaminants, which were invariably below levels of detection (10 ppb). On GD21, dams were anesthetized with isoflurane, the uterus opened and one-by-one for a total of three fetuses, the amniotic fluid was first extracted (~100 uL) and then the fetus and matching placenta was removed, rinsed briefly, dried, and snap frozen in liquid nitrogen. Afterwards, maternal blood was collected by cardiac puncture, placed on ice for 30 min, and centrifuged to separate serum (1000 g, 10 min, 4°C). Tissues and fluids were stored at -80°C, shipped to Virginia Commonwealth University on dry ice, and immediately stored at -80°C on arrival.

2.3. Amniotic and Serum Processing for Proteomic Analysis

For amniotic fluid, 100 µL was pipetted onto a Vivaspin 1,000 kDa filters before dilution with 100 µL of PBS. The samples were centrifuged at 12,000 g for 5 min at 4°C to remove extracellular vesicles and debris. The retentate of the filter was transferred to a new 500 µL tube. This vesicle fraction was stored for further analysis in future projects. The amniotic fluid filtrate was further processed by loaded 120 µL onto a washed Millipore Microcon YM-30 filter unit and centrifuged at 14,000 g for 30 min at 4°C to concentrate the fluid protein, which was collected by adding 35 µL of 200 mM Tris-HCl (pH: 8.0), vortexing for 1 min at 1,500 RPM, and flipping the filter into a collection tube when it was centrifuged at 1,000 g for 5 min. The exact same procedure was performed for maternal serum samples, except that only 20 µL of starting material was used, which was diluted 10-fold due to its significantly higher protein concentration when compared with amniotic fluid.

Biofluid protein fractions were standardized by volume across replicate animals. However, a pooled sample of amniotic fluid and serum was assessed for protein concentration in developing the

appropriate dilution factor ahead of filtration. Thus a 10 µL portion of the amniotic fluid and serum protein fractions was equivalent to ~20 µg of protein. A 0.5 µL sample of serum or 10 µL sample of amniotic fluid was diluted in TCEP reducing agent to a final volume of 10 µL. The reducing agent TCEP (tris(2-carboxyethyl)phosphine) was added to a concentration of 20 mM with the sample incubated at 60°C for 30 min. After cooling, iodoacetamide (IA) was added to a final concentration of 30 mM, with a pH of 8 verified, and incubated in the dark at room temperature for 30 min for thiol alkylation. The reaction was then quenched with 1.7 µL of 200 mM DDT to a final concentration of 20 mM. The solution was incubated for 30 min at RT in the dark. Trypsin was then added at 1:40 (w/w) ratio to the protein amount (0.5 µL = 0.5 µg per 20 µg of protein). Tubes were Parafilm sealed and incubated overnight at 37°C. Digestion was quenched with 21.3 µL of 0.5% FA, with pH verified at 3, resulting in a final peptide concentration of approximately 0.5 µg/µL.

2.4. Proteomic Analysis

Protein digests were analyzed in a group-interspersed order to minimize bias, for GD10 exposed animals to FA and 0.3 ppm O_3 and GD20 exposed animals to FA, 0.3 ppm and 1.0 ppm O_3 (n=6 animals per group). Digests were loaded (100 ng) onto a Symmetry C18 reversed-phase trap column ahead of a 150 mm x 75 µm HSS T3 reversed-phase capillary column for gradient separation (6% to 44% acetonitrile in 0.1% formic acid over 90 min) using a NanoAcquity UPLC online with a Waters Synapt G2-Si tandem mass spectrometer (Waters), as previously reported (Lizhnyak et al., 2019). The instrument was operated in UDMSe mode (Distler et al., 2016) for data-independent analysis at 25000 resolving power and the quadrupole optimized to exclude small-molecule ions below 500 m/z. UDMSe data were peak picked at either 300 and 30 or 350 and 60 ion count thresholds for low-energy and high-energy scans, respectively for amniotic fluid and serum, and then deisotoped and charge-collapsed using PLGS software v3.0.3. Resultant ion tables were aligned across replicates by retention time (±1.5 min), drift

time (±5 bins) and accurate mass (±6 ppm) measures with EndogeSeq. Precursor ion tables were then filtered to retain only highly-reproducible measures (n≥3/grp), with matched product ions (±15 ppm) retained if present in at least two biological replicates. Left censored data were imputed by random-generated value sets centered at the limit of quantification accounting for the datasets median ion variance and missingness across replicates (Cortes et al., 2012). The compiled peptide-level data were median centered and log2 transformed and then processed into a composite protein-level measure using the R-Rollup procedure in DanteR. Those data were then tested for an effect of ozone exposure using ANOVA (robust linear model) and Benjamini-Hochberg multiple-measures correction, set to a 5% false discovery rate, in DanteR. Proteins significantly responsive to ozone exposure were tabulated at the GD10 and GD20 time points, and their identifies evaluated using exploratory bioinformatics analysis. The ToppGene Suite (https://toppgene.cchmc.org) was utilized for broad-based enrichment analysis against gene ontology, multiple pathway, and other biological function and interaction databases, with all results restricted to a 5% false discovery rate. Protein-protein network interactions were additionally explored using STRING (https://string-db.org).

Tissue Processing: Upon extraction of the placenta from the dam, the tissues are first washed in phosphate buffer. The overlying decidual basalis and underlying umbilical insertion/yolk sac can be removed using fine forceps in order to more aptly inspect placental structure and consistently measure organ weight, but such tissues were left intact for our analysis of ECM effects. The junctional zone is distinguished by its pale appearance (due to lack of fetal blood) from the labyrinth zone, the highly vascularized zone of interest in vascular toxicological study such as this (Soares et al., 2006). Upon removal, tissues are immediately snap-frozen in liquid nitrogen and stored at -80°C until ready for sectioning. Snap-frozen placenta tissue was sectioned at 10 µm thickness using a freezing-stage microtome (Microm HM 450; Thermo Scientific, Waltham, MA, USA). In order to investigate the full spectrum of placental anatomy, all tissues were left intact after extraction. In dissection for sectioning,

the point of umbilical attachment is used as a reference point, and the organ is grossly cut along the transverse axis to present a cross section of all tissues. Once sectioned, tissues specimens are thaw mounted on frosted charged glass microscope slides from Globe Scientific optimal for cell adhesion to the glass medium. Six tissues were mounted per slide for antibody optimization, while 3 tissues per slide were used for final antibody analysis. After adhering a given tissue to a slide, condensation was dried in open air at room temperature prior to mounting each subsequent section to prevent freeze-thaw damage. Once mounted and dried, tissues were stored at -80°C until immunohistochemistry preparation.

Snap frozen fetal brains were detached from the body while frozen. The brain, if not already removed from the skull, was cut into left and right hemispheres along a mid-sagittal plane. From the exposed mid-sagittal medial hemisphere, the brain was cut laterally at 5 microns thickness using the same microtome used for placenta. In sectioning brain for histology, the generation of highly homologous images is of paramount importance. Obtaining such homology in rat brain can only come from adequate application of neuroanatomic landmarks such as the hippocampus to distinguish brain regions. BBB permeability in the adult rat has been shown to demonstrate heterogeneity (Villasenor et al., 2017). Because of this, comparison of ozone exposed animals to filtered air controls must maintain regiospecificity across samples. Areas of higher BBB permeability like the cortex, striatum and hippocampus will be assessed and compared to one another, as will areas of lower permeability such as interbrain and midbrain regions. The sagittal cut allows for a broad cross section of the brain, ideally giving a picture across the entire brain with minimal artifacts. Maintaining a constant blade angle perpendicular to the long axis is critical for consistent slicing.

2.5. Immunohistochemistry

Fresh-frozen slides were removed from -80°C storage and air dried for 15 min. Paired sections were encircled using a histo PAP pen. Slides were fixed in 3% paraformaldehyde for 15 min and then washed in PBS three times for five min. Slides were then incubated for 1 h in blocking solution (PBS containing 2.5% bovine serum albumin, 5% goat or donkey serum, 0.1% Triton X-100). Carefully selected mixtures of primary antibodies (**Table 2.1**) were then added for overnight incubation. Antibodies for PECAM , osteopontin, integrin alpha5-beta-3, galectin-1 and 4-HNE were mixed in solution with donkey serum based blocking buffer. Antibodies for MMP2, e-cadherin, galectin-1 and 4-HNE were mixed in solution in goat serum based blocking buffer. Similarly, a table of optimized antibodies and their concentrations proposed for BBB assessment is seen in **Table 2.**2. Primary antibody incubation was followed by incubation in fluorophore-conjugated secondary antibody mixtures corresponding to the host animal for corresponding primary antibodies. All secondary antibodies were obtained from Invitrogen and applied at concentrations from 1:250-1:1000. After washing in PBS two times for 5 min, DAPI (1:10000 in H_2O) was applied for 3 min before coverslip (0.17 mm) placement using ProLong Diamond Antifade dry-mounting medium (Invitrogen). Images of placenta collected at 40x magnification on a Zeiss AxioImager.M2 multi-channel fluorescence microscope oil objective equipped with a motorized X,Y,Z stage, a high-sensitivity 506m CCD camera and an Apotome.2 for focused structured illumination imaging.

Images were acquired using the aforementioned microscope and camera. Tile images were collected across the cortex, hippocampus, striatum, midbrain and hindbrain using DAPI staining and anatomical landmarks as references. Fiji software is used to generate semi-quantitative immunofluorescence. Markers for endothelial integrity, microglial reactivity and albumin leakage into the parenchyma are used to assess overall barrier integrity. The “Analyze Particles” feature of the FIJI software is used to first standardize fluorescence to mitigate background noise and quantify signals on a

given sample for comparative analysis. Local congregations of blood vessels are indicative of regions of high anatomical interest and are compared across samples. Similarly, placental staining utilized uterine attachment sites as reference points in an attempt to standardize anatomy for comparison between groups. The pale junctional zone is the primary site for investigating ECM abnormalities, whereas the labyrinth zone is the primary location of interest in assessing vascular abnormalities and barrier integrity. The metrial gland is of specific interest in investigating effects on spiral artery remodeling and will also be an area of focus. Using FIJI, these areas of interest can be standardized across samples for comparative analysis. Effects were measured comparing differing exposure timepoints (GD10 vs. GD20) and ozone doses (FA vs. 0.3 PPM vs 1.0 PPM). The collected values are mean center corrected. The effects of ozone exposure will be are assessed using a two tailed t-test.

Table 2.1 Antibodies Optimized for Placental Staining

Antigen	Company	Catalog Number	Host Species	Dilution	Channel	Assessment
Section A						
Osteopontin	R&D Systems	AF808	Goat	15µg/mL	488	ECM Cell adhesion
PECAM1	DSHB	P2B1-2	Mouse IgG1	15µg/mL	594	Vascular marker
A5B3-integrin	BioSS	Bs-1310B	Rabbit	1:100	680	ECM binding receptor
Section B						
MMP2	R&D Systems	AF1488	Goat	In Progress	488	ECM Proteolysis
E-Cadherin	DSHB	CPTC-CDH1-1	Mouse IgG2b	15µg/mL	594	Cadherins junctions
PECAM1	AB Clonal	A11525	Rabbit	1:50	680	Endothelial
Section C						
TIMP1	R&D Systems	AF580	Goat	In Progress	488	MMP Regulation
Galectin-1	Santa Cruz BioTechnology	Sc-166618	Mouse IgG2a	In Progress	594	Placenta ECM
4-HNE	BioSS	bs-6313R-A750	Rabbit	1:50	750	Oxidative stress

Table 2.1 Optimized Antibodies for Staining in Placenta

Optimized antibodies for staining in placenta are shown. Dilutions marked “In Progress” were being tested at the time of COVID-19 pandemic shutdown of the laboratory.

Table 2.2

Antigen	Company	Catalog #	Host Species	Dilution	Channel	Assessment
Section A						
Albumin	BioSS	Bs-2256R	Rabbit	1:300	488	BBB Permeability
GFAP	AbCam	AB4674	Chicken	1:3000	568	Astrocyte Activation
Pecam1	DSHB	P2B1-2	Mouse	1:7	680	BBB Endothelial
Section B						
Albumin	BioSS	Bs-2256R	Rabbit	1:300	488	BBB Permeability
IBA1	SySy	234004	Guinee Pig	1:2000	568	Microglial Reactivity
Pecam1	DSHB	P2B1-2	Mouse	1:7	680	BBB Endothelial
Section C						
Claudin 5	Thermo	35-2500	Ms IgG1	1:200	488	BBB Tight Junction
E-cadherin	DSHB	CPTC-CDH1-1-5	Ms IgG2b	1:25	568	BBB Adherens Junction
4-HNE	BioSS	bs-6313R-A750	Rabbit	1:200	750	Oxidative Stress

Table 2.2 Optimized Antibodies for Staining in Fetal Brain

Optimized staining protocols for BBB assessment in fetal brain are given with functionality for each assessment.

Figure 2.1

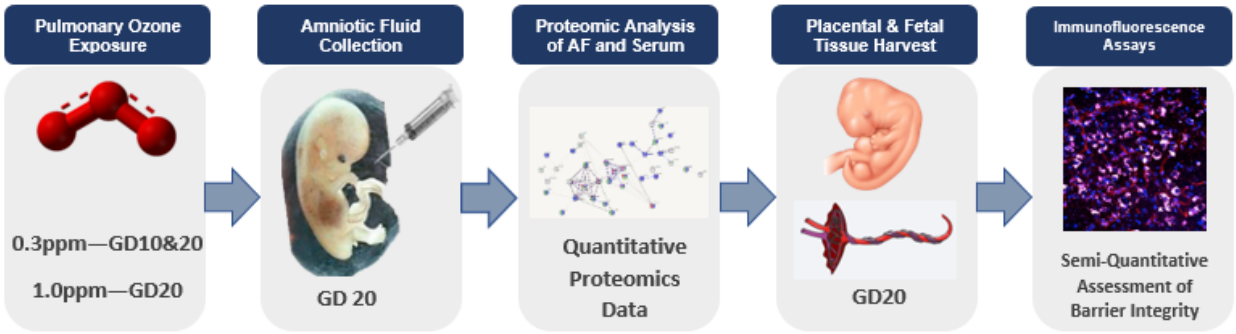

Figure 2.1 Visual Abstract of Experimental Model

Here we see a visual abstract of our experimental model. Ozone exposure at two different gestational timepoints is followed by amniocentesis, collection of maternal serum, fetal and placental tissues. Quantitative proteomic analysis of maternal serum and AF was used to develop a regimen of placental staining antibodies used for immunohistochemical assessment of placental integrity.

Chapter 3 – Results

3.1. Ozone responsive Amniotic Fluid Proteomes

Our amniotic fluid proteomic data were first assessed for normality to afford the use of parametric statistical testing with ANOVA with DanteR software (Pacific Northwest National Laboratories). Samples' data were plotted as histograms, **Figure 3.1A** for GD10 exposure samples and **Figure 3.2A** for GD20 exposure data, which were visually assessed for their normality of distribution within each given sample. To assist this assessment, a fit of the data was superimposed to provide an easy visualization of the classic "bell" shape. Samples sufficiently exhibited normality of distribution suitable for our ANOVA as per guidelines provided with DanteR. Additionally, the Benjamini-Hochberg procedure was applied to ANOVA results to control for false discovery rate to 5%.

To visualize the results here, we present the overarching peptide and protein level responses to ozone via volcano plots of post-hoc assessments between low (0.3 ppm ozone) and control (0 ppm ozone) exposure groups common to the GD10 and GD20 time points (**Figure 3.3**). Peptide (**Figure 3.3A,C**) and protein (**Figure 3.3B,D**) fold change data are plotted against p-values to visualize both the magnitude and statistical significance of each measured response. It should be noted that the actual analytical measures in these experiments are performed at the peptide level, generated through tryptic digestion during sample processing. In this "bottom-up" approach, protein measures are calculated using what is terms a rollup procedure, where the intensities of the top three peptide measures per protein are averaged together. This approach is well accepted by the proteomic community; however, it introduces potential for bias whereby a peptide measure may be influenced independently by post-translational events. After acknowledging this common limitation of proteomic output, we moved forward assessing the data at the higher protein level, as it afforded the most direct initial assessment of ozone exposure's effect on the amniotic fluid proteome. Once corrected for multiple measures using the

Benjamini-Hochberg procedure (5% FDR), 66 amniotic fluid proteins were significantly altered in abundance 10-days following a 4-h exposure to 0.3 ppm ozone at GD10, with just four protein exhibiting negative fold change. Given the prominent skew towards increased protein responses, we reviewed the full data distributions to ensure that there were no significant sample outliers causing this effect. Rather, we observed a consistent increase in the amniotic fluid protein distribution for 0.3 ppm ozone exposed animals that was consistent across all replicates (**Figure 3.1B**). This is important since samples were standardized by volume, not protein concentration, implying an ozone-induced shift in the fluid protein concentration as will be discussed in Chapter 4. Interestingly, as **Figure 3.3C** (peptide) and **3.3D** (protein) demonstrate, the GD20 low exposure group show the opposite effect. That is, a marked negative fold change in the majority of significant peptides and proteins. After correcting to a 5% false discovery rate, 105 unique proteins showed significant fold change shifts in the GD20 low exposure group, with 101 of these holding negative fold change values. Assessing the proteome distribution for each sample, we found a consistent decrease in concentration present within the animals acutely exposed for 4-h to 0.3 ppm ozone at GD20 (**Figure 3.2B**). In addition to the opposed effects of amniotic fluid proteome concentration observed between the GD10 and GD20 0.3 ppm exposure cohorts, we also observed distinctly different proteins as responsive to ozone. **Figure 3.4** displays a Venn diagram illustrating unique and shared proteins between the GD10 and GD20 cohorts, with only 12 proteins (7.5% of unique proteins) overlapping. Discussion of these differences is provided in Chapter 4.

A second objective of these studies was to examine how the dose of ozone exposure could influence the amniotic fluid proteome, which we assessed using the GD20 exposure, since we posited that we would see a more pronounced (and measurable) effect given the acute collection timing. Proteomic responses are shown as volcano plots in **Figure 3.5A** at peptide and **Figure 3.5B** at protein levels. The GD20 high exposure group showed a relatively equal distribution between positive and negative fold changes in peptide data, consistent with a similar proteome distribution between 1.0 ppm

and 0 ppm GD20 ozone exposure samples (**Figure 3.2B**). In all, 59 proteins showed significant fold changes in the GD20 high ozone exposure group relative to control, 28 of which showed negative fold changes. **Figure 3.6** displays a Venn diagram illustrating unique and shared proteins between the two ozone doses, with only 15 (10.1%) common proteins between exposure doses. **Figure 3.7** displays the responsive proteome overlap between low exposures at GD10 and GD20 time points as well as the high GD20 exposure data, relative to their respective 0 ppm ozone exposure control groups. Notably, there is only 1 protein in common across all three cohorts, indicating a very dynamic response by exposure time and dose within the amniotic fluid proteome. **Table 3.1** provides summary statistics for ozone-responsive proteins selected based on their known functional relevance to oxidative stress, vascular responses, and placental or neurobiological development. Further discussion of these observations can be found in Chapter 4.

3.2. Functional Review: GD10 Low Ozone Exposure Responsive Proteome

As an initial assessment of the potential functional relevance of amniotic fluid proteomic response to 0.3 ppm ozone exposure at GD10 (measured at GD20), we employed functional enrichment analysis on the statistically responsive proteins summarized earlier in **Figure 3.3B**. In this analysis, the list of responsive proteins is assessed against a wide range of ontologies using the ToppGene online tool (toppgene.cchmc.org), which includes standard Gene Ontology entries for biological processes, cellular components and molecular functions, but also data informative databases on molecular pathways, disease phenotypes, protein-protein interactions, among others. Importantly, results were effectively controlled via Benjamini-Hochberg correction for the multitude of analyses, to minimize false discovery to 5%. Relevant enriched association for the GD10 low exposure group are highlighted in **Table 3.2**. To further assess functional relevance of the low exposure proteomic results, protein-protein network analysis was performed using the STRING online suite (string-db.org), selecting for only “high

confidence" interaction scores of 0.7 or greater. The overall protein-protein interaction enrichment p value was <1.0E-16, suggesting a high-degree of specificity among the responsive proteins. A graphical view of the protein-protein interaction network is shown in **Figure 3.8**, with 22 interactive notes and 39 edges. Additionally, nodes are color-coded based on functional associations for each protein in the network with: response to oxygen containing compounds, response to oxidative stress, blood vessel development, central nervous system development, and extracellular region compartment. In order to expound on the involvement of matrix metalloproteinases, the shown network was seeded with MMP2 and MMP9 nodes, which were identified in the other exposure groups, and were identified as interactors with the present low-dose GD10 proteomic factors via enrichment analysis.

3.3. Functional Review: GD20 Low Ozone Exposure Responsive Proteome

As described above, we also assessed the broader functional relevance of the GD20 low-dose ozone exposure proteomic response using enrichment and protein-protein network analyses. The resulting functional categories significantly associated with this proteome are shown in **Table 3.3**, while the protein-protein interactive network is visually displayed in **Figure 3.9**. Parameters for each were kept identical to the analyses performed in section 3.2, except that MMP2 was already present within this dataset and MMP9 was not seeded. Instead, Lgals1 was added as a node given its significant enriched association with the present proteomic responsive (**Table 3.3**). The network was appreciably larger than that for the GD10 exposure proteome, having 35 nodes and 49 edges. As above, nodes are color-coded based on their associations with enriched functional categories: responsive to oxygen containing compounds; protein binding; inflammatory response; and extracellular region.

3.4. Functional Review: GD20 High Ozone Exposure Responsive Proteome

The broader functional relevance of the GD20 high-dose ozone exposure proteome was likewise explored using enrichment and protein-protein network analyses. Significant functionally enriched associations with this dataset are reported in **Table 3.4**. The protein-protein interaction network of this proteome is depicted in **Figure 3.10**, which included 20 nodes and only 21 edges, showing comparatively little interaction relative to the GD20 low-exposure proteome. Moreover, to attain this network, it was necessary to lower the interaction score threshold to 0.4 (considered moderately confident). Color coding of the nodes was associated with enriched categories for: cellular response to oxygen containing compound, neurogenesis, cytoplasm and extracellular region.

3.5. Comparative Ozone-responsive GD20 Maternal Serum Proteome

To begin assessing the potential source for the observed amniotic fluid responses, we evaluated the serum proteome from the dams exposed to 0.3 ppm and 1 ppm at the GD20 timepoint, with collection occurring at the same time for both fluids. Maternal serum was processed in the same manner as amniotic fluid for proteomic analysis (adjusted to a smaller volume of fluid, diluted to account for the higher protein concentration in serum than amniotic fluid). Overall, 135 serum proteins were reproducibly measured across all exposure groups, representing the most rigorous measures available to us. Following ANOVA analysis, 60 proteins were found statistically responsive to ozone exposure. Posthoc analysis found that 35 of the proteins were responsive at the low exposure group, 33 of which exhibited negative fold changes. The high exposure responsive included 33 proteins, of which 29 had negative fold changes. These patterns are reflected in the volcano plots seen in **Figure 3.11**. ToppGene enrichment analysis was completed for all significant proteins from both serum exposure groups, with the results shown in **Table 3.5**. Protein-protein network analysis was conducted across the full complement of 60 responsive proteins from both exposures as a generalized

serum responsive to be compared with the amniotic fluid results. Using an interaction score of 0.7 (high confidence), a total of 28 interactive nodes were used with 74 edges as shown in **Figure 3.12**. Additionally, STRING was used to analyze, under the same interaction score, for significant hits in high and low exposure serum groups as seen in **Figures 3.13 and 3.14**, respectively. As with previous STRING analyses, all serum proteins feature color coded functional associations defined at the base of each figure. The high exposure serum profile showed 30 nodes with 33 edges, whereas the low exposure group showed Between exposure doses, 16 (31.4%) overlap in responsive proteins was observed (**Figure 3.15B**), demonstrating a more consistent effect of ozone dose in the serum than in the amniotic fluid. Overlap between the amniotic fluid and maternal serum responses to ozone (irrespective of dose) was low, with only 14 (7.1%) common proteins (**Figure 3.15A**). Breaking overlap between the fluids down by exposure dose, there were only 8 (6.1%) common proteins at the 0.3 ppm exposure and just 2 (2.2%) at the 1 ppm exposure (**Figures 3.15D and 3.15C)**. As the measured serum proteins represent generally the more abundant proteins in blood, we can glean that the limited overlap between serum and amniotic fluid proteomic responses to ozone implies that crosstalk between the two of more abundant serum proteins from the dam was not the cause of the amniotic response. However, it is not possible to rule out more selective exchange (not due to overall high abundance in serum) between the two, perhaps by facilitated means. To gain a greater understanding of the overlap between maternal serum and amniotic fluid responses to ozone exposure, we focused on those proteins commonly responding between the fluids at the 0.3 ppm exposure dose as quantitatively depicted in **Figure 3.16** with further discussion provided in Chapter 4.

3.6. Optimization of Multi-channel Immunofluorescence for Targeted Assessments

The proteomic results described above point to interesting protein-specific findings that require further targeted assessment and validation. Our pre-COVID plan was to employ targeted

immunochemical assays, to include a battery of tissue-level immunofluorescence microscopy studies as described in Chapter 2. While the pandemic-related shutdown prevented completion of these studies, with animal tissues ready to ship on March 23rd, considerable effort had been made in optimizing multi-channel staining for placental and brain tissues.

An initial effort was to verify optimal fixation conditions for fresh-frozen placental tissue, which we expected would differ considerably from our brain tissue protocols. Evaluating the literature, we determined that PFA, as we have used in brain tissue, was commonly used in placenta (Fox et al., 1991). We thus focused on optimizing the percentage of PFA from 3% to 4%. Results showed that immunofluorescent signal-to-noise (S/N) was maximal at 9% PFA (**Figure 3.19**) when staining for e-cadherin.

We next set out to verify each primary antibody relative to negative control staining and optimize antibody concentration. Across sequential sections of the same tissue, we performed a serial dilution of each antibody along with a negative primary control. All other staining and microscopy parameters were kept constant. Replicate images were collected from within the same placental lamina to compare across dilutions where tissue structure was visible. Structures with clear positive and negative staining common to the laminar morphology across all dilutions were identified as regions of interest and assessed densitometrically to compute the mean immunofluorescent intensity for signal and background, respectively. These two numbers were then divided to produce a signal to noise ratio. This ratio was then used to determine which dilution produces the optimal amount of signal while minimizing background noise from nonspecific antibody binding. An example of this is provided in the MMP2 rabbit antibody dilution optimization images in **Figure 3.17** with S/N ratios per dilution noted. Similar region of interest fluorescence analysis would have been used across defined anatomical regions in the placenta for each antibody in these studies, such as the junctional zone for vascular permeability markers.

Next, we assessed combined multi-channel staining of these tissues. Our study design paired specific antibodies within the same tissue to allow for a co-localized analysis of protein targets with related functionality; thus, it was imperative to have effective combined staining (**Table 2.1**). Primary antibodies were specially selected to have distinct host species or immunogen isotypes that would allow independent probing upon mixing. Combined antibodies were evaluated for effective positive signal when combined that was consistent morphologically with that observed with prior optimization studies. An example of combined OPN, PECAM, and A5B3-integrin targets is shown in **Figure 3.20**. Multi-channel immunofluorescence of protein targets within the brain had been previously optimized in our laboratory for assessing the blood-brain barrier (albumin staining and tight-junction proteins) and glial reactivity (astrocytes and microglia) as shown in **Figure 3.18** and summarized in **Table 2.2**. Immunofluorescence densitometric and morphological analyses would have commonly been used for semi-quantitative and qualitative assessments at the GD20 collection time for an effect of maternal ozone exposure at different ages of exposure and doses

Table 3.1

Protein	GD10 0.3PPM	q value GD10 0.3PPM	GD20 0.3PPM	q Value GD20 0.3PPM	GD20 1.0PPM	q Value GD20 1.0PPM
	Fold Change ±SEM		Fold Change ±SEM		Fold Change ±SEM	
Osteopontin	+0.65 ±0.1999	0.0331	-1.70 ±0.1849	0.0448	No change	
Galectin-1	+3.78 ±0.4450	0.0025	No change		No change	
MMP-2	No Change		-0.88 ±0.3036	0.0269	-1.14 ±0.4863	0.0054
TIMP-1	+0.83 ±0.1894	0.0309	No change		No change	
TIMP-2	+0.93 ±0.1179	0.0024	No change		No change	
E-cadherin	+0.69 ±0.1722	0.0082	No change		No change	
Pkm1	+0.61 ±0.1831	0.0314	-1.59 ±0.3101	0.0049	No change	
Pkm2	No change		-4.09 ±0.4546	0.0004	-3.19 ±0.5433	0.0022
Superoxide Dismutase 1	No change		-0.63 ±0.2808	0.0492	No change	
Catalase	No change		-3.07 ±0.6915	0.0141	No change	
Collagen, Type I, Alpha 2	+0.60 ±0.2313	0.0148	-1.07 ±0.2851	0.0307	No change	
Vascular Cell Adhesion Molecule	No change		-2.09 ±0.1579	0.0128	No change	
Tissue Factor Pathway Inhibitor	-1.39 ±0.5199	0.0314	-2.22 ±0.5297	0.0025	No change	
Connective Tissue Growth Factor	+0.65 ±0.2296	0.0314	No change		-1.08 ±0.3671	0.0261
Sex Hormone Binding Globulin	No Change		+2.67 ±0.2516	1.28 E-05	+1.66 ±0.3388	0.0176
Rack1	No Change		+4.30 ±0.2715	7.68 E-08	No change	
Ubiquitin C	No Change		No Change		+2.18 ±0.6824	0.0096

Table 3.1 Selected Proteomic Fold Changes between Exposure Groups in Amniotic Fluid

Amniotic fluid proteome log(2) transformed fold change values for selected proteins of interest in amniotic fluid. All proteins in the planned staining protocol are seen. All fold changes achieved statistical significance of $p<0.05$.

Table 3.2

Enrichment Type	Name	p Value	Hit Count in Query List	Hit count in Genome	Proteins Enriched
Computational	Placenta Genes	1.291E-7	14	463	COL2A1, COL3A1, TGFBR3, RNASE1, TIMP2, SPP1, ENPP2, MMP2, APOE, PTGDS, CDH1, PNP, COL1A1, COL1A2
Mouse Phenotype	Abnormal Blood Vessel Morphology	4.540E-6	19	1382	COL3A1, HSPD1, TGFBR3,CD1D, SPP1, ENPP2, PON1, CCN2, MMP2, BCAM, APOE, MMP9, CDH1, PTGIS, SERPIND1, PROS1, COL1A1, NRP1, HSP90AB1
Pathway	Ensemble of Genes Encoding ECM and ECM-associated Proteins	4.189E-7	17	1026	COL2A1, COL3A1, IGFBP6, TIMP1, TIMP2, SPP1, HPX, CCN2, SERPINA10, MMP2, MMP9, SERPINA6, CTSB, SERPIND1, LGALS1, COL1A1, COL1A2
Pubmed	A Genetic Association Study of Maternal and Fetal Candidate Genes that Predispose to Preterm Prelabor Rupture of Membranes (PROM)	1.140E-14	11	186	COL3A1, TIMP1, TIMP2, PAFAH1B1, PON1, MMP2, APOE, MMP9, PROS1, COL1A1, COL1A2

Table 3.2 ToppGene Enrichment Results from GD10 Amniotic Fluid Proteome

ToppGene enrichment analysis for GD10 protein shifts in AF is seen. “Hit count in query list” refers to the number of significant protein shifts falling into the protein enrichment category. “Hit count in Genome” refers to the total number of proteins in the enrichment pathway. All protein systems enriched were p≤ .05.

Table 3.3

Enrichment Type	Name	p Value	Hit Count in Query List	Hit Count in Genome	Proteins Enriched
GO: Biological Process	Response to Oxidative Stress	3.25E-05	11	50	PSAP,PARK7,CAT,LDHA,PRDX6,RACK1,HP,PRDX1, MMP2,HSPA1A,SOD1
GO: Cellular Component	Extracellular Matrix	4.79E-13	21	598	A1BG,GPC1,PSAP,AZGP1,NCAM1,RPSA,DCN, SERPINH1,ITIH3,LGALS3BP,TGFB2,S100A11,MFGE8,HPX,PKM,C THRC1,SERPING1,HRG,MMP2,PLG,COL1A2
ToppCell Atlas	BrainMaps Endothelial	6.21E-07	8	155	SPP1,DCN,IGFBP2,SERPING1,SFTPA1,C6,MMP2, COL1A2
GO: Biological Process	Developmental Growth	1.55E-04	13	822	EZR,PSAP,SPP1,AZGP1,RBP4,SHBG,NCAM1,CHST11,PPIB,TGFB 2,PKM,PLG,SOD1
GO: Molecular Function	Cadherin Binding	1.31E-08	13	338	EZR,RAN,PARK7,LDHA,PRDX6,S100A11,RACK1, PRDX1,PKM,ALDOA,HSPA1A,HSPA5,HSPA8
Interaction	LGALS1 Interactions	3.06E-05	6	114	SERPINH1,LGALS3BP,ALDOA,HSPA5,VCAM1,SOD1
Disease	Cerebrovascular Disorders	6.83E-06	8	176	TCN2,SPP1,PON1,TUBB2B,TGFB2,HP,PLG,VCAM1

Table 3.3 ToppGene Enrichment Results for the GD20 Low Exposure Amniotic Fluid Proteome

ToppGene enrichment analysis for GD20 low exposure group protein shifts in AF is seen. “Hit count in query list” refers to the number of significant protein shifts falling into the gene enrichment category. “Hit count in Genome” refers to the total number of genes in the enrichment pathway. All gene systems enriched were $p \leq .05$.

Table 3.4

Enrichment Type	Name	p Value	Hit Count in Query List	Hit Count in Genome	Proteins Enriched
GO: Biological Process	Cellular Response to Oxygen Containing Compound	3.62E-05	13	1301	VIM,FBLN5,AOC1,IGFBP5,CFL1,PKLR,PKM,MMP2, NME1,HSPA5,CA2,PCSK9,MSN
GO: Cellular Component	Extracellular Matrix	3.58E-06	10	598	GPC1,S100A6,TGFBR3,FBLN5,PKM,SERPINB1,C1Q C,MMP,SERPINH1,PCOLCE
ToppCell Atlas	BrainMaps Endothelial	1.13E-05	5	188	VIM,TGFBR3,CAPG,SERPINH1,MSN,PCOLCE
GO: Biological Process	Response to Cytokine	1.48E-04	12	1287	VIM,UBC,IL1R2,CFL1,CAPG,ATIC,MMP2,FKBP1A, HSPA5,CA1,MSN,PCOLCE
GO: Molecular Function	Cadherin Binding	3.95E-04	6	338	NEO1,CAPG,PKM,ATIC,CDH6,HSPA5
GO: Cellular Component	Myelin Sheath	5.04 E-09	9	214	UBC,PDCD6IP,PKM,NME1,GDI2,HSPA5,CA2,EEF1 A1,MSN
GO: Cellular Component	Focal Adhesion	1.30 E-06	9	411	VIM,PDCD6IP,MRC2,CFL1,GDI2,HSPA5,MARCKS, CAP1,MSN

Table 3.4 ToppGene Enrichment Results for the GD20 High Exposure AF Proteome

ToppGene enrichment analysis for GD20 High exposure group protein shifts in AF is seen. “Hit count in query list” refers to the number of significant protein shifts falling into the enrichment category. “Hit count in Genome” refers to the total number of genes in the enrichment pathway. All protein systems enriched were p≤ .05.

Table 3.5

Enrichment Type	Name	pValue	Hit Count in Query List	Hit count in Genome	Proteins Enriched
GO: Molecular Function	Serin-type endopeptidase activity	2.127E-12	12	265	Ambp, Hp, Serping1, C1s, Plg, Serpina6, F2, Klkb1, Serpind1, F10, F12, Tfpi
GO: Molecular Function	Antioxidant Activity	4.690E-6	5	97	Apom, Hp, Gpx3, Apoa4, Alb
GO: Cellular Component	Blood microparticle	6.595E-17	23	147	Ambp, Fn1, Clu, Hp, Afm, Hpx, Ahsg, Serping1, C1qb, Psmc5, Cp, C1s, C3, Apoa1, Apoa4, Iglc2, C4bpa, Alb, Plg, C9, F2, Tf, Kng1
Pathway	Complement and coagulation cascades	9.733E-27	17	79	Clu, Serping1, C1qb, C1s, C3, Cpb2, C4bpa, C6, Plg, C9, F2, Kikb1, Serpind1, F10, F12, Kng1, Tfpi

Table 3.5 ToppGene Enrichment Results for the GD20 High and Low Exposure Serum Proteome ToppGene enrichment analysis for GD20 high and exposure groups protein shifts in maternal serum. “Hit count in query list” refers to the number of significant protein shifts falling into the enrichment category. “Hit count in Genome” refers to the total number of proteins in the enrichment pathway. All protein systems enriched were $p \leq 0.05$

Figure 3.1

A.

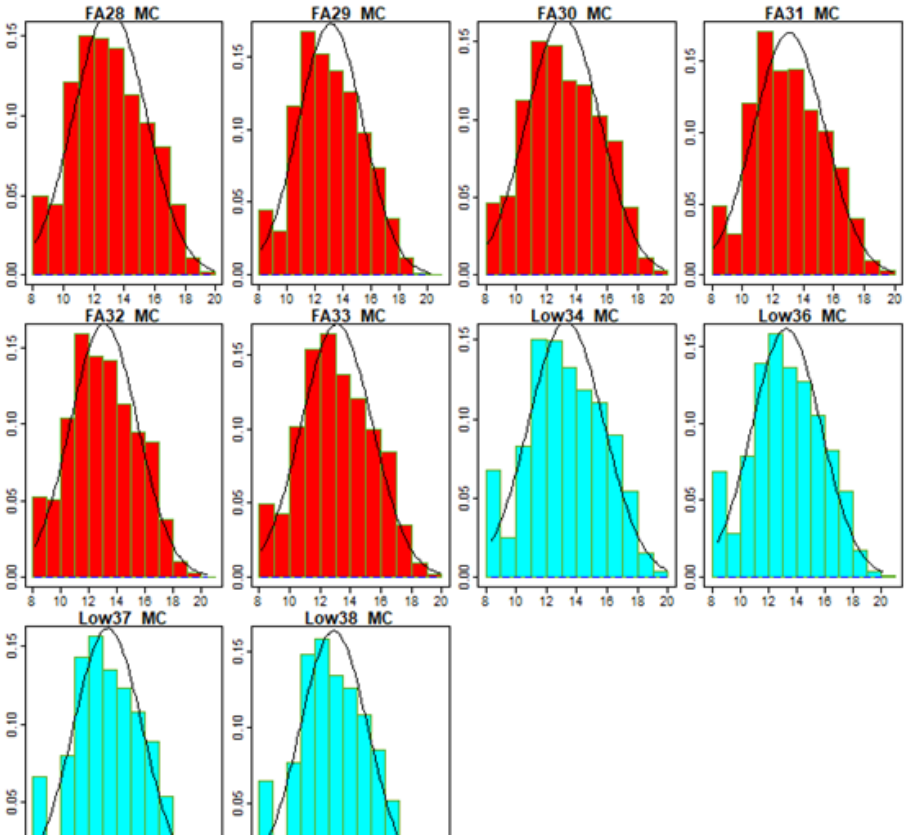

B.

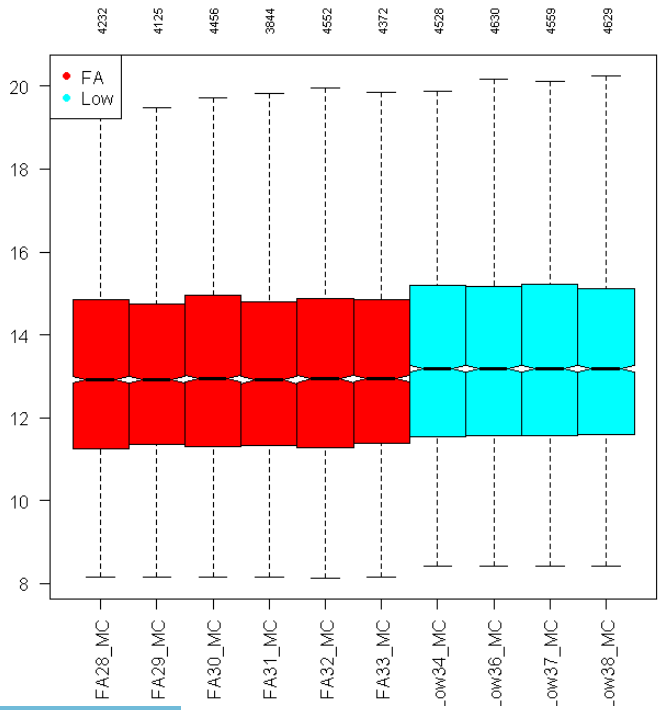

Figure 3.1 Assessing Normality of Distribution in GD10 Amniotic Fluid Animals

(A) Histograms for GD10 ozone exposed animals. Each histogram is an expression of normality of distribution for amniotic fluid proteomic data in a single dam. Red plots are filtered air exposed dams. Blue plots are from dams exposed to 0.3ppm ozone at GD10. **(B)** Box plot demonstrating consistent upregulation of proteome across GD10 0.3ppm exposed groups.

Figure 3.2:

A.

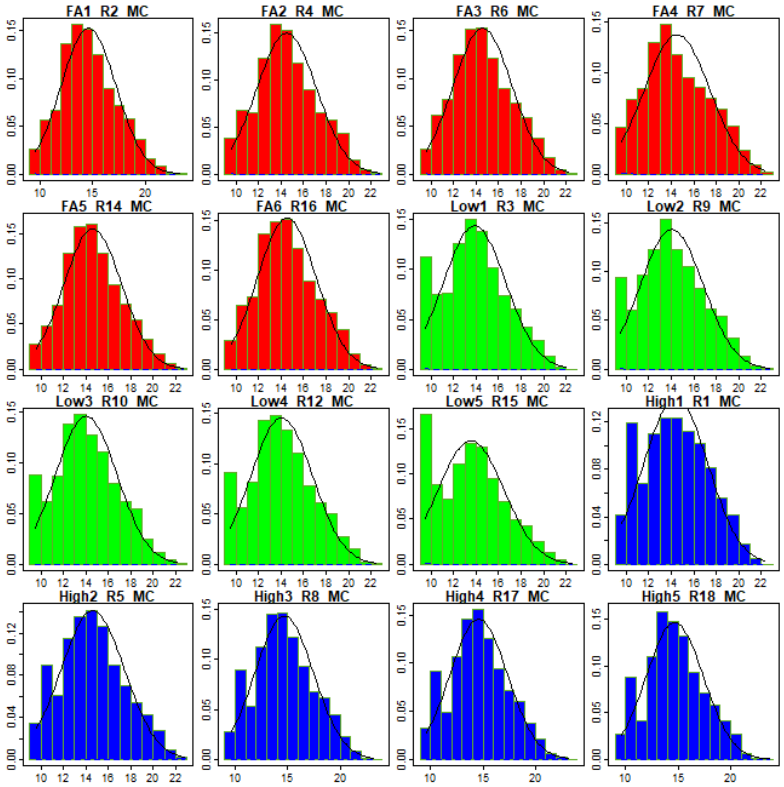

B.

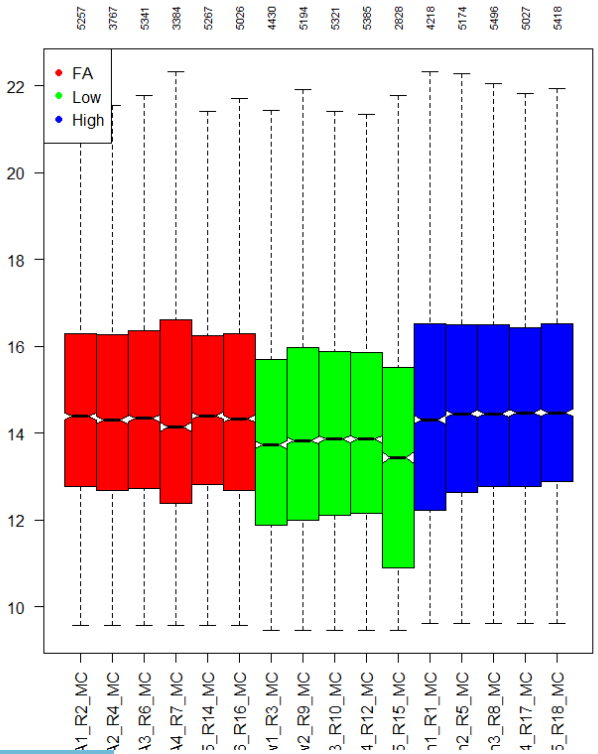

Figure 3.2 Assessing Normality of Distribution in GD20 Amniotic Fluid Groups

(A) Histograms for GD20 ozone exposed animals. Each histogram is an expression of normality of distribution for amniotic fluid proteomic data in a single dam. Red plots are filtered air exposed dams. Green plots are from dams exposed to 0.3ppm ozone at GD20. Blue plots are from dams exposed to 1.0ppm ozone at GD20. **(B)** Box plot demonstrating the overall downward trend in protein expression profiles between both GD20 groups and filtered air controls.

Figure 3.3

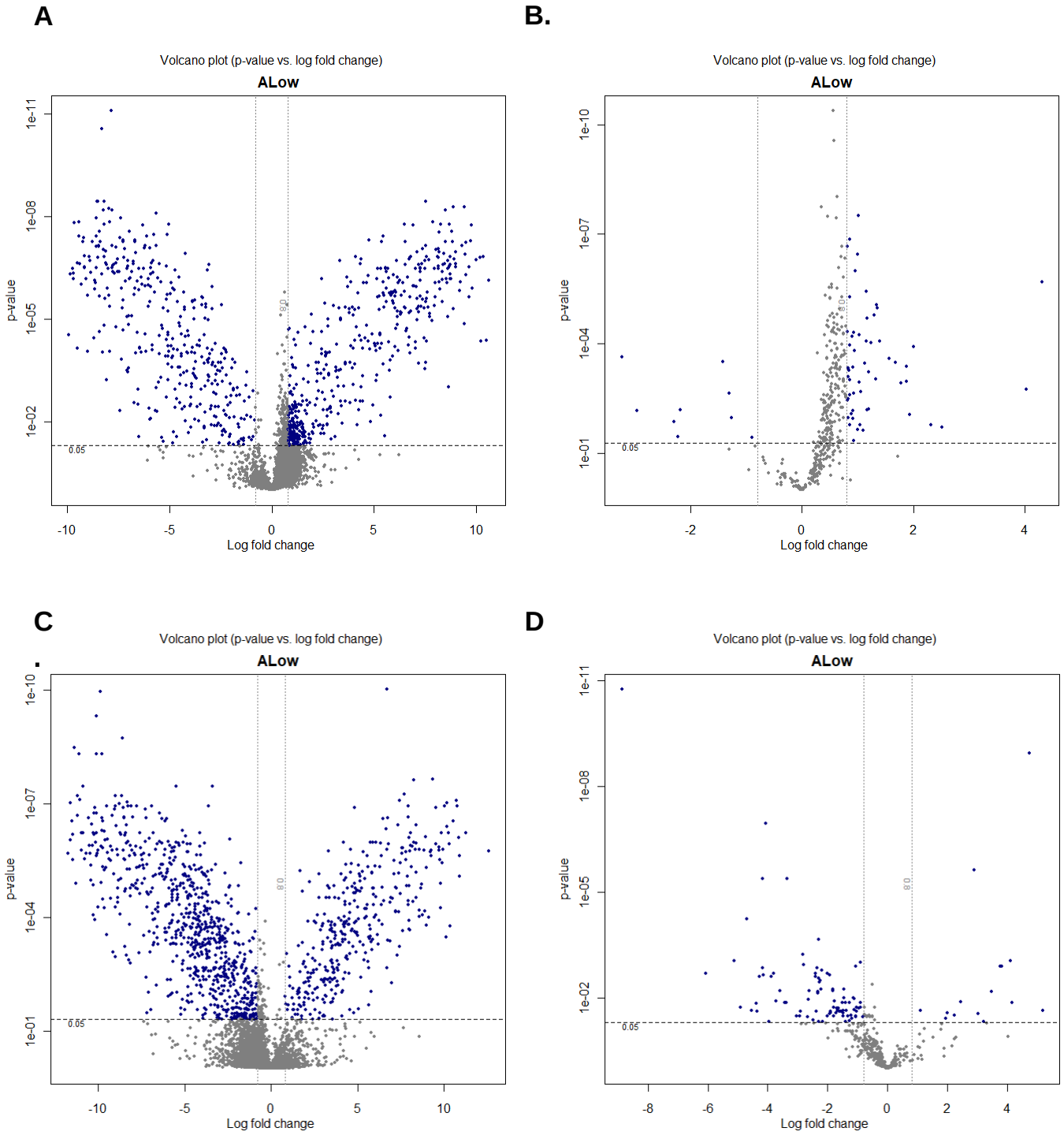

Figure 3.3 General Trends in Protein Fold Changes Between Exposure Timepoints in Amniotic Fluid

Volcano plots showing fold change differences in the overall proteome for the two timepoints exposed to low ozone concentrations (0.3ppm). Fold changes were assessed in reference to filtered air controls. **Each plot corresponds to the following group: A)** Peptide level expression fold changes in GD10 0.3ppm ozone exposed animals, **B)** Protein level expression fold changes in GD10 0.3ppm ozone exposed animals, **C)** Peptide level expression fold changes in GD20 0.3ppm ozone exposed animals, **D)** Protein level expression fold changes in GD20 0.3ppm ozone exposed animals. Statistical significance was demarcated by proteins whose fold change achieved $p \leq 0.05$.

Figure 3.4

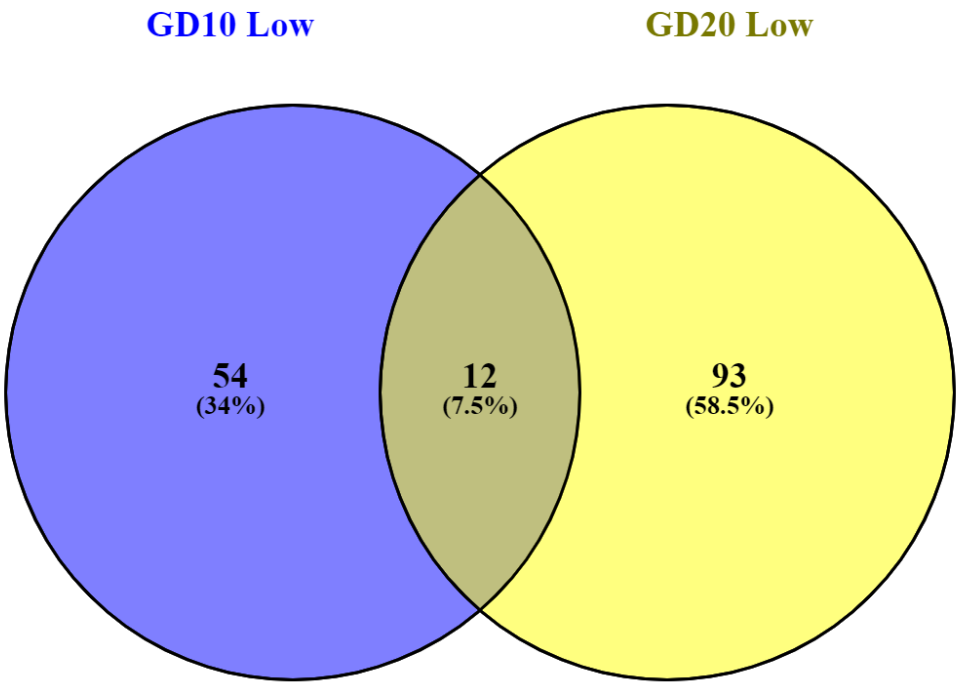

Figure 3.4 Comparing Overlap Between GD10 and GD20 Low Exposure Groups in Amniotic Fluid

Venn diagram illustrating shared and unique proteins between GD10 low exposure and GD20 low exposure groups in AF. Protein input was from significant protein shifts after statistical vetting. Courtesy: *Oliveros, J.C. (2007-2015) Venny 2.1. An interactive tool for comparing lists with Venn's diagrams.* https://bioinfogp.cnb.csic.es/tools/venny/index.html

Figure 3.5

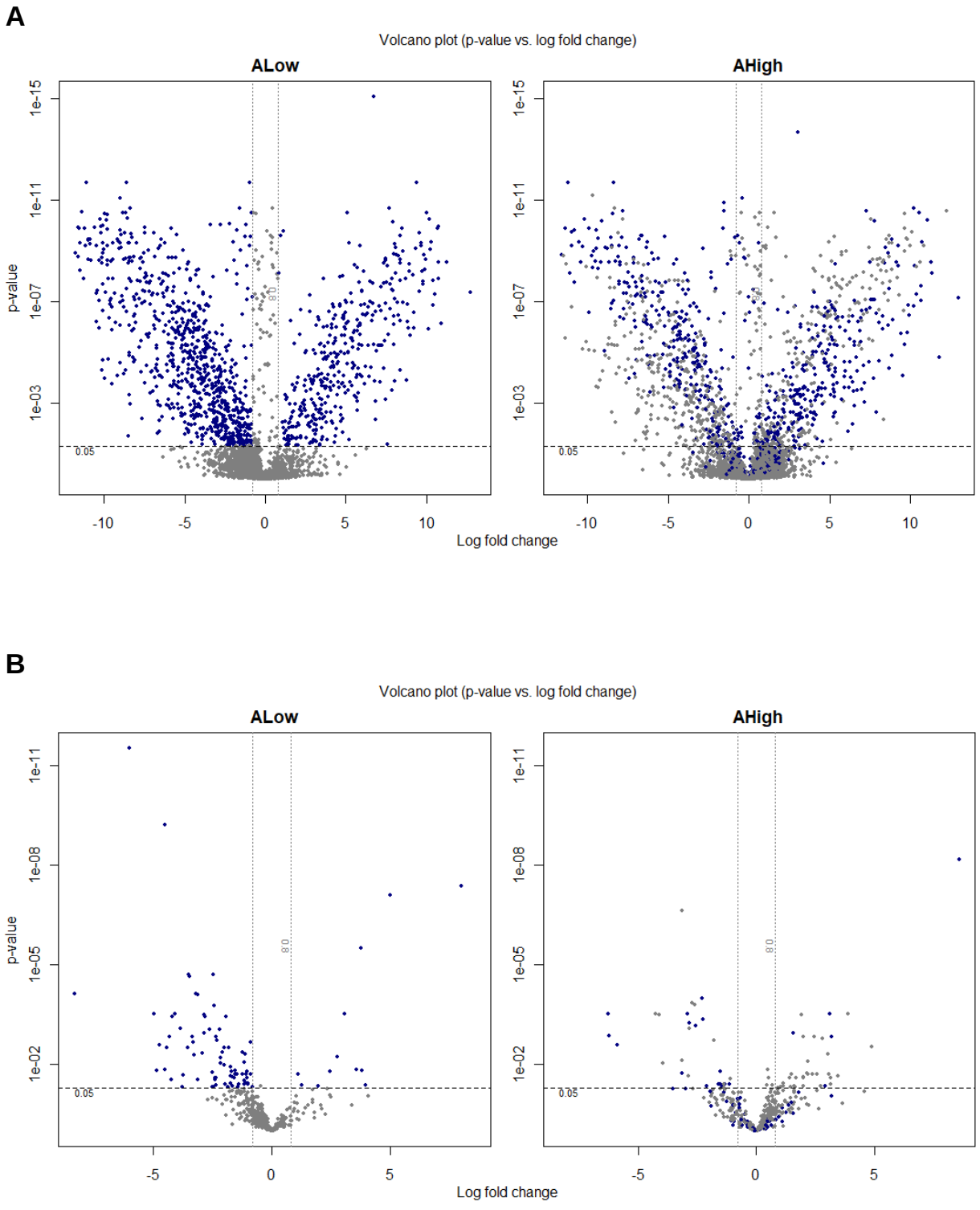

Figure 3.5 General Trends in Protein Fold Changes Between GD20 Dose Groups in Amniotic Fluid

Volcano plots showing fold change proteome differences for the two ozone exposure groups at GD20 in AF. **A)** Peptide level fold changes in GD20 exposed dams with "ALow" representing the 0.3ppm ozone exposed group and "AHigh" representing the 1.0ppm ozone exposed group. **B)** Peptide level fold changes in GD20 exposed dams with "ALow" representing the 0.3ppm ozone exposed group and "AHigh" representing the 1.0ppm ozone exposed group. Statistical significance was demarcated by proteins whose fold change achieved $p \leq 0.05$.

Figure 3.6

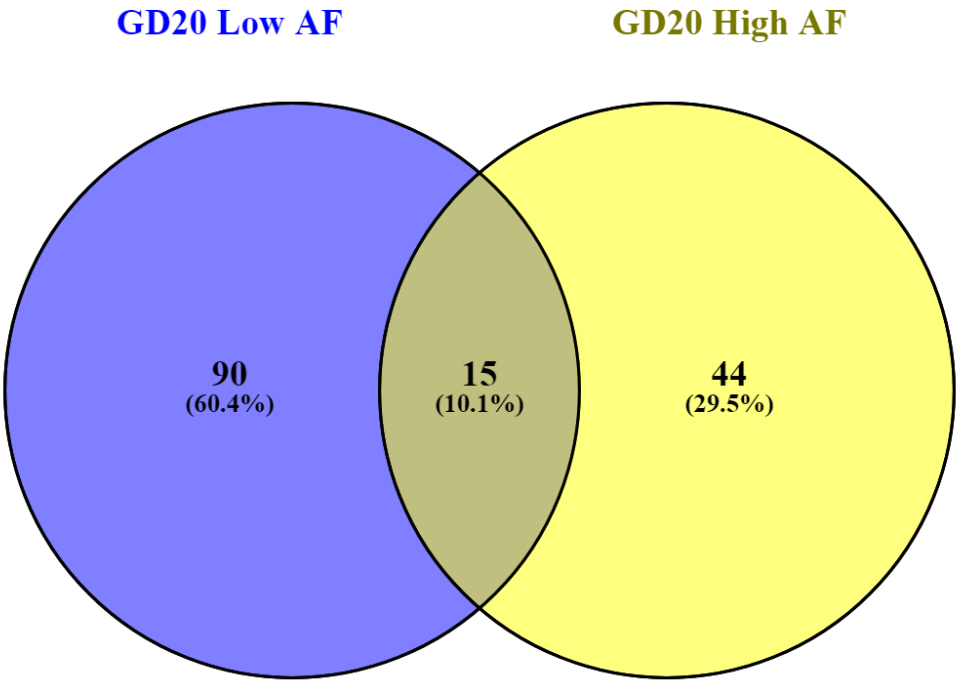

Figure 3.6 Comparing Overlap Between GD20 High and Low Exposure Groups in Amniotic Fluid

Venn diagram illustrating shared and unique proteins between ozone dosages at GD20. Protein input was from significant protein shifts after statistical vetting. Courtesy: *Oliveros, J.C. (2007-2015) Venny 2.1. An interactive tool for comparing lists with Venn's diagrams.* https://bioinfogp.cnb.csic.es/tools/venny/index.html

Figure 3.7:

Figure 3.7 Comparing Overlap Between GD10 and GD20 Exposure Groups in Amniotic Fluid

Venn diagram illustrating shared and unique proteins between the 3 exposure groups in amniotic fluid. Protein input was from significant protein shifts after statistical vetting. Courtesy: *Oliveros, J.C. (2007-2015) Venny 2.1. An interactive tool for comparing lists with Venn's diagrams.* https://bioinfogp.cnb.csic.es/tools/venny/index.html

Figure 3.8

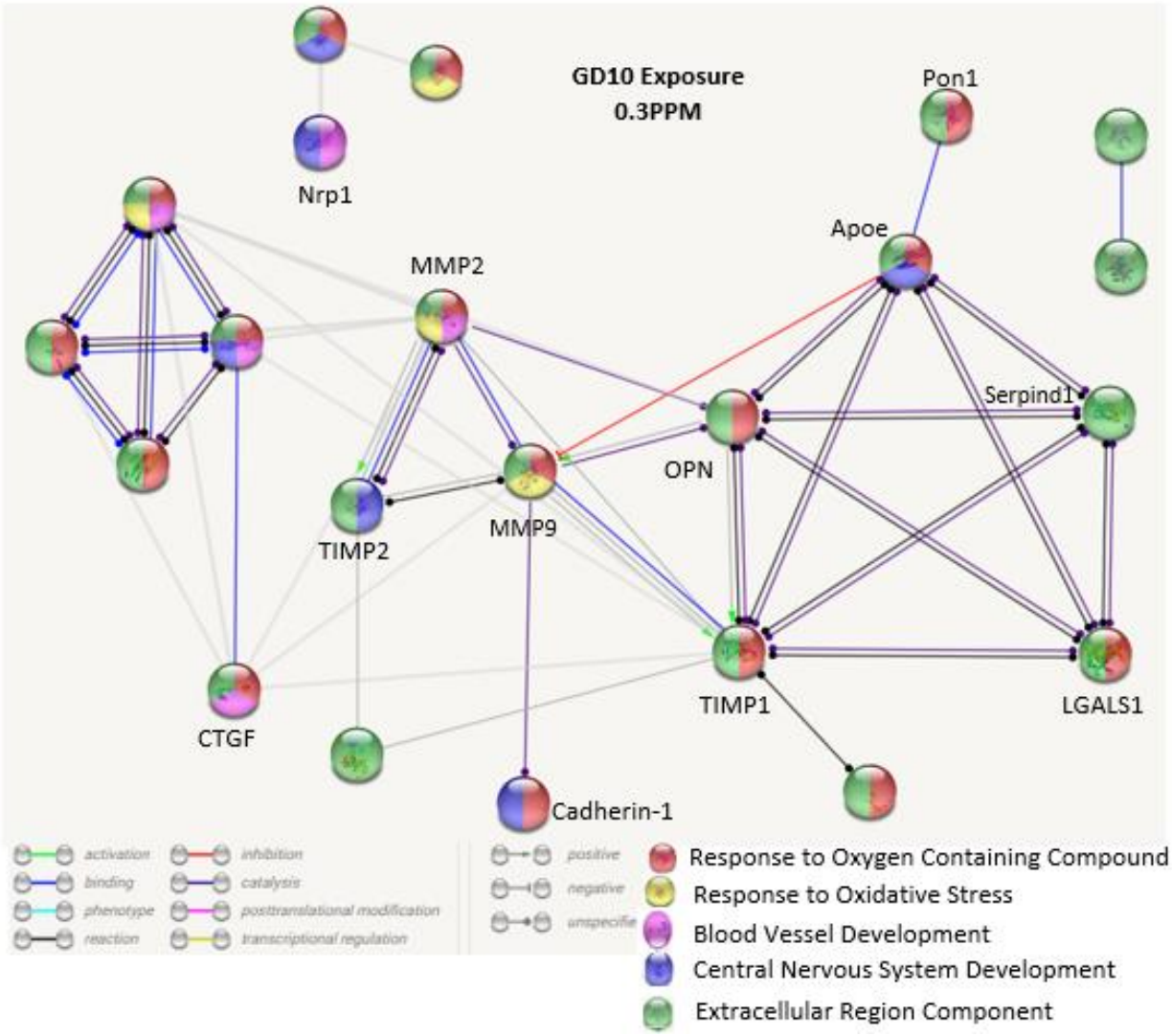

Figure 3.8 Protein-Protein Network Analysis in GD10 Low Exposure Amniotic Fluid

STRING database (version 11.0) analysis of enriched protein sets highlighted in **Table 3.1**. Protein network analysis minimum required interaction score was set to "High confidence (0.700)". Protein-protein interaction enrichment p-value was less than 1.0e-16. Overall, 33 proteins were assessed in enrichment analysis. Please note, MMP2 and MMP9 were added to this list and showed no significant fold change in the GD10 group.

Figure 3.9

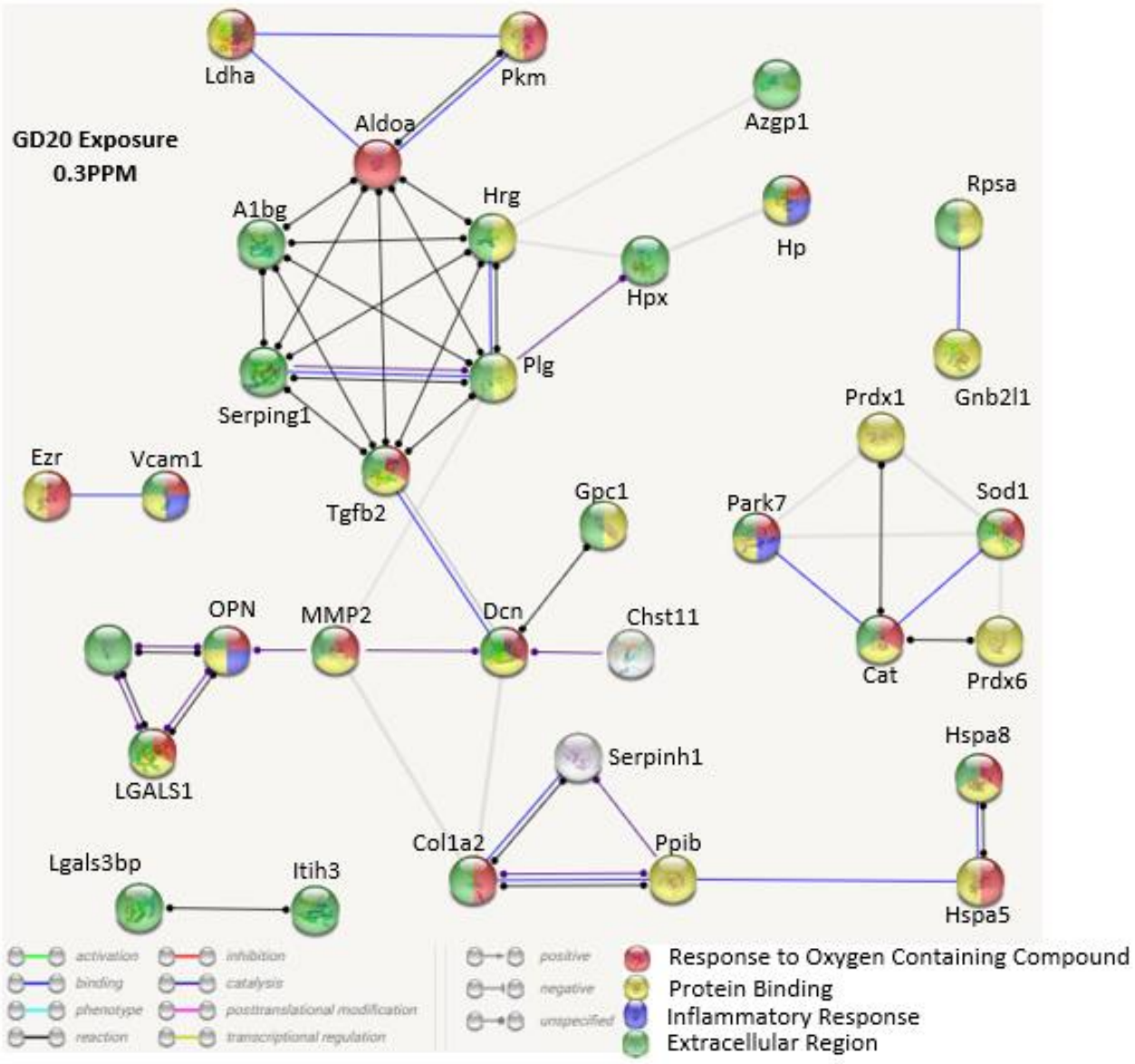

Figure 3.9 Protein-Protein Network Analysis in GD20 Low Exposure Amniotic Fluid

STRING database (version 11.0) analysis of enriched protein sets highlighted in **Table 3.2**. Protein network analysis minimum required interaction score was set to "High confidence (0.700)". Protein-protein interaction enrichment p-value was less than 1.0e-16. Overall, 48 proteins were assessed in enrichment analysis. Note, LGALS1 was added to this list and showed no significant fold change in the GD20 group.

Figure 3.10

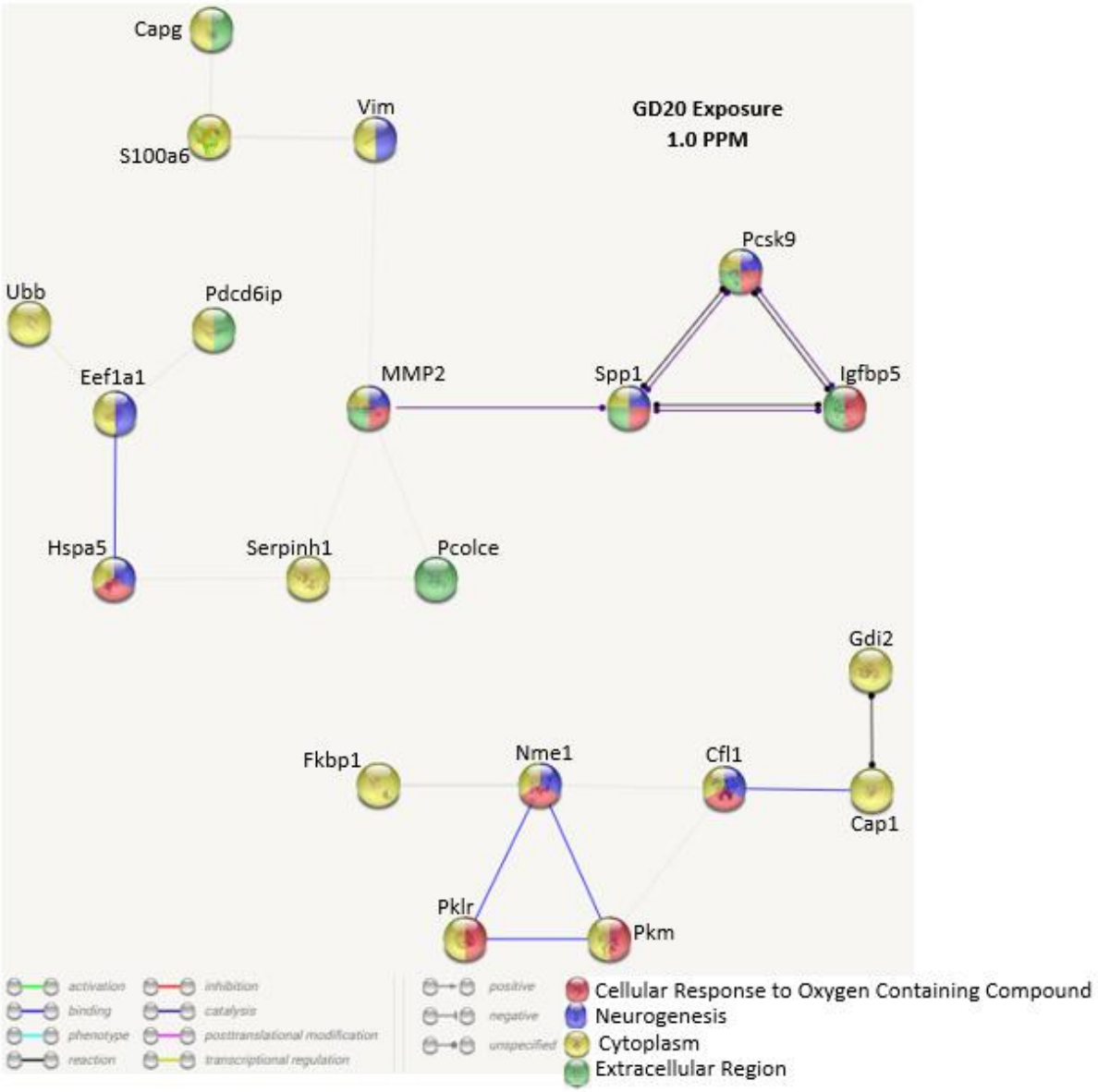

Figure 3.10 Protein-Protein Network Analysis in GD20 High Exposure Amniotic Fluid

STRING database (version 11.0) analysis of enriched protein sets highlighted in **Table 3.3**. Protein network analysis minimum required interaction score was set to "High confidence (0.700)". Protein-protein interaction enrichment p-value was less than 1.0e-16. Overall, 35 proteins were assessed in enrichment analysis. Note, OPN (spp1) was added to this list and showed no significant fold change in the GD20 high exposure group.

Figure 3.11

A.

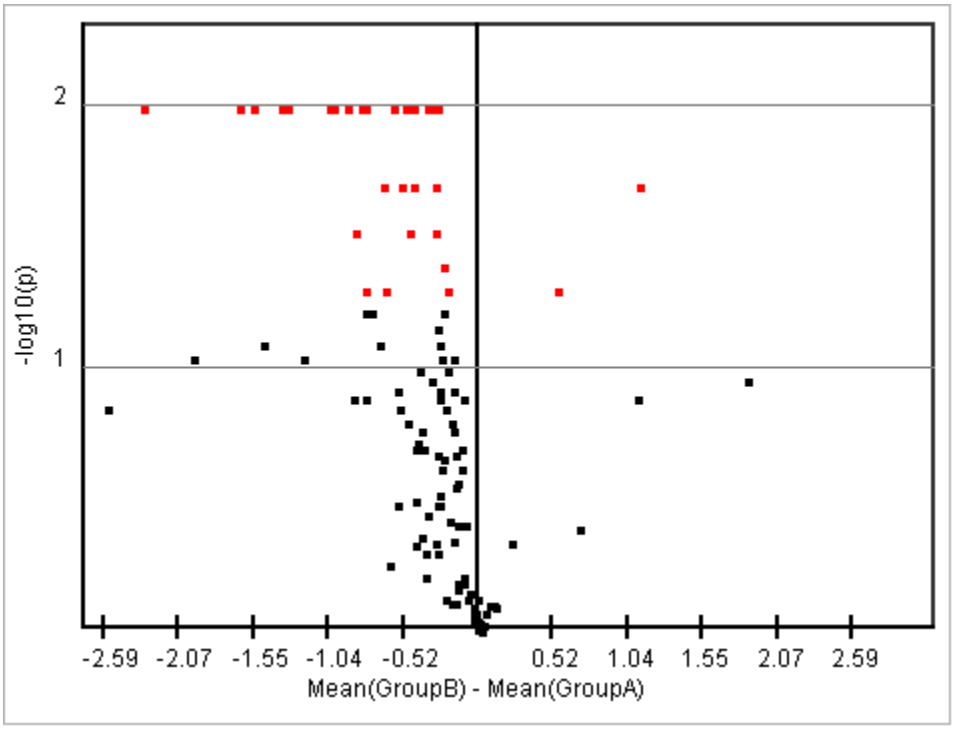

B.

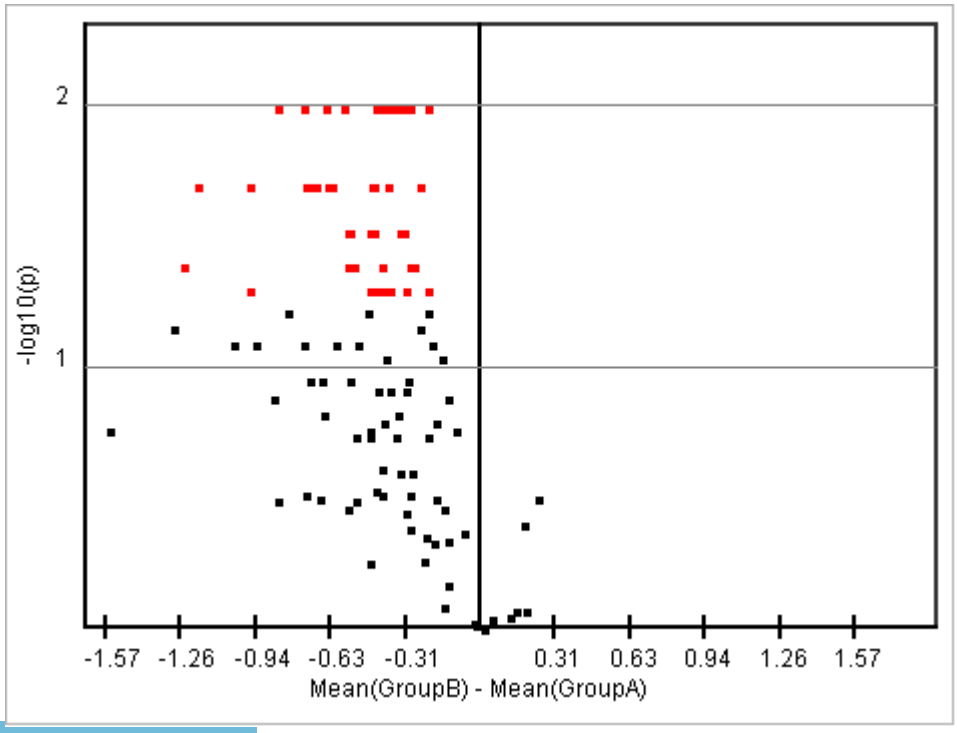

Figure 3.11 General Trends in Protein Fold Changes Between GD20 Dose Groups Serum

Volcano plots plotting trends in protein fold shifts for GD20 low ozone exposure group (**A**) and high exposure group (**B**). Both plots are protein data, with the overwhelming trend being negative fold change in protein expression.

Figure 3.12

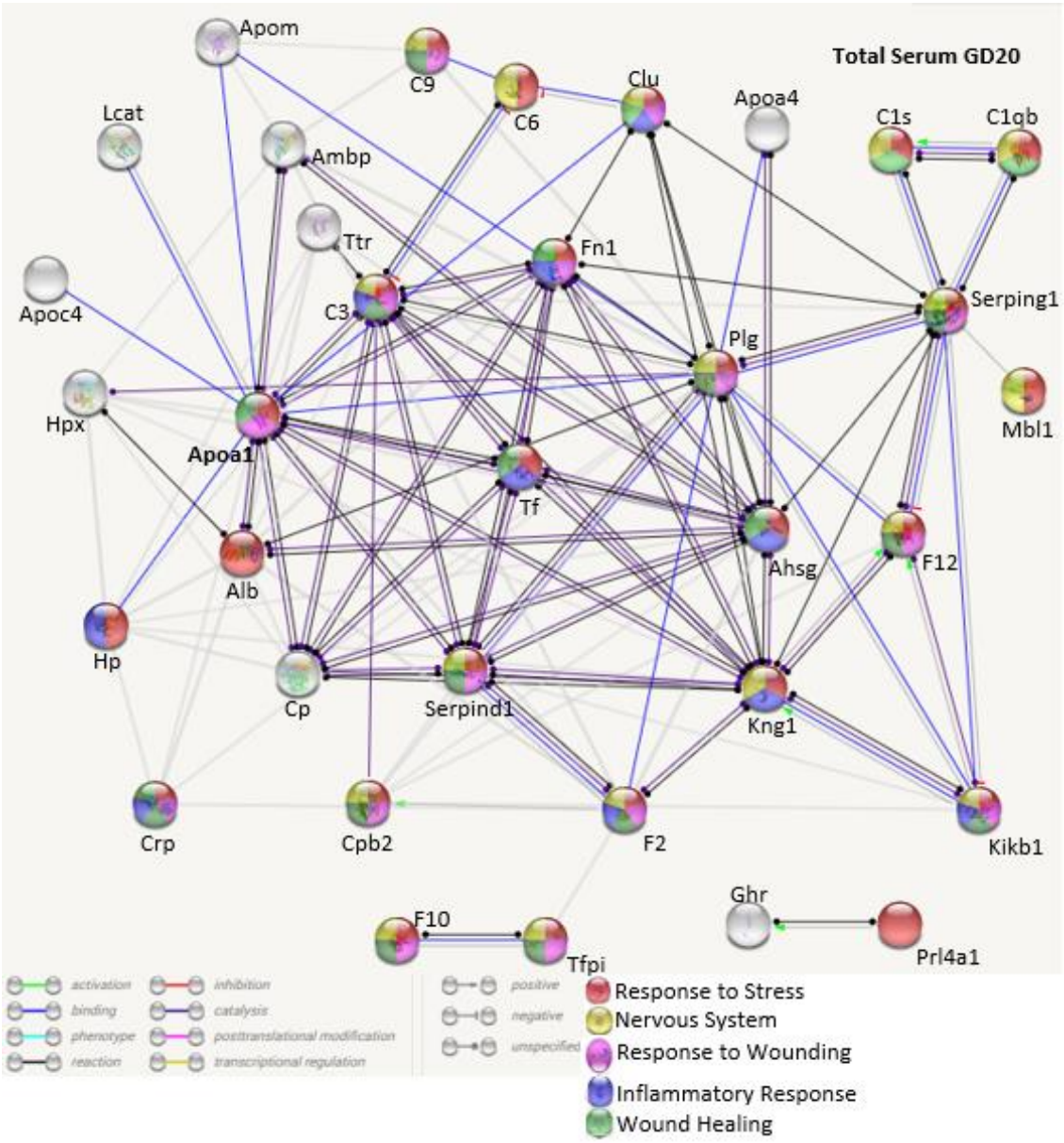

Figure 3.12 Protein-Protein Network Analysis in GD20 Exposure Groups in Maternal Serum

STRING database (Version 11.0) analysis of GD20 high and low serum results for protein-protein interactions is shown. The minimum required interaction score was set to "High confidence (0.700)". Proteins were obtained after ToppGene enrichment analysis of significant results.

Figure 3.13

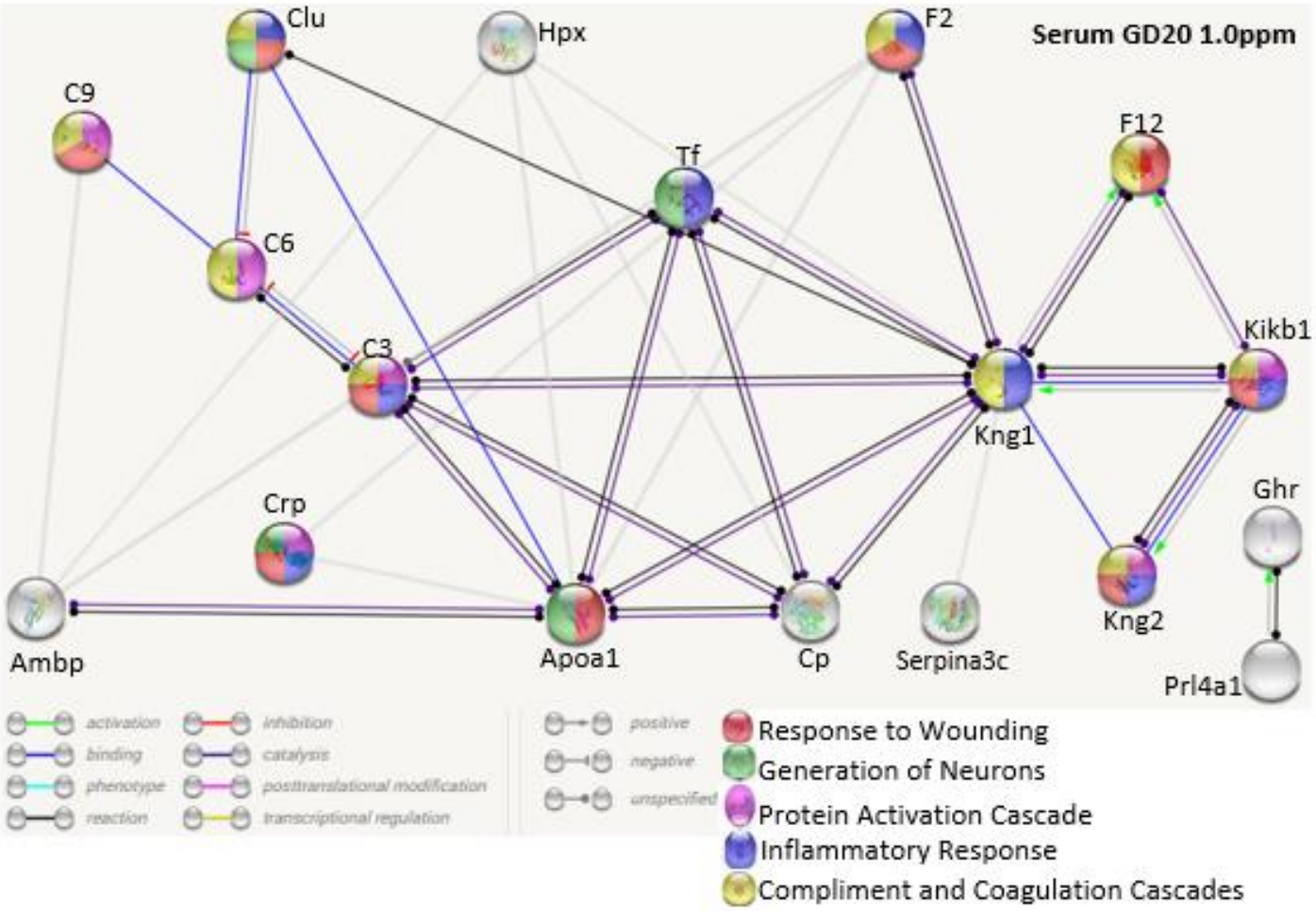

Figure 3.13 Protein-Protein Network Analysis in GD20 High Exposure Maternal Serum

STRING database (Version 11.0) analysis of GD20 1.0ppm ozone maternal serum results for protein-protein interactions is shown. The minimum required interaction score was set to "High confidence (0.700)". Proteins were obtained after statistical vetting for significant factors in the group.

Figure 3.14

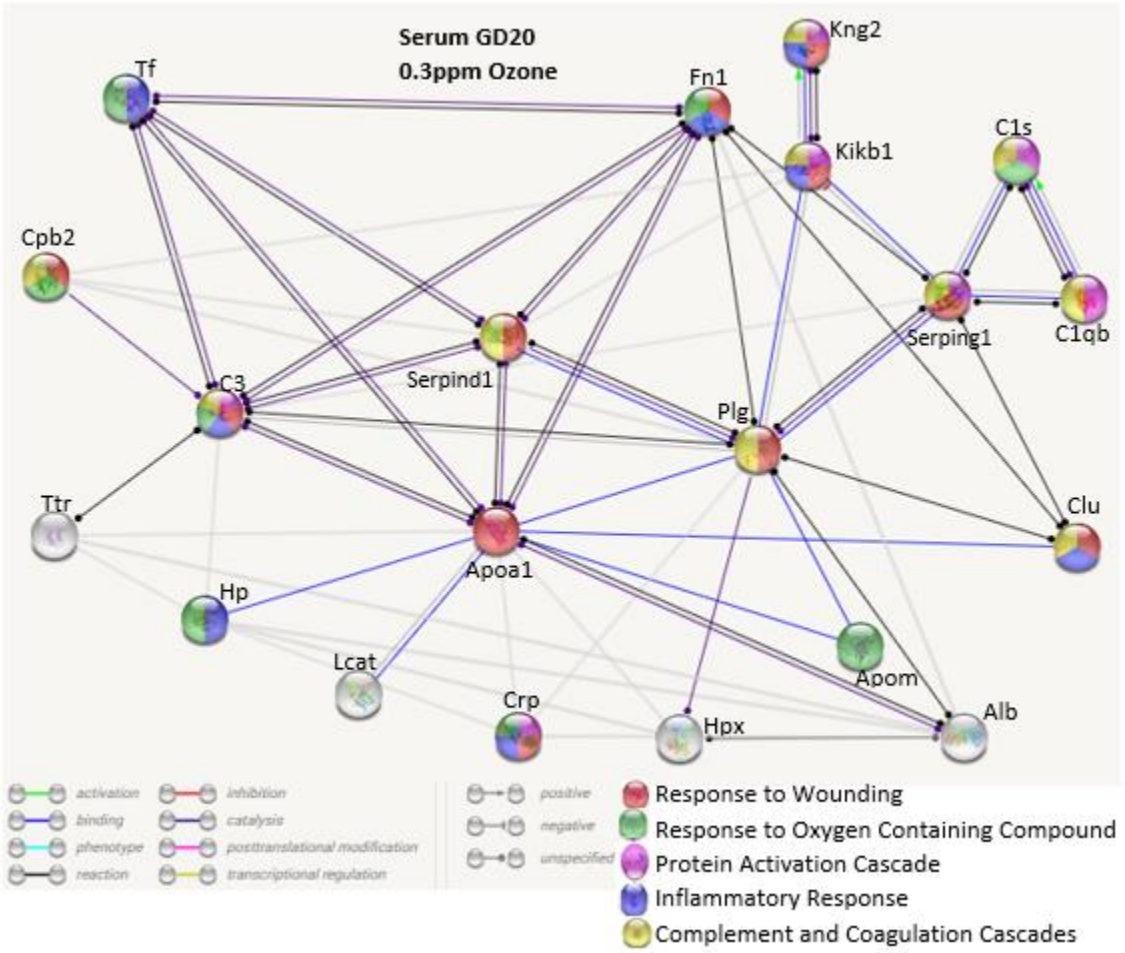

Figure 3.14 Protein-Protein Network Analysis in GD20 Low Exposure Serum

STRING database (Version 11.0) analysis of GD20 0.3ppm ozone maternal serum results for protein-protein interactions is shown. The minimum required interaction score was set to "High confidence (0.700)". Proteins were obtained after statistical vetting for significant factors in the group.

Figure 3.15

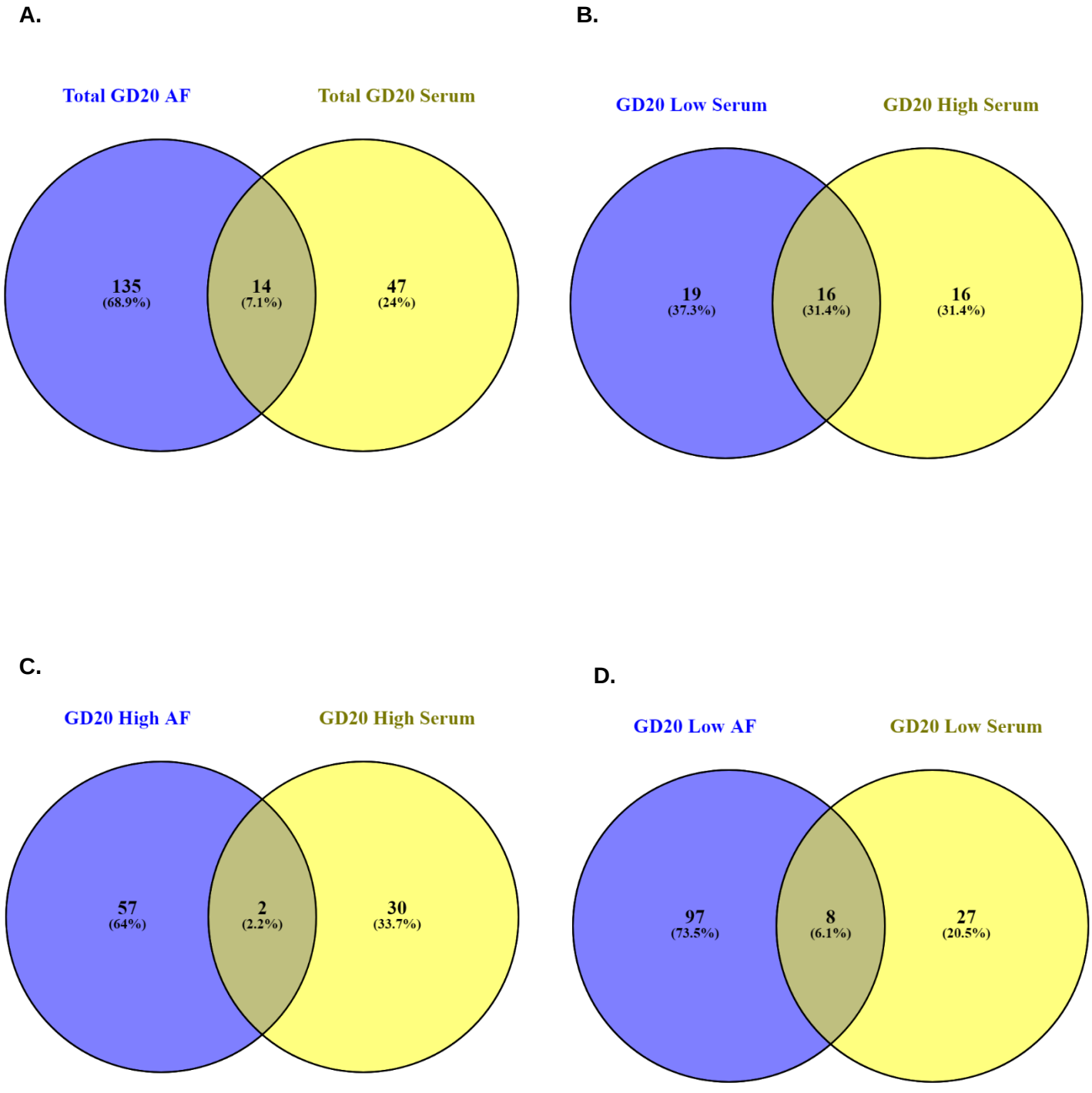

Figure 3.15 Comparing Shared Proteins Between Exposure Groups in Amniotic Fluid and Serum

Venn diagram illustrating shared and unique significant proteins across fluids and exposure groups per labels. Protein input was from significant protein shifts after statistical vetting. The comparisons analyzed are as follows: **(A)** total GD20 significant fold change in AF compared to total significant fold change in serum; **(B)** dose effect in serum from 0.3ppm and 1.0 ppm ozone exposed dams at GD20; **(C)** effects in GD20 AF and serum after 1.0ppm ozone exposure; **(D)** effects in GD20 AF and serum after exposure to 0.3ppm ozone. These findings indicate defined differences in each fluid's proteome based on ozone dose and gestational time of administration. Courtesy: *Oliveros, J.C. (2007-2015) Venny 2.1. An interactive tool for comparing lists with Venn's diagrams.* https://bioinfogp.cnb.csic.es/tools/venny/index.html

Figure 3.16

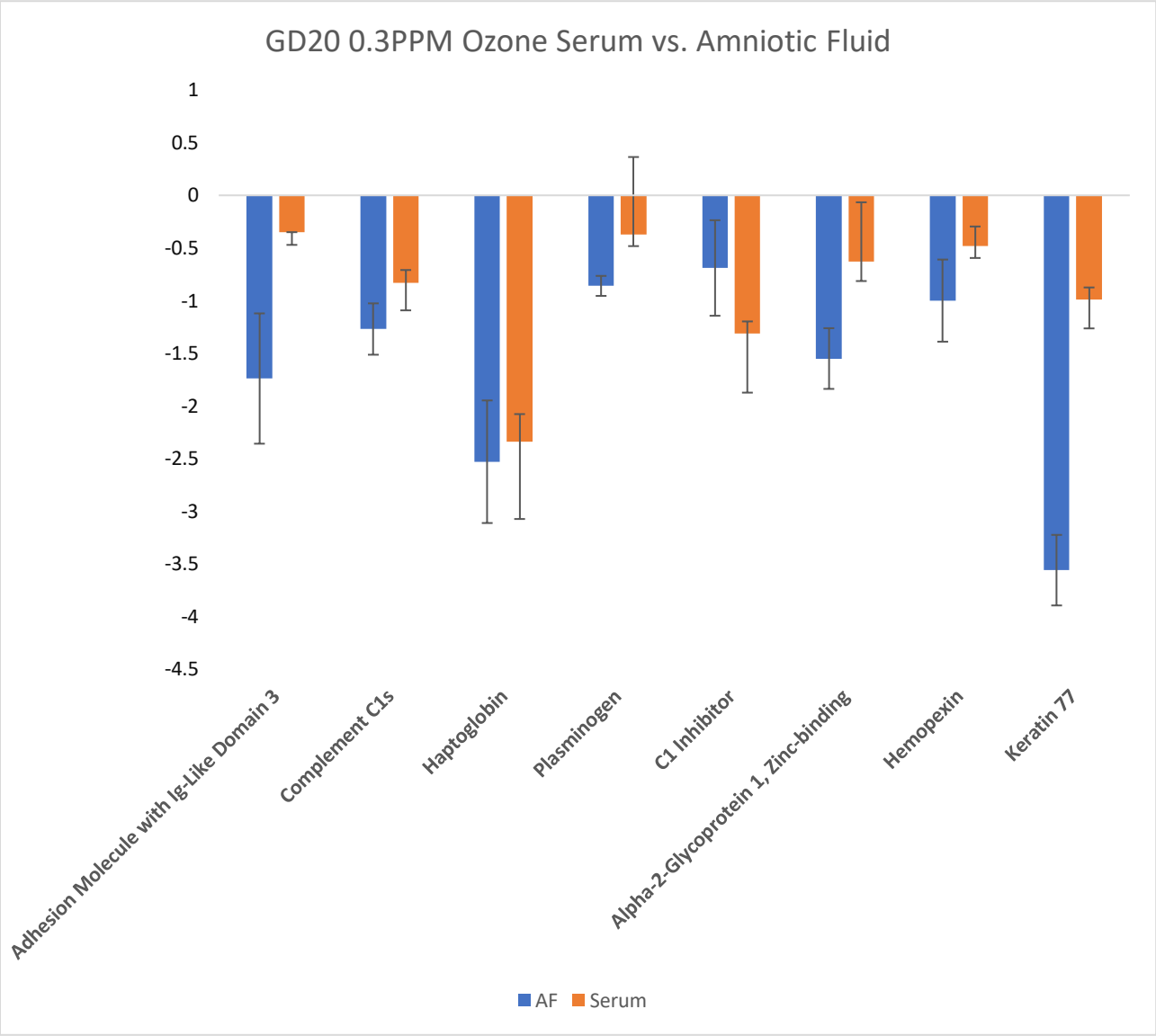

Figure 3.16 Significant Fold Changes for Selected Proteins in Amniotic Fluid and Maternal Serum

Graphical representation of fold change differences between shared proteins in serum and amniotic fluid from GD20 0.3PPM ozone exposed dams. All proteins achieved statistical significance in proteomic data processing.

Figure 3.17

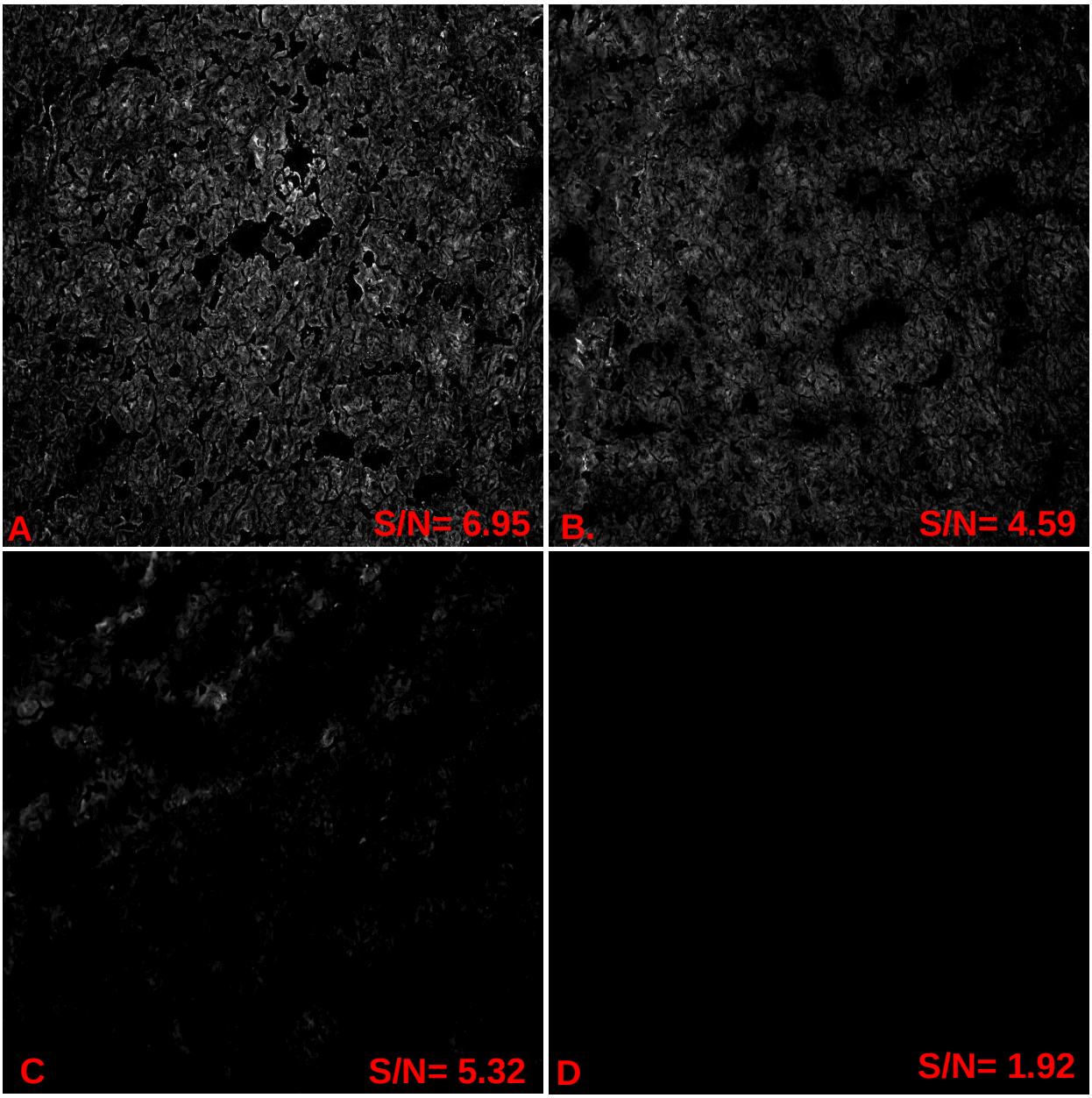

Figure 3.17 Example of Microscopy Optimization in Placenta

Optimization images for rabbit MMP2 antibody are shown at 1x **(A)**, 0.5x **(B)**, 0.25x **(C)**, and no primary **(D)** are shown. Signal to noise ratios are located at the bottom of each picture (S/N), with the 1x concentration offered the highest signal to noise ratio of 6.95.

Figure 3.18

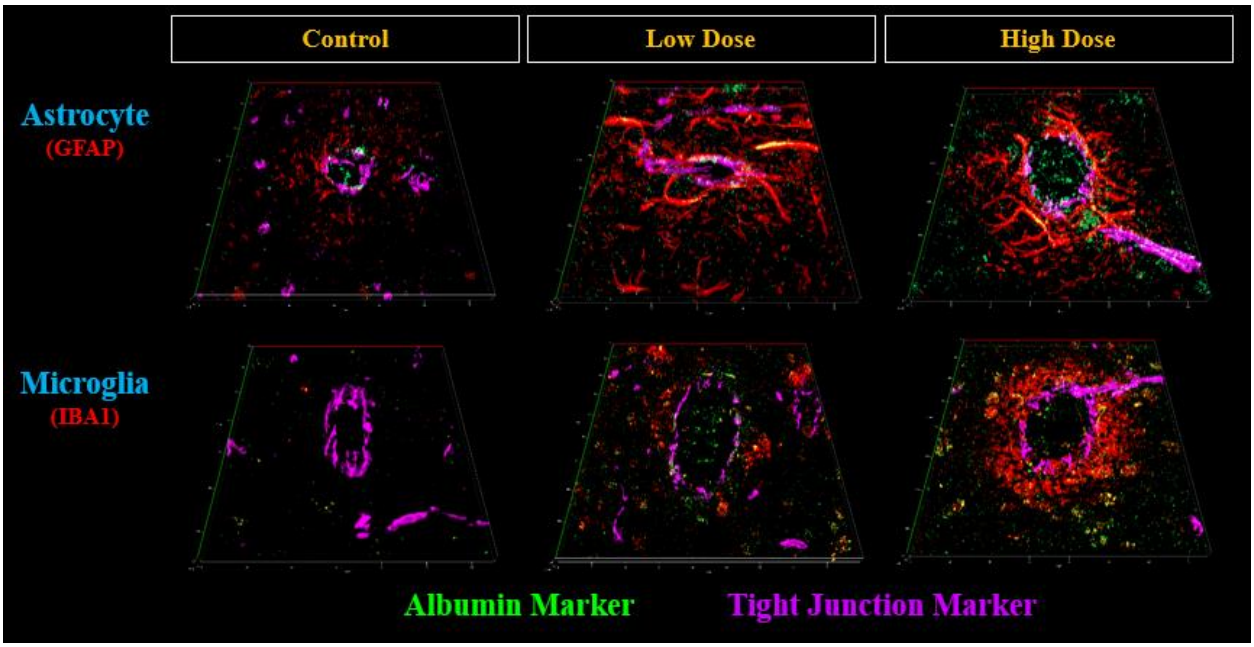

Figure 3.18 Demonstration of Antibody Regimen Used to Test BBB Integrity In Brain

Here we see a demonstration of our BBB integrity antibody staining regimen. Astrocyte and microglial reactivity are assessed in relation to vasculature in the brain. Albumin is used to assess permeability via leakage into the parenchyma.

Figure 3.19

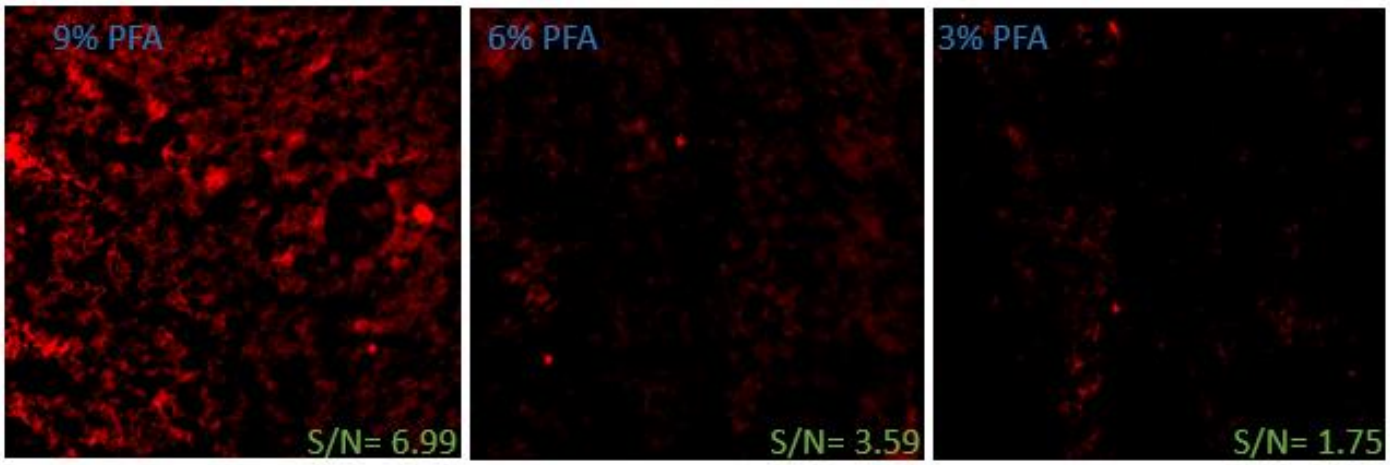

Figure 3.19 Demonstration of Placental Fixation Optimization Using E-Cadherin

Here we demonstrate optimization of fixation for mean signal to mean noise in placental tissue. Percentage PFA is indicated in the upper left hand corner, while mean signal to mean noise ratio is in the bottom righthand corner 9% PFA demonstrated the highest ratio and thus was chosen for experimentation.

Figure 3.20

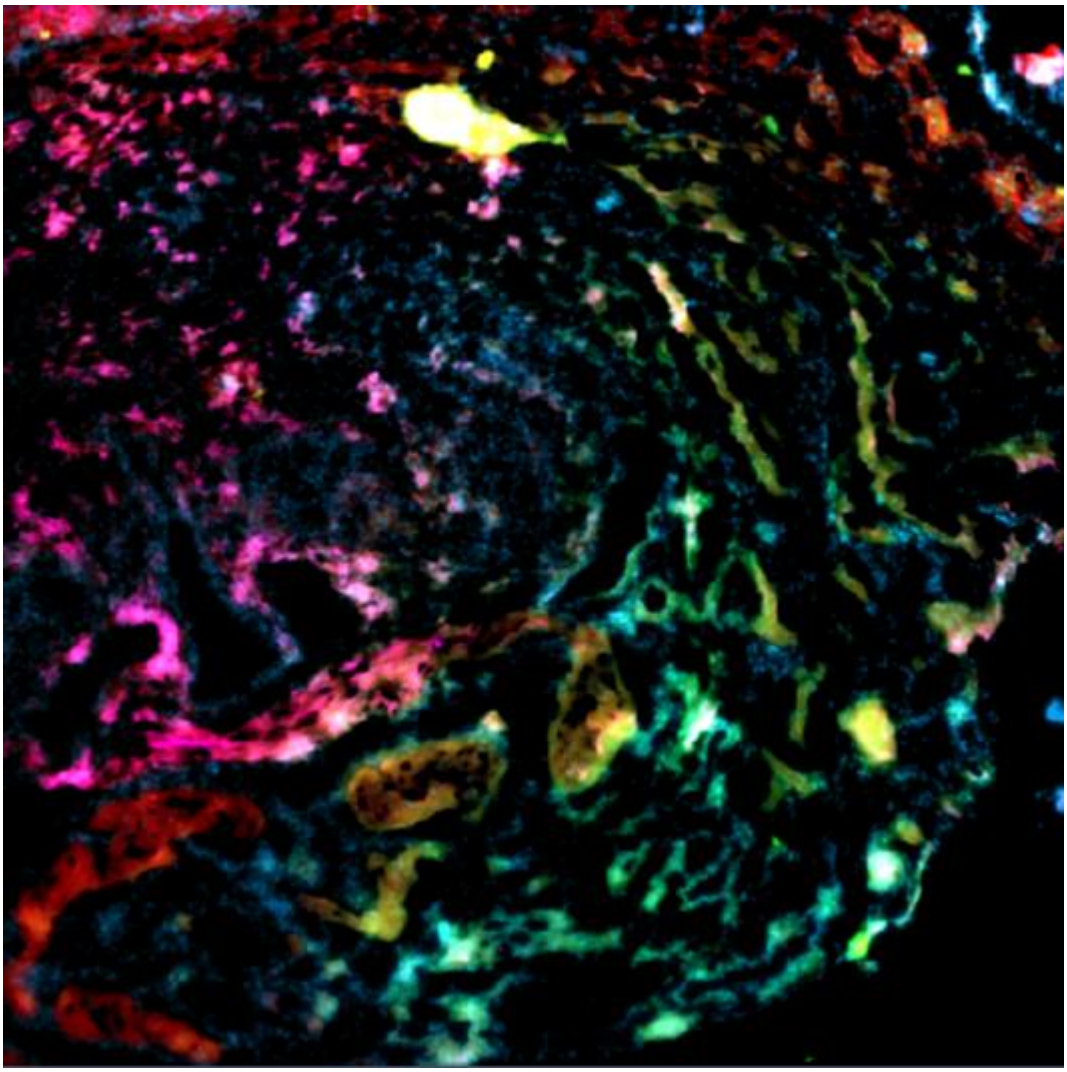

Figure 3.20 Demonstration of combined antibody staining regimen in placenta featuring OPN, PECAM1 and A5B3-integrin.

This is an example picture of our expected antibody regiment on outer placenta decidual tissue. OPN is on the green 488 channel, PECAM1 is on the red 568 channel and A5B3 integrin is on the pink 680 channel.

Chapter 4: Discussion

4.1. Effect of Ozone Exposure at Mid and Late Gestation on the Amniotic Fluid Proteome

In this study, an acute 4-h exposure to ozone was used to test how gestational age and separately dose impact the amniotic fluid (AF) proteome at term. When referring to gestational age, we are referring to differences in the AF proteome at GD10 and GD20 using a common 0.3 ppm ozone exposure and independent 0.0 ppm control exposures. What was very apparent was that the 0.3 ppm ozone exposure, normalized to control, reflected generalized shifts in the amniotic fluid proteomes that were opposite in directionality at the two time points. GD10 proteins showed a generalized shift to higher concentration while at GD20 there was a generalized shift to lower concentration. For example, of the 16 proteins in the GD20 exposure showing 2-fold or greater fold-change (+/-), all but one showed negative fold change. An explanation for these observations could be a dilution effect due to increases in overall AF volume, or polyhydramnios, at the GD21 (day of collection) in the amnion after late term ozone exposure. Similarly, the overall positive fold changes seen in the majority of GD10 exposed dams may be the result of a decreased AF volume, or oligohydramnios, at the GD20 collection date.

AF volume in healthy rats is dynamic with an almost 10-fold increase in volume at GD10-11, a timeframe aligning with the progress of major neurulation in these animals (Park and Shepard, 1994). AF volume continues to increase until GD18 before dropping until term, presumably as the result of increased fetal swallowing and intramembranous and intravascular absorption in both the developing GI tract and amniotic membranes. However, differences in AF volume are seen in complicated pregnancy states. Oligohydramnios, a decrease in AF volume, is commonly associated with hypertensive disorders during gestation in humans. Intuitively, this makes sense as the amniotic fluid near term is composed of what amounts to fetal urine. With the poor perfusion through the placenta observed in disorders like preeclampsia and hypertension, fetal urine output is similarly diminished (Mammaro et al, 2001).

After the placenta is developed near mid-gestation in rats, the uterine artery perfusion index in healthy individuals increases greatly as term approaches to meet the increasing metabolic and nutritional needs of the fetus (Browne et al., 2015). This perfusion index, along with uterine artery resistance are primary measures of placental function and can indicate hypertension in pregnancy. Interestingly, cardiovascular work conducted on the dams used in these studies by our collaborators at the University of New Mexico demonstrated an increased intrauterine artery resistance index at term in GD10 exposed animals (Figure 4.1). These data show that the normal decrease in intrauterine artery resistance expected between GD8.5 and GD20 is lessened with 0.3 ppm ozone exposure (Figure 4.1B). Subsequent post-hoc analysis showed that the effect was limited to the GD10 exposed cohort only (Figure 4.1C). These observations were also associated with decreased cardiac output and stroke volume in GD10 exposed dams, supporting a hypertensive condition and less artery perfusion at term in dams with mid-gestation ozone exposure. While AF volumes were not measured throughout pregnancy, such data suggests a hypertensive-state induced oligohydramnios, which is consistent with the biologically reproduced increased concentration of the AF proteome at term in GD10 exposed dams. Additionally, total AF protein concentration is negatively associated with birthweight at term in humans (Tisi et al., 2004). Unfortunately, fetal weights were not recorded for these studies, though as a surrogate, we could see that there was a negative trend, which did not reach significance, from 11.3 to 10.8 pups per 0.3 ppm GD10 exposed dams relative to control.

As previously mentioned, 0.3 ppm ozone GD20 exposed dams exhibited a general negative proteomic fold change in amniotic fluid, an opposite effect to that with GD10 exposure when assessed at term. Of importance, the cardiovascular effects observed in GD10 exposed dams were not apparent when testing the same parameters in GD20 exposed dams. However, treatment of excised uterine arteries from unexposed dams with the serum of GD20 exposed dams caused impaired vasorelaxation with acetylcholine and an enhanced contractile response to phenylephrine compared to serum from 0.0

ppm control GD20 exposed dams. It is possible that the acute ozone exposure results in a transient polyhydramnios (elevation in AF volume) and thus a transient "diluted" overall proteomic profile. However, such an acute effect would not be sustained the ten days following a GD10 exposure. Other explanations for the apparent polyhydramnios are less likely as the short period following GD20 exposure makes it unlikely that fetal swallowing or an increased fetal urination would have occurred to disturb the dynamic equilibrium controlling AF volume. However, a simpler explanation for polyhydramnios would be ozone induced dyspnea in the dams (Hamza et al., 2013), a "shortness-of-breath" that is a common acute symptom of ozone exposure (McDonnell 1999).

While ozone exhibited a generalized shift in the AF proteome that could be explained via generalized changes in fluid volume, there were distinctly elevated and diminished proteins that were significantly responsive to treatment (Table 3.1). In comparing time point similarities and differences of the AF proteome, some observations do relate to one another, though the interpretation is complicated be an incomplete set of observations across all treatments. For example, we measured a significant 1.84-fold decrease in MMP2 in the AF of GD20 exposed dams (decreased 2.2-fold in 1 ppm GD20 treated dams). In the GD10 treated cohort, MMP2 was not measured, however. Instead, there was a significant 1.9-fold increase in TIMP-2, MMP-2's direct inhibitor which may be a compensatory response. Unfortunately, it is not possible to relate these two because of the time different to collection of the amniotic fluid. However, it should be noted that MMP-2 and TIMP-2 dynamics have been demonstrated in human AF of preeclamptic and hypertensive pregnancies mid-gestation, though their profile at term is not defined (Lavee et al., 2009). Interestingly, umbilical arteries of preeclamptic pregnancies show a lowered expression of MMPs and heightened expression of collagens, the latter of which is the product of increased biosynthesis and decreased degradation by MMPs (Galewska et al., 2003). The decreased collagen breakdown contributes to the overall increase in vascular resistance associated with the disease. Our GD10 findings are indicative of decreased MMP-2 with elevated levels of four different

collagen motifs, factor patterns that are also associated with an anti-angiogenic state when measured in maternal blood during gestational hypertension (Tayebjee et al., 2005).

Studies of ozone toxicity have largely examined MMP levels in maternal serum and bronchoalveolar lavage fluid, which are notably elevated as part of the activated inflammatory and oxidative stress response when ozone comes in contact with lung surfactant at the epithelial interface (Yoon et al, 2007). However, the study of AF here gauges the level of stress within the privileged amniotic environment. It should, however, be noted that this raises the distinct limitation of these studies – that changes in the amniotic fluid can be simultaneously influenced by placental and fetal effects. This underlies the rationale for performing targeted assessments on the placenta and fetus, as has been planned out in this thesis. For example, MMP's play an important roles in early brain development after birth, but have been poorly investigated in the perinatal period (Ulrich et al., 2005). Additional studies on their role in toxicology and in rat fetal development could help to elucidate their full role in gestational pathogenesis in experimental models that are currently underexplored.

Osteopontin (OPN) is an example of a protein with measured changes observed at both time points. The GD20 0.3 ppm ozone exposure induced a 3.25-fold decrease while OPN was increased 1.57-fold in the cohort exposed at GD10. OPN is a proinflammatory cytokine that has be shown to play a direct role in the lungs (and seemingly other organ's) inflammatory response to ozone. During gestation, OPN plays a role in implantation, placental development and broadscale fetal tissue development, including in the CNS (Johnson et al., 2003; Choi et al., 2003). Recent evidence suggests its expression increases vascular permeability by controlling the expression of claudin-5 and ZO-1, both tight junction proteins (Zhang et al., 2018). This would align with our hypothesis of altered placental barrier function in the GD10 group. Interestingly, similar maternal serum elevations in OPN have been made with preeclamptic pregnancies (Stenczer et al., 2010). Yet, the acute (within 24-h) response to 0.3 ppm ozone

exposure resulted in a prominent decrease in AF OPN levels, which less obvious to explain and will be discussed later in this chapter as mechanisms of altered OPN expression.

Galectin-1 is a protein of particular interest here due to its established elevated state in maternal serum and AF collected from pregnancies complicated by preeclampsia. In our GD10 exposed group, the protein showed a massive 13.7-fold change. The protein is characterized as anti-inflammatory and pro-angiogenic in nature (Than et al., 2006). Its expression in trophoblast has been shown to be necessary for adequate development of the decidual vasculature following implantation, and lowered expression early in pregnancy is associated with placental resorption and early onset of a preeclamptic state (Freitag et al., 2014). Such observations come with enhancement of vascular endothelial growth factor receptor-2 signaling and enhanced activation of MMP-2, MMP-9 and TIMP-1 signaling (Freitag et al., 2014). However, early onset cases of human preeclampsia are not the norm, rather the condition typically presents after week 20 of gestation, firmly in mid- to late-gestation. Galectin-1 exhibits well established elevation in human placental tissue in late pregnancy with severe preeclampsia (Than et al., 2008). Its immunofluorescence and mRNA expression is demonstrated in both trophoblast lineages and placental endothelial cells in the previously referenced study, indicating possible roles in vascular and ECM remodeling. Its association with a TH2-type inflammatory response has led to its investigation as a marker of resolution in a highly engaged immune response, such as at the host-graft interface where it has a noteworthy amelioratory effect (Baum et al., 2003). Interestingly, ozone has been shown to induce TH2-like immune expression in mice after repeated exposure (Paul and Zhu, 2012). The mechanistic effect of gelactin-1 on the placenta is not currently deduced, however differing expression levels at alternative gestational timepoints is associated with development of preeclampsia (Hirashima et al., 2018). A discussion of possible mechanisms of elevated galectin-1 levels in the preeclamptic placenta at term is discussed later in this chapter.

Tissue factor pathway inhibitor (TFPI) is another shared protein between the two groups with noted effects on developmental processes. While its direct functionality is usually attributed to regulating coagulation through interactions with tissue factor, it appears to play a vital role in placental homeostasis. The protein was decreased in AF for both exposure groups, 2.62-fold with GD10 and 4.66-fold with GD20 exposures. TFPI knockout results in complete embryolethality, the majority of fetuses dying by GD11.5 (Huang et al., 1997). In a subsequent knockout study of the gene, rats still living by GD14 showed a marked disruption of the vascular network in the placental labyrinth zone with an almost complete loss of vascular channels required for maternal-fetal circulation. Additionally, these knockout mice showed increased fibrin deposition in the labyrinth zone and at the decidual interface, suggesting a role in placental ECM remodeling as well (Pederson et al, 2005). We'd expect to see similar observations in our placental tissues, particularly for the GD10 group with this exposure timepoint having the greatest potential for effect on the developing placental vasculature.

Of note, at the GD20 exposure time point, Rack1 was 19.7-fold increased, a protein with wide ranging functionality due to its role as a receptor for activated protein kinase C. It is classified as a scaffolding protein and thus integrates feedback from a myriad of signaling pathways to effect processes such as tissue migration and focal adhesion (Dave et al., 2013; Adams et al., 2011). While its overexpression has mostly been studied with tumor pathogenesis, the drastic fold change here suggests distinct effects on cell signaling, which we discuss later in this chapter. A similarly dramatic fold change in GD10 is seen with RNase1, a type of pancreatic ribonuclease exhibiting a 17.5-fold increase. The protein is the only known ribonuclease in plasma with high, nonspecific ribonucleolytic activity (Lomax et al., 2017). It can also enter the cytosol of other cells via endocytosis when secreted. In humans, it is widely expressed in endothelial cells. Generally, its expression is induced as the result of injury related stimuli and helps to clear RNA and damaged cells at inflammation sites (Lu, 2018). Hypoxic conditions are associated with an increase in extracellular RNA and proinflammatory cytokines, a response similar

to oxidative stress as would be expected with ozone exposure here. Administration of RNase1 has been shown to provide protection to the heart from proinflammatory cytokines, probably by clearance of these RNAs (Cabrera-Fuentes, 2014). The protein has additionally been shown to alleviate oxidative stress resulting from infection in blunt snout bream (Geng et al., 2019). It is important to note that RNase1 shows distinct structural and possibly functional diversity between species, and such diversity is poorly investigated in rodent models (Liu et al., 2015). However, it's highly elevated presence in our GD10 proteomic results is thought to be indicative of a prolonged activated immune response to the respiratory insult.

While distinct protein responses are informative, as discussed above, it is also important to examine differences between exposure times as a higher, functional level. Protein changes associated with an oxidative stress response as a biological process are demonstrated in both proteomes, but require different interpretations given time between exposure and collection. While the GD10 proteome exhibits downstream effects of oxidative stress days after the inducing event, the GD20 proteome profiles direct responses to ozone exposure in fold changes to catalase and superoxide dismutase (SOD1) enzymes. SOD1 exhibited a modest 1.55-fold decrease while catalase was down by 8.40-fold. While seemingly counterintuitive, these proteomic shifts are in line with established findings of ozone-induced inactivation of both of these enzymes due to the involvement of superoxide radicals (Whiteside and Hassan, 1988). Interestingly, this early study indicated an ozone dose-dependent effect on catalase inactivation, an observation not seen in our studies. In the GD10 group, it appears that with sufficient time passing, these enzymes returned to basal levels congruent with filtered air controls. Separately, the differential fold changes in heat shock protein Hsp1a1 (HSP70) were of note with a 2.79-fold increase in GD10 and a 12.0-fold decrease in GD20. Hsp1a1 has a potent anti-inflammatory effects (Wu et al., 2019), and elevation of the protein have been observed with oxidative stress, preterm labor, and chorioamnionitis when found in AF (Chaiworapongsa et al., 2008). However, ozone was found to not

cause a significant increase in Hsp1a1 in the lung, even in the presence of respiratory distress and inflammation (Wirth et al., 2002). This is unique as other stress inducers like temperature and cadmium exhibited notable upregulation. However, other studies have demonstrated the dramatic increase of the protein in the lung after ozone exposure for periods significantly longer than in this study (Bauer et al., 2009, Wong et al. 1996). Its increased expression in the placenta has been noted and associated with placental vascular disease, with Hsp1a1 being expressed in smooth muscle and endothelial cells of the placental microvasculature (Liu et al., 2008). The significant down regulation of Hsp1a1 in the GD20 exposure group, a finding consistent at the 0.3 and 1.0 ppm ozone doses, was not easily understood, as it ran counter to that expected for an acute response to oxidative stress conditions. Validation would be needed to affirm that these responses are accurate, but they do suggest that an acute response to ozone close to term substantially lessens the tolerance of the fetal environment to oxidative stress.

The GD10 and GD20 exposure groups shared only 12 proteins (7.5%) in common with significant fold change shifts, indicating a measured proteomic effect of ozone exposure in AF at these critical timepoints in development. Intuitively, this makes sense as the acute stress induced from a single exposure at GD10 had time to evolve while the GD20 exposure response was indicative of an acute phase response. While each AF proteome were largely unique, their enriched associations with common biological processes were evident. Clear associations between the GD10 and GD20 AF proteomic responses to 0.3 ppm ozone were with vasculature and ECM factors, and provide a perspective on analyzing acute ozone dosage just after exposure and analyzing downstream effects at term after mid-gestational exposure. Of note, an enrichment in association with placental tissue was only found with the GD10 AF proteomic response, which may relate to differences in acute vs chronic responses or perhaps in that the GD10 time point was proximal to implantation and placental growth. This is in line with our design logic, whereby the GD10 exposure was selected per its relevance to implantation and placental growth and thus having distinct effect on the vascular and ECM structure of the organ. Further

analysis of the GD10 AF proteome shows a compact, yet highly interconnected network of protein-protein interactions important in ECM remodeling and vascular development (Figure 3.8). We thus propose that the origin of most proteomic elements in AF derive from the placenta. In contrast, protein-protein interaction analysis of the GD20 0.3 ppm exposure AF proteomic response showed a much broader network of activation. Notably, those results implicate a link between the network of signaling/metabolic proteins and ECM proteins through TGF-β2 signaling. Further discussion of these mechanisms and their overall contribution to ozone mediated distress is provided later in this chapter.

4.2. Ozone Dose Effects on the Amniotic Fluid Proteome

To gain insight on dose-dependent effects of ozone, we exposed separate groups of GD20 dams to 0.3 ppm and 1.0 ppm for a common 4-h. As mentioned in Chapter 1, studies have determined that rodent modeling requires a 3-fold increase in concentration to produce the same baseline physiological and pulmonary pathological effects of ozone as seen in humans, with these doses correlating to 0.1 ppm and 0.3 ppm acute exposures. These selected doses are within the US EPA's "Very Unhealthy" and "Hazardous" categories of ozone exposure limits (American Heart Assocation, 2019). Many major cities in the US experience one or several days in these two categories, usually in the summer months, providing rationale for our single-exposure model during pregnancy. Los Angeles provides the most extreme example here in the U.S., with an average of 12 "Hazardous" days per year (2015-2017), a well-known hot-spot for high ozone exposure. Yet, even here in Central Virginia, Henrico County averaged at least 1 "Very Unhealthy" day per year in this same period. We selected the GD20 time point having previously found that the acute period exhibited prominent difference in the circulation with dose (Paffett et al., 2016), and thus a reasonable expectation that we would see a similar dose-dependent effect in the amniotic fluid. Overall, the 1.0 ppm exposed group demonstrated markedly fewer significant fold changes (59 proteins) than did the 0.3 ppm group (105 proteins). Unexpectedly, the AF

proteomic response between the two doses overlapped by only 10.1% (15 proteins, Figure 3.6), suggesting a prominent impact of dose. Yet unlike what was discussed above between GD10 and GD20 exposure differences, when examining dose-dependent effects on specific proteins at the GD20 exposure, the effect was directionally the same, with the higher dose producing a higher fold-change. For example, MMP-2 showed a 1.84-fold decrease at 0.3 ppm exposure and a 2.20-fold decrease at 1.0 ppm ozone. It was notable that MMP-2 levels within the AF were down acutely, which could suggest a protective response in the amniotic environment, as prior observations with this model showed that MMP-2 and MMP-9 were both increased acutely within the blood at these two doses (Paffett et al., 2016). Notably, MMP-2 and MMP-9 inhibition decreases cellular migration and angiogenesis in in vitro models (Webb et al., 2017) and antiangiogenic and decreased cell proliferation effects are seen in the shallowly invasive placenta associated with preeclampsia. Should a similar acute effect on these proteins be exhibited at the GD10 time point, this would impact trophoblast invasion and angiogenesis at the critical implantation stage that would be consistent with observations with preeclampsia. Yet it is also possible that these changes are an indication of an acute fetal response to the exposure, given that at term, the amniotic compartment is largely a reflection of exchange through the fetus. MMPs have a significant role in neurogenesis and network formation, for example, and their downregulation during critical periods would impact neurodevelopment.

Significant negative fold change expression was generally seen in shared proteins between the two doses. For example, pyruvate kinase-2 (PKM2) and amylase-2 both decreased dramatically. PKM2 decreased 17.0-fold and 9.13-fold while amylase-2 26.5-fold and 38.1-fold at the 0.3 ppm and 1.0 ppm doses, respectively. These proteins indicate altered carbohydrate/glucose metabolism induced shortly after acute ozone exposure. Such observations indicate distinct effects of ozone exposure on metabolism, likely in the fetus. PKM2 is the characteristic pyruvate kinase isoenzyme seen in rapidly proliferating tissues with a high rate of nucleic acid synthesis such as embryonic, adult stem and tumor

cells (Mazurek, 2011). The isoenzyme is typical in the fetus, but is replaced by tissue specific isoforms, such as pyruvate kinase M1 in brain at around term. If such a dramatic decrease in these proteins as an acute response to ozone were produced also at the GD10 timepoint, this would have been even more impactful on embryogenesis. At either time point, suppression of energetics would be detrimental to brain development which requires extensive energy input. Indeed, pyruvate kinase M1, the brain specific isoform, was found significantly decreased by 3.01-fold in the 0.3 ppm exposure group. This could be indicative of acutely altered brain glucose metabolism induced by ozone exposure at this concentration.

Yet, dose-dependent responses were not overtly consistent in showing a worse response at a higher dose. Negative fold changes seen in superoxide dismutase and catalase in the low exposure group were not seen in the high exposure group, which showed no significant fold change for either protein. This comes as somewhat of a surprise as the 1.0 ppm exposure would be expected to exacerbate the oxidative stress response. Enrichment analysis of the two exposure profiles indicated overlapping biological processes were being modulated, namely those involved in oxidative stress, extracellular matrix remodeling, and vascular function (Tables 3.3 and 3.4). However, the specific proteins enriched in each category are not the same. For instance, resolution of the oxidative stress response in the high exposure group may be augmented by vimentin, a structural protein with a 2.75-fold increase in the high exposure group only. A closer look at the protein-protein network analysis results for the 1.0 ppm exposure reported vimentin's interaction with MMP-2 (Figure 3.9). As a structural protein, vimentin is a target of MMP-2 proteinase activity after cytokine signaling. Vimentin has been demonstrated to have a profound suppressive effect on the oxidative stress response. Moreover, knockout of the vimentin gene in mice results in increased expression of CD36, a key endothelial receptor that mediates vascular dysfunction after ozone exposure (Haverson et al, 2018). Vimentin was also associated with significantly enriched protein subsets for cytokine, cellular response

to oxygen containing compound, endothelial cell, and focal adhesion processes, pointing to its broad functional importance as an increased ozone-responsive measure at this higher dose.

In contrast, proteins associated with similar processes were found decreased at the lower dose. Vcam (vascular cell adhesion molecule), for example, decreased 4.26-fold and its interacting partner ezrin decreased 2-fold. Their decreased abundance indicates induced vascular dysfunction, likely within the placenta. Knockout of Vcam results in abnormal placentation and embryonic death in mice (Gurtner et al., 1994). Ezrin is a cytoplasmic peripheral protein and component of microvilli known to be expressed in placenta (Berryman et al., 1995). The protein serves as a link between the plasma membrane and actin cytoskeleton. A combined decrease in Vcam and ezrin suggests an effect on cell migration, providing an inroad for extracellular signaling into the cytoplasm.

These findings from AF protein content with differential ozone doses at the GD20 timepoint could provide insight into the effects of differing ozone concentrations when applied to humans who live or work in areas where ozone concentrations could be dramatically different. In the context of our study, these measurements just 24 hours after ozone exposure demonstrate a dose-dependent acute-phase response to ozone within the amniotic environment. Overall, comparative analysis between the two doses reveals similar biological processes are impacted in this privileged environment, though not as a consistent linear response. The proteomic data point to a combinatorial set of mechanisms that are responsive, with differences in effects on vascular and ECM mediated dysfunction based on the concentration of ozone. Yet it is important to consider that the acute phase response observed at GD20 could have remarkably different impacts at other critical periods. For example, at GD10, one would expect that these acute vascular deficits would have a more drastic impact on implantation and establishing adequate placental function, with potential teratogenic fetal consequences that were not assessed in these studies. A future study should thus examine how to pool sufficient amniotic fluid from the GD10 time point to provide for an examination of acute-phase effects at this critical period.

4.3. Maternal Serum Proteomic Response to Ozone Exposure

Proteomic analysis was additionally performed on maternal serum from GD20 dams at both ozone doses. These studies had two goals: (1) to confirm established ozone induced effects in maternal serum and (2) to assess maternal serum as a source for the AF proteomic response to ozone. The total proteomic shift was more modest, with only 60 unique proteins demonstrating significant effects of ozone as opposed to 149 within AF across both doses (Figure 3.15A). However, protein-protein interaction analysis showed a highly connected network among responsive proteins (Figure 3.12). Comparing the two concentrations, the two shared 16 proteins (31.4% of those compared) in common (Figure 3.15B), a much higher degree of homology than seen in any of the AF comparative groups. Ozone exposure has been shown to increase levels of classical inflammatory mediators in the lung, such as Interleukin-6 and TNF-α and homeostatic markers such as fibrinogen and plasminogen activator inhibitor-1 (Zhang et al., 2019). These factors are often measured in brochoalveolar lavage fluid; however, we found no significant shifts in our serum results. Our collaborators have previously demonstrated that because ozone is completely reacted at the lung surfactant interface, there is a distinct mixture of secondary and tertiary reactants that appears across the lung-vascular interface (Frampton et al., 1999; Kafoury et al., 1999). However, these downstream reactants convey vascular dysfunction. Serum from ozone exposed animals (at these doses) elicits ex vivo vascular dysfunction in naïve vessels, demonstrating the systemic bioactivity of ozone-induced secondary and tertiary factors (Robertson et al., 2013; Paffett et al., 2015). Similar effects were seen in ex vivo experimentation with serum from our exposed dams (paper submitted to Toxicological Sciences). Thus, it was logical to examine proteomic changes within the maternal serum that may be indicative of this bioactivity, the first such study of the maternal blood proteome in response to ozone exposure during pregnancy.

In the 16 proteins shared between the experimental groups, the directionality of protein fold changes were homologous between the doses. In these 16 proteins, only two showed a positive fold change: (1) growth hormone receptor (up 27.5-fold at the low exposure and 30.5-fold at the high exposure), and (2) complement C1q subcomponent subunit B (up 6.87-fold at the low exposure and 4.76-fold at the high exposure). Growth hormone receptor is known to be upregulated in the blood of late-pregnant mice (Ilkbahar et al, 1999). However, little information about acute increases in the receptor is available in literature, nor why it would be observed in the blood, perhaps as a proteolytic breakdown product as a consequence of ozone-exposure induced MMPs. Interestingly, 25% of the proteins with an overlapping response between the doses were associated with the compliment cascade, a system involved in the inflammatory response and immune system attentiveness to cell damage and pathogen presence. Acute ozone exposure at a slightly higher concentration (2 ppm) for slightly less time (3 h) has been shown to increase neutrophil recruitment and protein concentration in bronchoalveolar lavage fluid (Park et al., 2004). Taken together, these data support consistency with prior secondary evidence of ozone systemic effects downstream of induced lung toxicity.

Differences between the doses were present. Plasminogen, an enzyme involved in fibrin clot clearance, was significantly downregulated only in the 0.3 ppm group. Decreased plasminogen due to an upregulation of its inhibitor is known to occur with oxidative stress induced lung fibrosis (Liu et al., 2008). Carboxypeptidase B was also significantly down 2.97-fold in the 0.3 ppm serum, a zymogen that circulates with plasminogen and is required for activation of the latter's ability to break down fibrin aggregates (Leung et al, 2018). It is interesting to consider whether ozone, though seemingly only at the low dose, would worsen the potential for blood clot formation during pregnancy. Not all findings in the low exposure cohort serum proteome were consistent with the literature, however. Haptoglobin, an acute phase protein known to be upregulated in conditions of oxidative stress, showed 5.06-fold decrease in the 0.3 ppm exposed group (Mumby et al., 2019; Bertaggia et al., 2014). Yet, the overall

serum proteome profile of the acute 0.3 ppm GD20 exposure was one of an engaged immune response, via increased expression in compliment cascade proteins, and inhibited breakdown of fibrin formations.

There were some unique observations within the high ozone exposed serum as well. Most dramatic was the 897-fold decrease in the pro-hormone for relaxin at the 1.0 ppm dose, which had a much more modest 6.02-fold downward trend at the 0.3 ppm dose that did not reach significance. Relaxin is integral in preparing the endometrium for implantation and subsequent angiogenesis earlier in pregnancy (Goldsmith and Weiss, 2009), but its role at term is not clear. Knockout studies outside of pregnancy have revealed its intimate relationship with estrogen, portending distinct effects near-term, as well as vital roles in reducing airway fibrosis, airway smooth muscle thickening, and cardiac hypertrophy (Lekgabe et al., 2006). Yet, overall, the serum proteomic response to 1.0 ppm ozone was similarly indicative of compliment cascade activation and impaired degradation of ECM fibrotic clusters. Such evidence is indicative of the effects of acute ozone exposure and demonstrates an altered serum proteome in the pregnant rat after exposure.

4.4. Maternal Serum as a Source for the Amniotic Fluid Proteomic Response to Ozone

As the AF is at least partially a filtrate of the maternal blood, it would be possible for ozone-augmented protein content from the serum to end up in the AF. Intriguingly, overlap between the serum and AF was dose-dependent, with 8 common proteins at the 0.3 ppm exposure and only 2 at the 1.0 ppm exposure. The 8 common proteins for the low exposure were: Ali3 (aka Amigo3), C1s, Hp, Plg, Serping1, Azgp1, Hpx and Krt77. C1s, Serping1 and Plg, which are all known components of the compliment cascade system. Azgp1 is known to be expressed in secretory cells of the lung epithelium and has never been demonstrated in placenta, though it was detected in the AF. Hemopexin (Hpx), haptoglobin(Hp), and plasminogen (Plg) are defined serum proteins with previously discussed roles in the serum proteome. Krt77 is a keratin known to be expressed in development of embryonic epithelial

tissue, but its origins and functionality are largely uncharacterized (Bazzi et al., 2007). While there is possibility for Krt77 to have embryonic origins in the AF fluid, the remaining shared proteins between 0.3 ppm AF and maternal serum appear to have clear origins in the serum. In support of this statement, negative fold change was seen throughout all shared proteins in both groups (**Figure 3.16**). While specific differences between serum and AF proteomes exist, both indicate an altered inflammatory state induced by ozone exposure leading to differential tissue processing of vasculature and ECM components after exposure. However, the low proteomic homology observed between serum and AF provides leaves open an alternative placental and/or fetal origin for the majority of AF proteomic shifts. Such a conclusion further validates investigation into the true placental and fetal nature of proteomic shifts in AF. Due to expression of different proteins such as MMPs, by both maternal and fetal subtypes, it is challenging to fully eliminate serum contributions to the AF proteome. However, further studies by immunofluorescence microscopy have been devised to examine certain targets of the AF proteomic response within placental tissue. In the next section, we devise a proposed mechanism of placental origin that would be tested using the planned set of targeted immunochemical experimentation.

4.5 Possible Mechanisms for Ozone Mediated Placental Dysfunction

In assessing mechanisms of ozone related placental dysfunction, AF proteomic data from the GD10 time point undoubtedly provided greater insight given this time's criticality to placental development. However, we also consider for our discussion an extrapolation of the GD20 time point results to suggest placental effects that ozone may have acutely at GD10 that could not be assessed in this study. As explained above, GD20 serum data showed significant activation of the maternal complement system, indicating extensive immune activation in ozone exposed dams just one day after exposure. During the early period of placentation, maternal blood comes into contact with invasive trophoblast cell lines for the first time. Additionally, the development of new blood vessels during this

period is substantial to establish maternal-fetal circulation while rapidly increasing placenta size. Others have shown that the induction of maternal inflammation through a single low dose injection with lipopolysaccharide at GD13.5, followed by successively higher injections daily until GD16.5, increased maternal mean arterial pressured and produced deficiencies in trophoblast invasion and spiral artery remodeling in Wistar rats (Cotechini et al., 2014). If ozone is viewed as an acute driver of inflammation, as suggested by the GD20 acute-response data, one might infer that shortly after the GD10 exposure, there would be an exacerbated influence of ozone on placental angiogenesis in its early stages. Of course, ozone is nowhere near as potent in driving inflammation as LPS, and our model involves a single exposure, but the effects of ozone on inflammation and hypertensive effect have been outline extensively to this point, so such inference of similar trophoblast and spiral artery effect is within reason.

In proposing mechanisms for placental dysfunction based on our proteomic findings, we will begin by using data from our proteomic findings in the serum related to complement system activation, as this data has provided useful insight for our lab's current investigation in placenta and subsequent fetal effects. The expression of paternal antigens on the fetus and placenta results in presentation of these tissues as foreign to the maternal immune system. In hemochorial placentation, as seen in rodents and humans, maternal blood comes into direct contact with fetal vasculature. The trophospongium, or junctional zone, in rodent placenta is both fetal and maternal in origin, featuring invasive trophoblast lines invading maternal tissues to remodel maternal spiral arteries to high flow, low resistance vessels. The labyrinth zone, or villous space in humans, is strictly fetal in origin, carrying developing fetal blood vessels into the lacunae, analagous to the intervillous space in humans, to be bathed in maternal blood. The principle placental barrier is the outer layer of trophoblast surrounding the fetal vessels which comes into direct contact with the maternal blood allowing for oxygen and nutrient exchange. Given that the fetal trophoblast is the only cell line in contact with maternal blood, this is an important site for

complement interact to maintain viability of the organ through term. The balance of maternal innate immune complement response is critical in maintaining viability of the conceptus through term while protecting both mother and fetus from infection as the trophoblast layer lining fetal vasculature is impermeable to maternal immune cell invasion.

While extensively investigated, the research community has yet to come to a true consensus on the nature of specific complement cascade factors universally exhibited in preeclamptic or hypertensive pregnancies in humans and rodent models (Regal et al., 2015; Regal et al., 2017; Pierik et al., 2020). Depleted C3 in plasma along with increased C3a/C3 ratio, measured from serum of human preeclamptic pregnancies, is hypothesized to be the result of C3 activation exceeding C3 synthesis (Derzsy et al., 2010). This observation in humans is congruent with our findings of modest C3 negative fold changes for C3 at both GD20 doses. However, other proteomic findings ran opposite to established research, like the increased fold change in C1q observed at both doses. Hypertension has been associated rather with C1q deficiency in mice, namely in defective decidual invasion (Singh et al., 2011). Many studies on maternal serum content are done in humans as serum is readily available and noninvasive to collect, complicating conclusive extrapolation of results from other animal models. The true mechanistic nature of complement mediated placental dysfunction is yet to be truly elucidated; however, increased activation of the maternal complement system is observed across categorizations of inflammation and gestational hypertensive disorders. Due to the nature of complement cascade, a peptidomic approach may produce more enlightening results than the current proteomic approach due to extensive fragmentation inherently seen in the compliment cascade. With the applied rollup procedure, it is possible such details are lost. Peptidomic analysis could provide insight to the content of anaphylatoxins and other activated complement protein fragments, providing an even greater level of specificity in analysis.

Acute AF changes in the GD20 group also provides distinctive insight into what occurs acutely after exposure. When analyzing protein-protein interactions in AF from the GD20 group (Figure 3.9),

important interactions were observed. Most notable was the interaction between plasminogen, seen in both AF and serum, and MMP-2. Both showed distinct negative fold change shifts and are highly connected with different parts of the network. In the interaction network, plasminogen is linked with other proteins of serum origin, hemoplexin and haptoglobin. Plasminogen requires activation via an enzymatic cascade to produce the broad spectrum serine protease plasmin, the form capable of degrading fibrin and other connective tissue proteins (Tarango, 2014). The expression of plasminogen activator inhibitor type 1 is observed in trophoblasts of invasive and vascular cell lines and is elevated in preeclampsia (Ye et al., 2017). Literature suggests a clear functional overlap between the two proteins and expression of the two together has been demonstrated as essential for proper placental development (Solberg et al., 2003). Each is known to play a role in both biologically normative and pathogenic angiogenesis due to their role in endothelial cells and ability to rapidly degrade ECM content (Pepper et al, 2001). The acute downregulation of each seen 24 hours after ozone exposure could be indicative of an acute inhibition of angiogenic and ECM remodeling activity. Further investigation of the network reveals a direct connection between plasminogen and TGFβ in a highly connected network of 6 proteins. A direct link between this network and a network containing multiple ECM proteins including MMP-2, OPN and galectin-1, is seen through the aforementioned MMP-2—plasminogen linkages, as well as direct interaction between TGFβ and decorin, a small proteoglycan that is a component of connective tissue and plays a role in matrix assembly (Zhang et al., 2014). Decorin is an established general inhibitor of TGFβ (Yamaguchi et al., 1990; Kolb et al., 2001). The downregulation of both suggests an attenuated signaling effect after acute exposure. TGFβ has generally been described as a diffusely expressed and highly potent profibrogenic cytokine (Katre et al., 2013). It has been implicated in induced lung fibrosis by several agents, including ozone, and in multiple fibrotic lung diseases (Katre et al., 2013; Coker et al, 1997; Churg et al, 2009). In vitro experiments revealed differentially increased invasiveness in trophoblast lines by TGFβ, further adding to the complexity of the protein's role in

regulated tissue invasion of placenta (Lafontaine et al., 2011). Due to the extremely diverse nature of TGFβ signaling, however, further insight into its expression in placenta after pulmonary insult will be needed. However, a common negative fold change of proteins involved in remodeling of the ECM and vasculature, can be functionality associated with placental dysfunction and a possible preeclamptic state. These functional distinctions are mirrored in the GD10 AF, with acute upregulation of ECM proteins after resolution of an initial ozone insult.

The role of OPN as a significant responsive factor within the AF proteome cannot be overlooked. Its primary expression in the decidua, as well as invasive trophoblast, has been shown to have distinct interaction with uterine natural killer cells and notably galectin-1 (Barrientos, et al., 2014; Herington et al., 2007). Such interactions implicate the protein in nearly every important process for adequate placental development, including maternal immune tolerance, trophoblast migration and angiogenesis (Johnson et al., 2003). Ozone exposure has already been shown to increase OPN-mediated neutrophil recruitment in the lung (Barreno et al., 2013). It is reasonable to postulate then that ozone treatment may enhanced recruitment of maternal immune cells in the decidua. An acute negative fold change of OPN (as demonstrated with GD20 data) followed by a positive-fold change ten days after exposure (as observed with GD10 data) suggests a suppressive effect immediately after inhalation, followed by a compensatory increase. Such recovery is likely the result of further cytokine signaling. If the acute negative fold change seen in GD20 is mirrored following GD10 exposure, we would expect to see decreased invasion into the decidua evident in our microscopy, along with diffusely decreased OPN immunofluorescence in the term placenta, particularly at the junctional trophospongium and labyrinth zones, where the two cells expressing OPN in placenta are most concentrated. Furthermore, such findings would be consistent with immunostaining for OPN in preeclamptic placentae (Gabinskaya et al., 2011; Xia et al., 2009). Interestingly, the association of OPN and its integrin receptor, alpha-5-beta-3 integrin, has been investigated in preeclamptic pregnancies, with the complicated pregnancies showing

decreased OPN immunostaining, but no difference in its integrin receptor (Xia et al, 2009). The role of this specific integrin has been investigated during pregnancy in sheep and ruminant placenta has produced conflicting results on its role in uterine attachment (Wan et al., 2011; Kimmins et al., 2004). However, given the vastly different placental invasiveness and overall placental structure in these animals, such observations are hardly conclusive when applying findings to the hemochorial placenta. Integrin binding is also seen with galectin-1 in placenta, indicating the role of these receptor proteins in mediation of cell-matrix interactions and possible signal transduction (Xu et al., 2020). Further research is needed to establish defined temporal and anatomical guidelines in these interactions in placental models applicable to humans. The well-defined rise in galectin-1 late in preeclamptic pregnancies is poorly explored mechanistically. This is most likely due to the investigation of the molecule for use as a diagnostic biomarker, rather than a therapeutic target (Tirado-Gonzalez et al, 2013).

The two most highly upregulated proteins in the low exposure groups, Rack1 (GD20) and RNase1 (GD10), provide only slight insight. RNase1 has not been demonstrated in any literature on placenta, suggesting a fetal or serum origin for its presence in AF. Rack1, however, has been shown to have a possible role in placental cell migration and invasion (Whang et al., 2013). The protein is thought to act as a scaffold for many other proteins inherent to functionality in diverse signaling pathways, and promote translational efficiency. However, molecular mechanisms for such roles are uncharacterized (Gallo et al., 2015). Further investigation in such broad scale translational monitors and scaffolding proteins could provide insight into the largely underexplored and extraordinarily complex world of placental cell signaling.

4.6. Comparison of Rat and Human Placental Models

The qualities that make the rat placenta an attractive model for extrapolation of comparative effects in humans are primarily related to its structure. A brief assessment of similarities and differences

between the species can be seen in **Figure 4.2**. The bidiscoid implantation seen in rats is similar to the discoid implantation of human placenta in the uterine endometrium. Additionally, the hemochorial structure of the rat is similar in nature, with defined layers of analogous function. An abundance of uterine natural killer cells associated with spiral arteries is shared, along with bidirectional blood supply. Invasion into the endometrium is deep in both, allowing for assessments of over-invasiveness and poorly invasive placenta (Pijnenborg et al., 1981). Overall, the well-established physiology in and small size of rats also serve to boost its viability as an experimental model in placentation (Soares et al., 2011). Additionally, the multi-placental nature of rat pregnancy makes it a good candidate for study by increasing n without increasing the number of dams used, thus saving cost and life expenses.

Differences do exist in extrapolating analogous effect from rat to human placenta, however. A key difference is the significantly lessened defined structure in the area of circulatory exchange. The junctional zone structure of the rat is bathed in maternal blood through irregular formation of lacunae, or patches of decidualized tissue cleared of connective tissue to form blood pools. Moreover, the fetal vascular interface is formed by angiogenesis of capillary beds of significantly less defined structure than the human villous structure (Furukawa et al., 2012). In contrast, the human circulatory interface is formed by highly regulated development of villous vascular trees surrounded by highly differentiated trophoblast subpopulations (Enders and Blankenship et al., 1999). The development of these trees and their invasion into maternal tissue is seen in coordination with highly regulated apoptotic events to surround the villi with open spaces capable of being filled with maternal blood upon establishment of the maternal-fetal circulation termed the intervillous space. However, these structural differences present little in the way of differing gas and nutrient transfer across trophoblast layers. One study indicated that the rat placenta is an inadequate model for extrapolating indicators of human developmental toxicity after exposure to teratogenic insult because of the differing endocrine functions of the organ between rat and placental models. Namely, the placenta is the primary source of estrogen

biosynthesis by mid-gestation in humans. In rats, the ovaries remain the primary source of estrogen through term due to the lack of catalytic enzymes such as aromatase expressed in rat placenta (Nakanishi, 2007). Additionally, the smaller size of the rat placenta can make it harder to surgically remove prior to term without significant artifact effect. Overall, for our assessments of ECM and vascular proteins, the rat shares more morphological similarities than differences. The rat model's extensive uterine artery remodeling, deep decidualized tissue region and analogous point of maternal-placental circulatory interface provide definitive targets for the microscopy experiments proposed in this thesis.

4.7. Evidence for Ozone-Mediated BBB Dysfunction

Ozone exposure at GD10 presents the potential for brain teratogenesis as it is a critical timepoint for neurogenesis in rats (Shepard and Park, 1994). Given the vascular nature of ozone mediated dysfunction and exposure effect on the AF proteome, we postulated that the developing rat BBB is a target for ozone mediated dysfunction in the developing fetus. Previous data from our lab has documented a primed microglial response in the BBB after ozone exposure (Mumaw et al., 2016). In this response, microglia remained activated 24 hours after ozone exposure, indicative of an increased inflammatory response resulting from pulmonary exposure that is not quickly resolved. Tight junction opening and BBB leakage has been demonstrated under conditions of oxidative stress induced reactive oxygen species in ozone and non-ozone mediated adult animal models (Mumaw et al., 2016; Schreibelt et al., 2007). Additionally, assessment of BBB and neurogenesis proteins in 25 week old rats after daily air pollutant exposure from early gestation into postnatal life showed induced vascular leakage in the hippocampus and impaired neurogenesis (Woodward et al., 2018). Their data showed a remarkable 75% decrease in vascular tight junction protein ZO-1. We expect that our model of single-dose ozone at the GD10 critical period would produce a similar, though lessened, state of BBB perturbation at term.

As with the placenta, the time of administration should prove crucial for outcome at term. Vascularization of the cortex in rats begins at approximately GD11 (Daneman et al., 2010). BBB development first begins with invasion of the neuroepithelium by endothelial tissue. Induction of these endothelial cells via specific signaling pathways from neural tissue leads to the expression of the BBB-specific phenotype characterized by specific tight junction, adheren ,and gap junction proteins such as ZO-1, claudin-5 ,and vascular endothelial cadherin as early as GD12 (Stamatovic et al., 2016; Daneman et al., 2010). Specific nutrient transporter channels also help to classify this phenotype, such as the expression of the Glut1 glucose transporter. The recruitment of pericytes aids in strengthening the endothelial barrier, limiting the rate of transcytosis, and inhibiting the expression of leukocyte adhesion molecules (Rudziak et al., 2019). Astrocytes, the final fundamental structural component of the NVU are first detected at GD16, but continue to mature even after birth, leaving BBB structural maintenance largely to pericytes before this point (Liu et al., 2002). Glial precursor cells begin to differentiate by GD11, but myelination is not seen until late embryonic and early postnatal days (Liu et al., 2002; Compston et al., 1997). These observations indicate the period from mid-gestation until birth as a critical period for brain and BBB development. Functionality of the early BBB in rat is achieved before full development of astrocytes, indicating pericytes as key players in this establishment (Daneman et al., 2010). Importantly, microglia are seen in the rat forebrain as early as GD13 (Ashwell, 1991). All of these signs point to the GD10 timepoint as having potential to influence early BBB formation, while GD20 exposure would allow assessment of an acute challenge to the established fetal BBB, with both assessed at term.

States of inflammation during gestation, such as chorioamnionitis, are well established for their negative effect on neurological outcomes in fetal development such as cerebral palsy (Shatrov et al., 2010). This maternal inflammatory state is shown to induce oxidative stress defensive mediators in the fetal brain as a means of protecting the conceptus (Beloosesky et al., 2016). The adverse neural effects

of maternal uterine inflammation during development are seen in offspring later in life with significantly higher rates of neuropsychiatric and neurobehavioral disorders like schizophrenia and autism (Ginsberg et al., 2017). Combining these factors with the acute cerebrovascular impairments we have observed with ozone, we hypothesized that this exposure model would produce distinct increased tight junction permeability and glial reactivity in the fetal brain. Our AF proteomic results proposed cerebrovascular dysfunction. Enrichment analysis of significant proteins in the GD20 low exposure group indicated a set of genes involved in cerebrovascular disorder. Two of these, OPN and TGFβ, have been discussed in reference to possible placental disfunction. TGFβ is well documented in effects on endothelial-pericyte cell adhesion via paracrine and autocrine secretion from both cell types (Seo et al., 2014). Additionally, TGFβ stimulates ECM production in pericytes resulting in upregulation of cadherin-2 in cerebral endothelial cells (Dohgu et al., 2005). Glial precursor cells have been shown to increase BBB tightness via upregulating tight junction proteins, indicating a further complexity of multi-cell type regulation in BBB integrity (Seo et al., 2014). If the acute negative fold change in TGFβ seen 24 hours after GD20 exposure holds true immediately following exposure at GD10, the effects could be drastic. Given the vital importance of the cytokine in BBB development, OPN presents an interesting role in mediation of the BBB insult response. After subarachnoid hemorrhage in rats, OPN cytokine release was induced in reactive astrocytes and capillary endothelial beds. Blockage of endogenous OPN expression exacerbated BBB disruption and neurological impairment. Further, delayed upregulation of OPN restored BBB functionality (Suzuki et al., 2010). Our results indicated a negative fold change in OPN after GD20 exposure. Alternatively, GD10 exposed animals showed increased OPN in the AF at term. These data point to an acute ozone-mediated downregulation of OPN, which if viewed from a fetal origin perspective, would suggest a negative vascular effect. While the positive OPN fold change observed ten days following GD10 exposure points to a likely compensatory upregulation, an effect proven to restore BBB functionality after subarachnoid hemorrhage in adult rats (Suzuki et al., 2010).

Both PKM1 and PKM2 are expressed in brain tissue, however PKM2 is shown to mainly have a role in embryonic tissue in humans (Zhang et al., 2019). Loss of PKM2 is shown to have an effect in limiting growth and activating innate immune response in endothelial cells, limiting endothelial proliferation and angiogenic sprouting (Stone et al., 2018). The drastic 17.0-fold decrease in PKM2 after acute ozone exposure in GD20 AF, the potential connection with fetal neurodevelopment would manifest as decreased, irregular expression of cerebral tight junction proteins and increased albumin leakage into the parenchyma at birth indicative of an impaired BBB. Additionally, the altered glucose metabolism suggested by this large negative fold change indicates distinct alteration of energy resource processing in the conceptus. We thus devised a microscopic approach that would have investigated this possibility. Yet, data from GD10 exposed animals showed that PKM levels were restored ten days after, at term, suggesting a return to normal glucose metabolism. However, a similar acute downward fold change in PKM at the GD10 critical stage would represent a significant impact on fetal BBB and overall neurodevelopment that we posited would remain evident at term.

MMP's and TIMP's are also fundamental in brain development. Significantly higher levels of MMP-2 and TIMP-1 were found in brain and spinal cord 1 week after birth compared to later in postnatal life (Ulrich et al., 2005). MMP-9 and TIMP-2 were also upregulated in brain only. The upregulation coincided with maximal extension of the transient cerebellar external granular layer, a process used to demarcate neuronal progenitor proliferation and migration. While this association has been established, the function of MMP's and their specific proteolytic substrates in brain development is poorly understood. MMP's 2 and 9 have demonstrated importance in dendritic spine development via intracellular adhesion molecule-5 and the NMDA receptor mediated pathway in hippocampal neurons (Tian et al., 2007). The acute negative fold change in MMP-2 in AF after GD20 exposure would indicate their downregulation just after ozone exposure. The subsequent positive fold changes in TIMP1

and TIMP2 in GD10 exposed animals without significant fold change in MMPs suggests a prolonged suppression of MMP activity after ozone exposure.

Two additional proteins detected in our AF proteomic assessment appear to have significant contributions in neurodevelopment. Neuropilin-1, a transmembrane protein, showed modest 1.58-fold increase. In brain, it's interaction with vascular endothelial growth factor is required for angiogenesis (Gu et al., 2003). However, interactions with interferon-gamma in the adult brain microvasculature are associated with CNS inflammatory disease, such as multiple sclerosis (Wang et al., 2016). Thus, interactions of neuropilin-1 in cerebrovascular appear to be highly complex. Much like many of the other proteins discussed, the true role of this protein in our AF results and prefacing response to ozone will need follow-up targeted assessments to fully be elucidated. Galectin-1, already discussed for its role as an established marker in preeclampsia, is shown to induce astrocyte differentiation while strongly inhibiting astrocyte proliferation in culture. Interestingly, these differentiated astrocytes then show greatly enhanced production of brain-derived neurotrophic factor, a neuroprotective polypeptide implicated in neuron proliferation, differentiation, and survival (Sasaki et al., 2004). Galectin-1 is shown to deactivate microglia via activation of multiple cell signaling pathways to protect against inflammation-induced neurodegeneration (Starossom et al., 2012; Aalinkeel and Mahajan, 2016). However, such findings have yet to be established in the fetal brain. Given the establish effect of ozone on adult microglial activation and that galectin-1 was substantially elevated in the AF of GD10 exposed dams, these findings support the alternative source of elevated galectin-1 in AF as a compensatory response to neuroinflammation in the developing fetus. The proposed targeted immunofluorescence studies are aimed at further differentiating between placental and fetal sources of the AF proteomic response to ozone.

In summary, our AF proteomic findings include fold changes in proteins imperative for proper BBB and neural development. We expect ozone exposure in dams to have induce changes in

development of cerebrovasculature in fetal brains to be tested by immunohistological analyses already used in identifying ozone-induced barrier dysfunction and glial reactivity in the adult brain. We further posit from our AF proteomic findings that a TGFβ signaling mechanism is involved, with this cytokine's multi-functionality in BBB development and diffuse influences on the ECM and vasculature. While our hypothesis of a vastly altered amniotic fluid proteome after ozone exposure was confirmed, these proteomic findings are not enough along to confirm a true preeclamptic state. Such conclusory evidence would require blood pressure readings and urinalysis from dams throughout pregnancy. However, the proposed targeted immunohistological studies will aide in distinguishing neurodevelopmental consequences of acute ozone exposure at different gestational periods, and provide a greater understanding of the AF proteomic findings initially explored in this thesis.

Figure 4.1

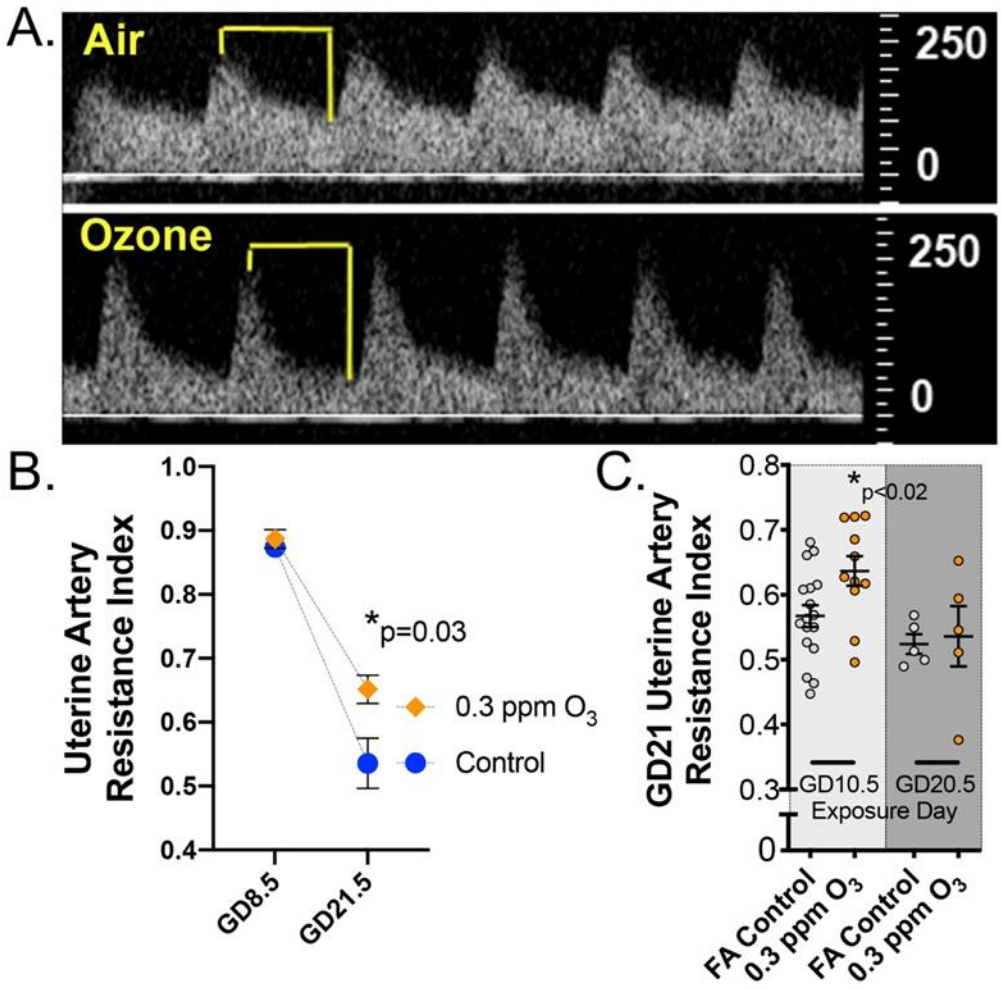

Figure 4.1 Assessing Ozone-Mediated Effects on Maternal Vascular Function: Data From Our Collaborators

(A) Uterine artery index resistance was derived based on peak systolic and trough diastolic flow ratios. **(B)** Uterine artery resistance index decreased in all dams from GD8 to GD20, but this change was diminished in dams exposed to 0.3 ppm O_3 at GD10 (n=5/group). **(C)** Examining uterine artery resistance cross-sectionally in all dams from the collected GD10 and GD20 exposure studies also revealed increased resistance in GD10-exposed dams compared to all other groups. Data is presented as mean ± SEM. Asterisks indicate significant difference between FA controls by two-way repeated measures ANOVA **(B)** or one-way ANOVA with a two-stage linear step-up procedure of Benjamini, Krieger and Yekutieli, which reveals that GD10 O_3-exposed dams have higher resistance index values compared to each other group **(C)**. This data was generated by our collaborators in the Campen Lab at New Mexico State University and is currently under review for publication in *Toxicological Sciences*.

Figure 4.2

	Rat	Human
Embryo/Fetal period	3 (Embryo) / 1 (Fetus)	1 (Embryo) / 4 (Fetus)
Implant type	Eccentric implantation	Interstitial implantation
Yolk sac placenta	The yolk sac placenta contributes special functions throughout gestation.	The yolk sac placenta is a temporary organ essential during organogenesis and degenerates at the end of the first trimester.
Chorio-allantoic placenta	Labyrinthe type ・Labyrinth zone (L) ・Syncytiotrophoblast ・Cytotrophoblast ・Basal zone (B) ・Spongiotrophoblast ・Glycogen cell ・Trophoblastic giant cell ・Decidua basalis (DB) 	Vullous type ・Fetal placenta (FP) ・Syncytiotrophoblast ・Basal plate (BP) ・Cytotrophoblastic cell column ・Interstitial trophoblast ・Endovascular trophoblast ・Decidua basalis (DB) 
Placental barrier	Maternal blood (MB) ↓ Cytotrophoblast (Cy) ↓ Syncytiotrophoblast I (SI) ↓ Syncytiotrophoblast II (SII) ↓ Basement membrane (BM) ↓ Fetal capillary (FC) ↓ Fetal blood (FB) 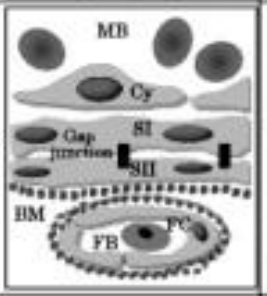	Maternal blood (MB) ↓ Syncytiotrophoblast (Sy) ↓ Basement membrane (BM) ↓ Fetal capillary (FC) ↓ Fetal blood (FB) 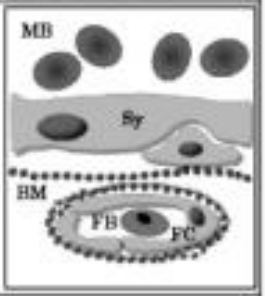
Trophoblast-associated vascular remodeling	Vascular remodeling effected by endovasucular trophoblasts in metrial gland.	Vascular remodeling effected by endovasucular and interstitial trophoblasts in metrial gland.
Placental steroidogenesis	The placenta synthesizes androgen from cholesterol. Estrogen is produced in the ovary due to the absence of aromatase.	The placenta synthesizes pregnenolone from cholesterol. Estrogen is produced in the placenta after the fetal adrenal gland converts dehydroepiandrosterone due to the absence of CYP17.
Glycoprotein hormone synthesis	Glycoprotein hormone is not produced due to not producing LH/hCG α chain.	HCG is produced in placenta.

Figure 4.2 Comparing Human and Rat Placenta for Toxicological Assessment

Assessing similarities and differences between rat and human placenta. Differing cell types in the exchange zone are highlighted along with unique barrier characteristics. Courtesy of Furukawa et al., 2011. Copyright Japanese Society of Toxicologic Pathology. License. Original text available at: https://dx.doi.org/10.1293%2Ftox.24.95

Literature Cited

Aalinkeel, R., & Mahajan, S. D. (2016). Neuroprotective role of galectin-1 in central nervous system pathophysiology. *Neural Regeneration Research, 11*(6), 896–897. https://doi.org/10.4103/1673-5374.184455

Abbott, N. J., Rönnbäck, L., & Hansson, E. (2006). Astrocyte-endothelial interactions at the blood-brain barrier. In *Nature Reviews Neuroscience*,*7*(1), 41–53. Nat Rev Neurosci. https://doi.org/10.1038/nrn1824

Adams, D. R., Ron, D., & Kiely, P. A. (2011, October 6). RACK1, A multifaceted scaffolding protein: Structure and function. Cell Communication and Signaling, Vol. 9, pp. 1–24. https://doi.org/10.1186/1478-811X-9-22

Allen, J. L., Klocke, C., Morris-Schaffer, K., Conrad, K., Sobolewski, M., & Cory-Slechta, D. A. (2017). Cognitive Effects of Air Pollution Exposures and Potential Mechanistic Underpinnings. In *Current environmental health reports*, *4*(2), 180–191. Springer. https://doi.org/10.1007/s40572-017-0134-3

Amburgey, Ö. A., Chapman, A. C., May, V., Bernstein, I. M., & Cipolla, M. J. (2010). Plasma from preeclamptic women increases blood-brain barrier permeability: Role of vascular endothelial growth factor signaling. *Hypertension*, *56*(5), 1003–1008. https://doi.org/10.1161/HYPERTENSIONAHA.110.158931

Amenta, P. S., Gay, S., Vaheri, A., & Martinez-Hernandez, A. (1986). The Extracellular Matrix is an Integrated Unit: Ultrastructural Localization of Collagen Types I, III, IV, V, VI, Fibronectin, and Laminin in Human Term Placenta. *Topics in Catalysis*, *6*(2), 125–152. https://doi.org/10.1016/S0174-173X(86)80021-8

Amiel-Tison, C., & Pettigrew, A. G. (1991). Adaptive changes in the developing brain during intrauterine stress. *Brain and Development*, *13*(2), 67–76. https://doi.org/10.1016/S0387-7604(12)80109-4

Aragón, F. M., Miranda, J. J., & Oliva, P. (2017). Particulate matter and labor supply: The role of caregiving and non-linearities. *Journal of Environmental Economics and Management*, *86*, 295–309. https://doi.org/10.1016/j.jeem.2017.02.008

Ashwell, K. (1991). The distribution of microglia and cell death in the fetal rat forebrain. *Developmental Brain Research, 58*(1), 1–12. https://doi.org/10.1016/0165-3806(91)90231-7

Balogh, A., Toth, E., Romero, R., Parej, K., Csala, D., Szenasi, N. L., Hajdu, I., Juhasz, K., Kovacs, A. F., Meiri, H., Hupuczi, P., Tarca, A. L., Hassan, S. S., Erez, O., Zavodszky, P., Matko, J., Papp, Z., Rossi, S. W., Hahn, S., … Than, N. G. (2019). Placental galectins are key players in regulating the maternal adaptive immune response. *Frontiers in Immunology*, *10*(JUN), 1240–1240. https://doi.org/10.3389/fimmu.2019.01240

Barreno, R. X., Richards, J. B., Schneider, D. J., Cromar, K. R., Nadas, A. J., Hernandez, C. B., Hallberg, L. M., Price, R. E., Hashmi, S. S., Blackburn, M. R., Haque, I. U., & Johnston, R. A. (2013). Endogenous osteopontin promotes ozone-induced neutrophil recruitment to the lungs and airway hyperresponsiveness to methacholine. *American journal of physiology. Lung cellular and molecular physiology*, *305*(2), L118–L129. https://doi.org/10.1152/ajplung.00080.2013

Barrientos, G., Freitag, N., Tirado-Gonzalez, I., Unverdorben, L., Jeschke, U., Thijssen, V., & Blois, S. (2014). Involvement of galectin-1 in reproduction: past, present and future. *Human Reproduction Update*, *20*(2), 175–193. https://doi.org/10.1093/humupd

Baschat, A. A. (2011). Neurodevelopment following fetal growth restriction and its relationship with antepartum parameters of placental dysfunction. *Ultrasound in Obstetrics and Gynecology*, *37*(5), 501–514. https://doi.org/10.1002/uog.9008

Bauer, A., Rondini, E., DeGraff, L., Hummel, K., Walker, C., & Kleeberger, S. (2009). Role of Heat Shock Protein 70 (HSP70) in O 3 -Induced Lung Inflammation. American Thoracic Society International Conference Meetings Abstracts American Thoracic Society International Conference Meetings Abstracts, A2569. https://doi.org/10.1164/ajrccm-conference.2009.179.1_meetingabstracts.a2569

Baum, L. G., Blackall, D. P., Arias-Magallano, S., Nanigian, D., Uh, S. Y., Browne, J. M., … Baldwin, G. C. (2003). Amelioration of graft versus host disease by galectin-1. *Clinical Immunology*, 109(3), 295–307. https://doi.org/10.1016/j.clim.2003.08.003

Bazzi, H., Fantauzzo, K. A., Richardson, G. D., Jahoda, C. A. B., & Christiano, A. M. (2007). Transcriptional profiling of developing mouse epidermis reveals novel patterns of coordinated gene expression. *Developmental Dynamics, 236*(4), 961–970. https://doi.org/10.1002/dvdy.21099

Becerra, T. A., Wilhelm, M., Olsen, J., Cockburn, M., & Ritz, B. (2013). Ambient air pollution and autism in Los Angeles County, California. *Environmental Health Perspectives*, *121*(3), 380–386. https://doi.org/10.1289/ehp.1205827

Beloosesky, R., Khatib, N., Ginsberg, Y., Anabosy, S., Shalom-Paz, E., Dahis, M., Ross, M. G., & Weiner, Z. (2016). Maternal magnesium sulfate fetal neuroprotective effects to the fetus: inhibition of neuronal nitric oxide synthase and nuclear factor kappa-light-chain-enhancer of activated B cells activation in a rodent model. *American Journal of Obstetrics and Gynecology, 215*(3), 382.e1-382.e6. https://doi.org/10.1016/j.ajog.2016.03.032

Ben-Zvi, A., Lacoste, B., Kur, E., Andreone, B. J., Mayshar, Y., Yan, H., & Gu, C. (2014). Mfsd2a is critical for the formation and function of the blood-brain barrier. *Nature*, *509*(7501), 507–511. https://doi.org/10.1038/nature13324

Berryman, M., Gary, R., & Bretscher, A. (1995). Ezrin oligomers are major cytoskeletal components of placental microvilli: a proposal for their involvement in cortical morphogenesis. *The Journal of cell biology*, *131*(5), 1231–1242. https://doi.org/10.1083/jcb.131.5.1231

Bertaggia, E., Scabia, G., Dalise, S., Lo Verso, F., Santini, F., Vitti, P., Chisari, C., Sandri, M., & Maffei, M. (2014). Haptoglobin is required to prevent oxidative stress and muscle atrophy. *PLuS ONE, 9*(6). https://doi.org/10.1371/journal.pone.0100745

Bolton, J. L., Marinero, S., Hassanzadeh, T., Natesan, D., Le, D., Belliveau, C., Mason, S. N., Auten, R. L., & Bilbo, S. D. (2017). Gestational Exposure to Air Pollution Alters Cortical Volume, Microglial Morphology, and Microglia-Neuron Interactions in a Sex-Specific Manner. *Frontiers in Synaptic Neuroscience*, *9*(MAY), 10. https://doi.org/10.3389/fnsyn.2017.00010

Bolton, J. L., Smith, S. H., Huff, N. C., Gilmour, M. I., Foster, W. M., Auten, R. L., & Bilbo, S. D. (2012). Prenatal air pollution exposure induces neuroinflammation and predisposes offspring to weight gain in adulthood in a sex-specific manner. *The FASEB Journal*, *26*(11), 4743–4754. https://doi.org/10.1096/fj.12-210989

Brew, K., Dinakarpandian, D., & Nagase, H. (2000). Tissue inhibitors of metalloproteinases: Evolution, structure and function. In *Biochimica et Biophysica Acta - Protein Structure and Molecular Enzymology*, *1477*(1–2), 267–283. Elsevier. https://doi.org/10.1016/S0167-4838(99)00279-4

Brown, L. F., Berse, B., Van De Water, L., Papadopoulos-Sergiou, A., Perruzzi, C. A., Manseau, E. J., Dvorak, H. F., & Senger, D. R. (1992). Expression and Distribution of Osteopontin in Human

Tissues: Widespread Association with Luminal Epithelial Surfaces. In *Molecular Biology of the Cell* (Vol. 3).

Browne, V. A., Julian, C. G., Toledo-Jaldin, L., Cioffi-Ragan, D., Vargas, E., & Moore, L. G. (2015). Uterine artery blood flow, fetal hypoxia and fetal growth. Philosophical Transactions of the Royal Society B: Biological Sciences, Vol. 370. https://doi.org/10.1098/rstb.2014.0068

Burghardt, R. C., Johnson, G. A., Jaeger, L. A., Ka, H., Garlow, J. E., Spencer, T. E., & Bazer, F. W. (2002). Integrins and extracellular matrix proteins at the maternal-fetal interface in domestic animals. *Cells Tissues Organs*, *172*(3), 202–217. https://doi.org/10.1159/000066969

Burton, G. J., Woods, A. W., Jauniaux, E., & Kingdom, J. C. P. (2009). Rheological and Physiological Consequences of Conversion of the Maternal Spiral Arteries for Uteroplacental Blood Flow during Human Pregnancy. *Placenta*, *30*(1), 473–482. https://reader.elsevier.com/reader/sd/pii/S0143400409000666?token=A03B6A90B9A0D9DA065AB22DD5B043C4C57BBEB62F73D047293CA12F30AAE52010845B804E4E2EC1843036EB4448B9C8

Bushway, M. E., Gerber, S. A., Fenton, B. M., Miller, R. K., Lord, E. M., & Murphy, S. P. (2014). Morphological and Phenotypic Analyses of the Human Placenta Using Whole Mount Immunofluorescence1. *Biology of Reproduction*, *90*(5). https://doi.org/10.1095/biolreprod.113.115915

Cabrera-Fuentes, H. A., Ruiz-Meana, M., Simsekyilmaz, S., Kostin, S., Inserte, J., Saffarzadeh, M., … Preissner, K. T. (2014). RNase1 prevents the damaging interplay between extracellular RNA and tumour necrosis factor-α in cardiac ischaemia/reperfusion injury. *Thrombosis and Haemostasis*, 112(6), 1110–1119. https://doi.org/10.1160/TH14-08-0703

Calderon-Garcidueñas, L., Rodriguez-Alcaraz, A., Garcia, R., Sanchez, G., Barragan, G., Camacho, R., & Ramirez, L. (1994). Human nasal mucosal changes after exposure to urban pollution. *Environmental Health Perspectives*, *102*(12), 1074–1080. https://doi.org/10.1289/ehp.102-1567497

Carson, D. D., Lagow, E., Thathiah, A., Al-Shami, R., Farach-Carson, M. C., Vernon, M., Yuan, L., Fritz, M. A., & Lessey, B. (2002). Changes in gene expression during the early to mid-luteal (receptive phase) transition in human endometrium detected by high-density microarray screening. *Molecular human reproduction*, *8*(9), 871–879. https://doi.org/10.1093/molehr/8.9.871

Chaiworapongsa, T., Erez, O., Kusanovic, J. P., Vaisbuch, E., Mazaki-Tovi, S., Gotsch, F., … Romero, R. (2008). Amniotic fluid heat shock protein 70 concentration in histologic chorioamnionitis, term and preterm parturition. *Journal of Maternal-Fetal and Neonatal Medicine*, 21(7), 449–461. https://doi.org/10.1080/14767050802054550

Chen, C. P., & Aplin, J. D. (2003). Placental extracellular matrix: Gene expression, deposition by placental fibroblasts and the effect of oxygen. *Placenta*, *24*(4), 316–325. https://doi.org/10.1053/plac.2002.0904

Cheung, C. Y., & Brace, R. A. (2020). Altered proteomics profile in the amnion of patients with oligohydramnios. *Physiological Reports, 8*(4). https://doi.org/10.14814/phy2.14381

Choi, J. S., Park, H. J., Cha, J. H., Chung, J. W., Chun, M. H., & Lee, M. Y. (2003). Induction and temporal changes of osteopontin mRNA and protein in the brain following systemic lipopolysaccharide injection. *Journal of neuroimmunology*, *141*(1-2), 65–73. https://doi.org/10.1016/s0165-5728(03)00223-6

Chuang, G. C., Yang, Z., Westbrook, D. G., Pompilius, M., Ballinger, C. A., White, C. R., Krzywanski, D. M., Postlethwait, E. M., & Ballinger, S. W. (2009). Pulmonary ozone exposure induces vascular dysfunction, mitochondrial damage, and atherogenesis. *Am J Physiol Lung Cell Mol Physiol*, *297*, 209–216. https://doi.org/10.1152/ajplung.00102.2009

Chuang, K. J., Chan, C. C., Su, T. C., Lee, C. T., & Tang, C. S. (2007). The effect of urban air pollution on inflammation, oxidative stress, coagulation, and autonomic dysfunction in young adults. *American journal of respiratory and critical care medicine*, *176*(4), 370–376. https://doi.org/10.1164/rccm.200611-1627OC

Churg, A., Zhou, S., Preobrazhenska, O., Tai, H., Wang, R., & Wright, J. L. (2009). Expression of profibrotic mediators in small airways versus parenchyma after cigarette smoke exposure. *American Journal of Respiratory Cell and Molecular Biology, 40*(3), 268–276. https://doi.org/10.1165/rcmb.2007-0367OC

Coker, R. K., Laurent, G. J., Shahzeidi, S., Lympany, P. A., Du Bois, R. M., Jeffery, P. K., & McAnulty, R. J. (1997). Transforming growth factors-β1, -β2, and -β3 stimulate fibroblast procollagen production in vitro but are differentially expressed during bleomycin-induced lung fibrosis. *American Journal of Pathology, 150*(3), 981–991. /pmc/articles/PMC1857875/?report=abstract

Compston, A., Zajicek, J., Sussman, J., Webb, A., Hall, G., Muir, D., Shaw, C., Wood, A., & Scolding, N. (1997). Review: Glial lineages and myelination in the central nervous system. Journal of Anatomy, 190(2), 161–200. https://doi.org/10.1046/j.1469-7580.1997.19020161.x

Corradi, M., Alinovi, R., Goldoni, M., Vettori, M. V., Folesani, G., Mozzoni, P., Cavazzini, S., Bergamaschi, E., Rossi, L., & Mutti, A. (2002). Biomarkers of oxidative stress after controlled human exposure to ozone. *Toxicology Letters*, *134*(1–3), 219–225. https://doi.org/10.1016/S0378-4274(02)00169-8

Cortes, D. F., Landis, M. K., & Ottens, A. K. (2012). High-capacity peptide-centric platform to decode the proteomic response to brain injury. *Electrophoresis*, *33*(24), 3712–3719. https://doi.org/10.1002/elps.201200341

Cotechini, T., Komisarenko, M., Sperou, A., Macdonal-Goodfellow, S., Adams, M. A., & Graham, C. H. (2014). Inflammation in rat pregnancy inhibits spiral artery remodeling leading to fetal growth restriction and features of preeclampsia. *Journal of Experimental Medicine*, *211*(1), 165–179. https://doi.org/10.1084/jem.20130295

Courchesne, E., Press, G. A., & Yeung-Courchesne, R. (1993). Parietal lobe abnormalities detected with MR in patients with infantile autism. *American Journal of Roentgenology*, *160*(2), 387–393. https://doi.org/10.2214/ajr.160.2.8424359

D'Angiulli, A. (2018). Severe Urban Outdoor Air Pollution and Children's Structural and Functional Brain Development, From Evidence to Precautionary Strategic Action. *Frontiers in Public Health*, *6*, 95. https://doi.org/10.3389/fpubh.2018.00095

Daneman, R. (2012). The blood-brain barrier in health and disease. *Annals of Neurology*, *72*(5), 648–672. https://doi.org/10.1002/ana.23648

Daneman, R., Zhou, L., Kebede, A. A., & Barres, B. A. (2010). Pericytes are required for blood-brain barrier integrity during embryogenesis. *Nature*, *468*(7323), 562–566. https://doi.org/10.1038/nature09513

Dave, J. M., Kang, H., Abbey, C. A., Maxwell, S. A., & Bayless, K. J. (2013). Proteomic profiling of endothelial invasion revealed receptor for activated C kinase 1 (RACK1) complexed with vimentin to regulate focal adhesion kinase (FAK). *Journal of Biological Chemistry*, 288(42), 30720–30733. https://doi.org/10.1074/jbc.M113.512467

de Jager, C. A., Linton, E. A., Spyropoulou, I., Sargent, I. L., & Redman, C. W. G. (2003). Matrix metalloprotease-9, placental syncytiotrophoblast and the endothelial dysfuntion of pre-eclampsia. *Placenta*, *24*(1), 84–91. https://doi.org/10.1053/plac.2002.0871

De Rijk, E. P. C. T., Esch, E. Van, & Flik, G. (2002). Pregnancy Dating in the Rat: Placental Morphology and Maternal Blood Parameters, *Toxicologic Pathology, 30*(2).

Derzsy, Z., Prohászka, Z., Rigó, J., Jr, Füst, G., & Molvarec, A. (2010). Activation of the complement system in normal pregnancy and preeclampsia. *Molecular immunology*, *47*(7-8), 1500–1506. https://doi.org/10.1016/j.molimm.2010.01.021

Distler, U., Kuharev, J., Navarro, P., & Tenzer, S. (2016). Label-free quantification in ion mobility-enhanced data-independent acquisition proteomics. *Nature protocols*, *11*(4), 795–812. https://doi.org/10.1038/nprot.2016.042

Dohgu, S., Takata, F., Yamauchi, A., Nakagawa, S., Egawa, T., Naito, M., Tsuruo, T., Sawada, Y., Niwa, M., & Kataoka, Y. (2005). Brain pericytes contribute to the induction and up-regulation of blood-brain barrier functions through transforming growth factor-β production. *Brain Research, 1038*(2), 208–215. https://doi.org/10.1016/j.brainres.2005.01.027

Duley, L. (2009). The Global Impact of Pre-eclampsia and Eclampsia. In *Seminars in Perinatology*, 33(3), 130–137. https://doi.org/10.1053/j.semperi.2009.02.010

Eiland, E., Nzerue, C., & Faulkner, M. (2012). Preeclampsia 2012. *Journal of Pregnancy*, *2012*(1), 1–7. https://doi.org/10.1155/2012/586578

Enders, A. C., & Blankenship, T. N. (1999). Comparative placental structure. *Advanced Drug Delivery Reviews, 38(*1), 3–15. https://doi.org/10.1016/S0169-409X(99)00003-4

Endeshaw, G., & Berhan, Y. (2015). *Perinatal Outcome in Women with Hypertensive Disorders of Pregnancy: A Retrospective Cohort Study*. *2015*(208043), 1–8. https://doi.org/10.1155/2015/208043

Erickson, M. A., Jude, J., Zhao, H., Rhea, E. M., Salameh, T. S., Jester, W., Pu, S., Harrowitz, J., Nguyen, N., Banks, W. A., Panettieri, R. A., & Jordan-Sciutto, K. L. (2017). Serum amyloid A: an ozone-induced circulating factor with potentially important functions in the lung-brain axis. *The FASEB Journal*, *31*(9), 3950–3965. https://doi.org/10.1096/fj.201600857RRR

Fang, X., Xiao, H., Sun, H., Liu, C., Zhang, Z., Xie, Y., Liang, Y., & Wang, F. (2020). Characteristics of Ground-Level Ozone from 2015 to 2018 in BTH Area, China. *Atmosphere*, *11*(2), 130. https://doi.org/10.3390/atmos11020130

Fonseca, B. M., Correia-da-Silva, G., & Teixeira, N. A. (2012). The rat as an animal model for fetoplacental development: A reappraisal of the post-implantation period. In *Reproductive Biology*, 12(2), 97–118. Elsevier B.V. https://doi.org/10.1016/S1642-431X(12)60080-1

Fox, G. E., Van Wesep, R., Resau, J. H., & Sun, C. C. (1991). The effect of immersion formaldehyde fixation on human placental weight. *Archives of pathology & laboratory medicine*, *115*(7), 726–728.

Frampton, M. W., Pryor, W. A., Cueto, R., Cox, C., Morrow, P. E., & Utell, M. J. (1999). Ozone Exposure Increases Aldehydes in Epithelial Lining Fluid in Human Lung. In *Am J Respir Crit Care Med*, 159. www.atsjournals.org

Freitag, N., Tirado-Gonzaĺez, I., Barrientos, G., Herse, F., Thijssen, V. L. J. L., Weedon-Fekjær, S. M., … Blois, S. M. (2013). Interfering with Gal-1-mediated angiogenesis contributes to the pathogenesis of preeclampsia. *Proceedings of the National Academy of Sciences of the United States of America*, *110*(28), 11451–11456. https://doi.org/10.1073/pnas.1303707110

Furukawa, S., Hayashi, S., Usuda, K., Abe, M., Hagio, S., & Ogawa, I. (2011). Toxicological pathology in the rat placenta. In *Journal of Toxicologic Pathology*, *24*(2), 95–111. The Japanese Society of Toxicologic Pathology. https://doi.org/10.1293/tox.24.95

Furukawa, S., Tsuji, N., & Sugiyama, A. (2019). Morphology and physiology of rat placenta for toxicological evaluation. In *Journal of Toxicologic Pathology*, *32*(1), 1–17. Japanese Society of Toxicologic Pathology. https://doi.org/10.1293/TOX.2018-0042

Gabinskaya, T., Salafia, C. M., Gulle, V. E., Holzman, I. R., & Weintraub, A. S. (2011). Gestational Age-Dependent Extravillous Cytotrophoblast Osteopontin Immunolocalization Differentiates Between Normal and Preeclamptic Pregnancies. *American Journal of Reproductive Immunology*, *40*(5), 175–193. https://doi.org/10.1111/j.1600-0897.1998.tb00063.x

Gackière, F., Saliba, L., Baude, A., Bosler, O., & Strube, C. (2011). Ozone inhalation activates stress-responsive regions of the CNS. *Journal of Neurochemistry*, *117*(6), 961–972. https://doi.org/10.1111/j.1471-4159.2011.07267.x

Galewska, Z., Bańkowski, E., Romanowicz, L., & Jaworski, S. (2003). Pre-eclampsiaa (EPH-gestosis)-induced decrease of MMP-s content in the umbilical cord artery. *Clinica Chimica Acta*, *335*(1–2), 109–115. https://doi.org/10.1016/S0009-8981(03)00296-1

Gallo, S., & Manfrini, N. (2015). Working hard at the nexus between cell signaling and the ribosomal machinery: An insight into the roles of RACK1 in translational regulation. *Translation, 3*(2), e1120382. https://doi.org/10.1080/21690731.2015.1120382

Garantziotis, S., Li, Z., Potts, E. N., Lindsey, J. Y., Stober, V. P., Polosukhin, V. V., Blackwell, T. S., Schwartz, D. A., Foster, W. M., & Hollingsworth, J. W. (2010). TLR4 is necessary for hyaluronan-mediated airway hyperresponsiveness after ozone inhalation. *American Journal of Respiratory and Critical Care Medicine*, *181*(7), 666–675. https://doi.org/10.1164/rccm.200903-0381OC

Geer, L. A., Weedon, J., & Bell, M. L. (2012). Ambient air pollution and term birth weight in Texas from 1998 to 2004. *Journal of the Air and Waste Management Association*, *62*(11), 1285–1295. https://doi.org/10.1080/10962247.2012.707632

Geng, R., Jia, Y., Chi, M., Wang, Z., Liu, H., & Wang, W. (2019). RNase1 alleviates the Aeromonas hydrophila-induced oxidative stress in blunt snout bream. *Developmental and comparative immunology*, *91*, 8–16. https://doi.org/10.1016/j.dci.2018.09.018

Ghulmiyyah, L., & Sibai, B. (2012). Maternal Mortality From Preeclampsia/Eclampsia. In *Seminars in Perinatology*, *36*(1), 56–59. W.B. Saunders. https://doi.org/10.1053/j.semperi.2011.09.011

Ginsberg, Y., Khatib, N., Weiner, Z., & Beloosesky, R. (2017). Maternal Inflammation, Fetal Brain Implications and Suggested Neuroprotection: A Summary of 10 Years of Research in Animal Models. *Rambam Maimonides Medical Journal, 8*(2), e0028. https://doi.org/10.5041/rmmj.10305

Goldsmith, L. T., & Weiss, G. (2009). Relaxin in human pregnancy. Annals of the New York Academy of Sciences, 1160, 130–135. https://doi.org/10.1111/j.1749-6632.2008.03800.x

González-Guevara, E., Martínez-Lazcano, J. C., Custodio, V., Hernández-Cerón, M., Rubio, C., & Paz, C. (2014). Exposure to ozone induces a systemic inflammatory response: Possible source of the neurological alterations induced by this gas. *Inhalation Toxicology*, *26*(8), 485–491. https://doi.org/10.3109/08958378.2014.922648

Gupta, A., Agarwal, R., & Shukla, G. S. (1999). Functional impairment of blood ± brain barrier following pesticide exposure during early development in rats. *Human & Experimental Toxicology*, *18*(1), 174–179. http://www.stockton-press.co.uk/het

Gurtner, G. C., Davis, V., Li, H., McCoy, M. J., Sharpe, A., & Cybulsky, M. I. (1995). Targeted disruption of the murine VCAM1 gene: Essential role of VCAM-1 in chorioallantoic fusion and placentation. *Genes and Development, 9*(1), 1–14. https://doi.org/10.1101/gad.9.1.1

Gu, C., Rodriguez, E. R., Reimert, D. V., Shu, T., Fritzsch, B., Richards, L. J., Kolodkin, A. L., & Ginty, D. D. (2003). Neuropilin-1 conveys semaphorin and VEGF signaling during neural and cardiovascular development. *Developmental cell*, *5*(1), 45–57. https://doi.org/10.1016/s1534-5807(03)00169-2

Hallmann, R., Horn, N., Selg, M., Wendler, O., Pausch, F., & Sorokin, L. M. (2005). Expression and function of laminins in the embryonic and mature vasculature. *Physiological Reviews*, *85*(3), 979–1000. American Physiological Society. https://doi.org/10.1152/physrev.00014.2004

Hamza, A., Herr, D., Solomayer, E. F., & Meyberg-Solomayer, G. (2013, December 21). Polyhydramnios: Causes, diagnosis and therapy. Geburtshilfe Und Frauenheilkunde, Vol. 73, pp. 1241–1246. https://doi.org/10.1055/s-0033-1360163

Håversen, L., Sundelin, J. P., Mardinoglu, A., Rutberg, M., Ståhlman, M., Wilhelmsson, U., Hultén, L. M., Pekny, M., Fogelstrand, P., Bentzon, J. F., Levin, M., & Borén, J. (2018). Vimentin deficiency in macrophages induces increased oxidative stress and vascular inflammation but attenuates atherosclerosis in mice. *Scientific Reports, 8*(1), 1–13. https://doi.org/10.1038/s41598-018-34659-2

Hellström, M., Kalén, M., Lindahl, P., Abramsson, A., & Betsholtz, C. (1999). Role of PDGF-B and PDGFR-β in recruitment of vascular smooth muscle cells and pericytes during embryonic blood vessel formation in the mouse. Development, 126(14), 3047–3055.

Herington, J. L., & Bany, B. M. (2007). The conceptus increases secreted phosphoprotein 1 gene expression in the mouse uterus during the progression of decidualization mainly due to its effects on uterine natural killer cells. *Reproduction*, *133*(6), 1213–1221. https://doi.org/10.1530/REP-07-0085

Hirashima, C., Ohkuchi, A., Nagayama, S., Suzuki, H., Takahashi, K., Ogoyama, M., Takahashi, H., Shirasuna, K., & Matsubara, S. (2018). Galectin-1 as a novel risk factor for both gestational hypertension and preeclampsia, specifially its expression at a low level in the second trimester and a high level after onset. *Hypertension Research*, *41*, 45–52. https://doi.org/10.1038/hr.2017.85

Hu, D., & Cross, J. C. (2010). Development and function of trophoblast giant cells in the rodent placenta. *International Journal of Developmental Biology*, *54*(2–3), 341–354. https://doi.org/10.1387/ijdb.082768dh

Huang, Z. F., Higuchi, D., Lasky, N., & Broze, G. J. (1997). Tissue factor pathway inhibitor gene disruption produces intrauterine lethality in mice. *Blood*, 90(3), 944–951. https://doi.org/10.1182/blood.V90.3.944

Hubel, C. A. (1999). Oxidative Stress in the Pathogenesis of Preeclampsia. *Proceedings of the Society for Experimental Biology and Medicine*, *222*(3), 222–235. http://ebm.rsmjournals.com/content/222/3/222#BIBLhttp://ebm.rsmjournals.com/content/222/3/222%23otherarticleshttp://ebm.rsmjournals.com/

Huisman, M. A., Timmer, A., Zeinstra, M., Serlier, E. K., Hanemaaijer, R., Goor, H. V., & Erwich, J. J. H. M. (2004). Matrix-metalloproteinase activity in first trimester placental bed biopsies in further complicated and uncomplicated pregnancies. *Placenta*, *25*(4), 253–258. https://doi.org/10.1016/j.placenta.2003.10.006

Huppertz, B., Kertschanska, S., Demir, A. Y., Frank, H. G., & Kaufmann, P. (1997). Immunohistochemistry of matrix metalloproteinases (MMP), their substrates, and their inhibitors (TIMP) during trophoblast invasion in the human placenta. *Cell and Tissue Research*, *291*(1), 133–148. https://doi.org/10.1007/s004410050987

Hynes, R. O. (1987). Integrins: A family of cell surface receptors. *Cell*, *48*(4), 549–554. https://doi.org/10.1016/0092-8674(87)90233-9

Iadecola, C. (2017). The Neurovascular Unit Coming of Age: A Journey through Neurovascular Coupling in Health and Disease. *Neuron*, *96*(1), 17–42. Cell Press. https://doi.org/10.1016/j.neuron.2017.07.030

Ilkbahar, Y. N., Southard, J. N., & Talamantes, F. (1999). Transcriptional upregulation of hepatic GH receptor and GH-binding protein expression during pregnancy in the mouse. *Journal of Molecular Endocrinology*, *23*(1), 85–96. https://doi.org/10.1677/jme.0.0230085

Isaka, K., Usuda, S., Ito, H., Sagawa, Y., Nakamura, H., Nishi, H., Suzuki, Y., Li, Y. F., & Takayama, M. (2003). Expression and activity of matrix metalloproteinase 2 and 9 in human trophoblasts. *Placenta*, *24*(1), 53–64. https://doi.org/10.1053/plac.2002.0867

Jawerbaum, A., & José López-Costa, J. (2005). Increased matrix metalloproteinases 2 and 9 in placenta of diabetic rats at midgestation. https://doi.org/10.1016/j.placenta.2004.06.011

Jiang, W., & Bond, J. S. (1992). Families of metalloendopeptidases and their relationships. In *FEBS Letters*, *312*(2–3), 110–114. John Wiley & Sons, Ltd. https://doi.org/10.1016/0014-5793(92)80916-5

Johnson, E. (2017). Cars and ground-level ozone: how do fuels compare? *European Transport Research Review*, *9*(47), 1–13. https://doi.org/10.1007/s12544-017-0263-7

Johnson, G. A., Burghardt, R. C., & Bazer, F. W. (2014). Osteopontin: A leading candidate adhesion molecule for implantation in pigs and sheep. In *Journal of Animal Science and Biotechnology*, *5*(1), 1–14. BioMed Central Ltd. https://doi.org/10.1186/2049-1891-5-56

Johnson, G. A., Burghardt, R. C., Bazer, F. W., & Spencer, T. E. (2003). Osteopontin: Roles in Implantation and Placentation. *Biology of Reproduction*, *69*(5), 1458–1471. https://doi.org/10.1095/biolreprod.103.020651

Jollie, W. P. (1964). Fine structural changes in placental labyrinth of the rat with increasing gestational age. *Journal of Ultrasructure Research*, *10*(1–2), 27–47. https://doi.org/10.1016/S0022-5320(64)90018-8

Jung, C. R., Lin, Y. T., & Hwang, B. F. (2015). Ozone, particulate matter, and newly diagnosed Alzheimer's disease: A population-based cohort study in Taiwan. *Journal of Alzheimer's Disease*, *44*(2), 573–584. https://doi.org/10.3233/JAD-140855

Kafoury, R. M., Pryor, W. A., Squadrito, G. L., Salgo, M. G., Zou, X., & Friedman, M. (1999). Induction of inflammatory mediators in human airway epithelial cells by lipid ozonation products. *American Journal of Respiratory and Critical Care Medicine*, *160*(6), 1934–1942. https://doi.org/10.1164/ajrccm.160.6.9902025

Kampfrath, T., Maiseyeu, A., Ying, Z., Shah, Z., Deiuliis, J. A., Xu, X., Kherada, N., Brook, R. D., Reddy, K. M., Padture, N. P., Parthasarathy, S., Chen, L. C., Moffatt-Bruce, S., Sun, Q., Morawietz, H., & Rajagopalan, S. (2011). Chronic fine particulate matter exposure induces systemic vascular dysfunction via NADPH oxidase and TLR4 pathways. *Circulation Research*, *108*(6), 716–726. https://doi.org/10.1161/CIRCRESAHA.110.237560

Kao, L. C., Tulac, S., Lobo, S., Imani, B., Yang, J. P., Germeyer, A., Osteen, K., Taylor, R. N., Lessey, B. A., & Giudice, L. C. (2002). Global gene profiling in human endometrium during the window of implantation. *Endocrinology*, *143*(6), 2119–2138. https://doi.org/10.1210/endo.143.6.8885

Katre, A., Ballinger, C., Akhter, H., Fanucchi, M., Kim, D. K., Postlethwait, E., & Liu, R. M. (2011). Increased transforming growth factor beta 1 expression mediates ozone-induced airway fibrosis in mice. *Inhalation Toxicology, 23*(8), 486–494. https://doi.org/10.3109/08958378.2011.584919

Kaur, C., Rathnasamy, G., & Ling, E.-A. (2017). Biology of Microglia in the Developing Brain. *Journal of Neuropathology & Experimental Neurology*, *76*(9), 736–753. https://doi.org/10.1093/JNEN/NLX056

Kavlock, R., Daston, G., & Grabowski, C. T. (1979). Studies on the developmental toxicity of ozone. I. Prenatal effects. *Toxicology and Applied Pharmacology*, *48*(1 PART 1), 19–28. https://doi.org/10.1016/S0041-008X(79)80004-6

Kim, J., Erikson, D. W., Burghardt, R. C., Spencer, T. E., Wu, G., Bayless, K. J., Johnson, G. A., & Bazer, F. W. (2010). Secreted phosphoprotein 1 binds integrins to initiate multiple cell signaling pathways, including FRAP1/mTOR, to support attachment and force-generated migration of trophectoderm cells. *Matrix Biology*, *29*(5), 369–382. https://doi.org/10.1016/j.matbio.2010.04.001

Kim, M. S., Yu, J. H., Lee, M. Y., Kim, A. L., Jo, M. H., Kim, M. G., Cho, S. R., & Kim, Y. H. (2016). Differential expression of extracellular matrix and adhesion molecules in fetal-origin amniotic epithelial cells of preeclamptic pregnancy. *Plus One, 11*(5). https://doi.org/10.1371/journal.pone.0156038

Kim, Y.-H., Hwang, H.-S., Kim, Y.-T., Kim, H.-S., & Park, Y.-W. (2008). Modulation of matrix metalloproteinase secretion by adenosine A3 receptor in preeclamptic villous explants. *Reproductive Sciences (Thousand Oaks, Calif.)*, *15*(9), 939–949. https://doi.org/10.1177/1933719108322431

Kimmins, S., Lim, H. C., & MacLaren, L. A. (2004). Immunohistochemical localization of integrin alpha V beta 3 and osteopontin suggests that they do not interact during embryo implantation in ruminants. *Reproductive Biology and Endocrinology, 2*, 19. https://doi.org/10.1186/1477-7827-2-19

Kioumourtzoglou, M. A., Schwartz, J. D., Weisskopf, M. G., Melly, S. J., Wang, Y., Dominici, F., & Zanobetti, A. (2016). Long-term PM2.5 exposure and neurological hospital admissions in the northeastern United States. *Environmental Health Perspectives*, *124*(1), 23–29. https://doi.org/10.1289/ehp.1408973

Kirrane, E. F., Bowman, C., Davis, J. A., Hoppin, J. A., Blair, A., Chen, H., Patel, M. M., Sandler, D. P., Tanner, C. M., Vinikoor-Imler, L., Ward, M. H., Luben, T. J., & Kamel, F. (2015). Associations of ozone and PM2.5 concentrations with Parkinson's disease among participants in the agricultural health study. *Journal of Occupational and Environmental Medicine*, *57*(5), 509–517. https://doi.org/10.1097/JOM.0000000000000451

Klein, T., & Bischoff, R. (2011). Physiology and pathophysiology of matrix metalloproteases. *Amino Acids*, Vol. 41, pp. 271–290. https://doi.org/10.1007/s00726-010-0689-x

Kling, D., Fingerle, J., & Harlan, J. M. (1992). Inhibition of leukocyte extravasation with a monoclonal antibody to CD18 during formation of experimental intimal thickening in rabbit carotid arteries. *Arteriosclerosis and Thrombosis*, *12*(9), 997–1007. https://doi.org/10.1161/01.atv.12.9.997

Kumano-Kuramochi, M., Shimozu, Y., Wakita, C., Ohnishi-Kameyama, M., Shibata, T., Matsunaga, S., Takano-Ishikawa, Y., Watanabe, J., Goto, M., Xie, Q., Komba, S., Uchida, K., & Machida, S. (2012). Identification of 4-hydroxy-2-nonenal-histidine adducts that serve as ligands for human lectin-like oxidized LDL receptor-1. *Biochemical Journal*, *442*(1), 171–180. https://doi.org/10.1042/BJ20111029

Lafontaine, L., Chaudhry, P., Lafleur, M.-J., Van Themsche, C., Soares, M. J., & Asselin, E. (2011). Transforming Growth Factor Beta Regulates Proliferation and Invasion of Rat Placental Cell Lines1. *Biology of Reproduction, 84*(3), 553–559. https://doi.org/10.1095/biolreprod.110.086348

Lavee, M., Goldman, S., Daniel-Spiegel, E., & Shalev, E. (2009). Matrix metalloproteinase-2 is elevated in midtrimester amniotic fluid prior to the development of preeclampsia. *Reproductive Biology and Endocrinology*, 7, 85. https://doi.org/10.1186/1477-7827-7-85

Lekgabe, E. D., Royce, S. G., Hewitson, T. D., Tang, M. L. K., Zhao, C., Xiao, L. M., Tregear, G. W., Bathgate, R. A. D., Du, X. J., & Samuel, C. S. (2006). The effects of relaxin and estrogen deficiency on collagen deposition and hypertrophy of nonreproductive organs. *Endocrinology, 147*(12), 5575–5583. https://doi.org/10.1210/en.2006-0533

Leung, L. L. K., & Morser, J. (2018). Carboxypeptidase B2 and carboxypeptidase N in the crosstalk between coagulation, thrombosis, inflammation, and innate immunity. *Journal of Thrombosis and Haemostasis*, *16*(8), 1474–1486. https://doi.org/10.1111/jth.14199

Lippmann, E. S., Azarin, S. M., Kay, J. E., Nessler, R. A., Wilson, H. K., Al-Ahmad, A., Palecek, S. P., & Shusta, E. V. (2012). Derivation of blood-brain barrier endothelial cells from human pluripotent stem cells. *Nature Biotechnology*, *30*(8), 783–791. https://doi.org/10.1038/nbt.2247

Li, Z., Potts-Kant, E. N., Garantziotis, S., Foster, W. M., & Hollingsworth, J. W. (2011). Hyaluronan signaling during ozone-induced lung injury requires TLR4, MyD88, and TIRAP. *PLuS ONE, 6*(11). https://doi.org/10.1371/journal.pone.0027137

Liu, R. M. (2008). Oxidative stress, plasminogen activator inhibitor 1, and lung fibrosis. *Antioxidants and Redox Signaling, 10*(2), 303–319. Antioxid Redox Signal. https://doi.org/10.1089/ars.2007.1903

Liu, J., Wang, X. P., Cho, S., Lim, B. K., Irwin, D. M., Ryder, O. A., Yu, L. (2014). Evolutionary and functional novelty of pancreatic ribonuclease: A study of musteloidea (order Carnivora). Scientific Reports, 4(1), 1–11. https://doi.org/10.1038/srep05070

Liu, X., Zhao, W., Liu, H., Kang, Y., Ye, C., Gu, W., Hu, R., & Li, X. (2016). Developmental and Functional Brain Impairment in Offspring from Preeclampsia-Like Rats. *Molecular Neurobiology*, *53*(2), 1009–1019. https://doi.org/10.1007/s12035-014-9060-7

Liu, Y., Wu, Y., Lee, J. C., Xue, H., Pevny, L. H., Kaprielian, Z., & Rao, M. S. (2002). Oligodendrocyte and astrocyte development in rodents: An in situ and immunohistological analysis during embryonic development. *GLIA, 40*(1), 25–43. https://doi.org/10.1002/glia.10111

Liu, J., Wang, X. P., Cho, S., Lim, B. K., Irwin, D. M., Ryder, O. A., … Yu, L. (2014). Evolutionary and functional novelty of pancreatic ribonuclease: A study of musteloidea (order Carnivora). *Scientific Reports*, *4*(1), 1–11. https://doi.org/10.1038/srep05070

Lomax, J. E., Eller, C. H., & Raines, R. T. (2017). Comparative functional analysis of ribonuclease 1 homologs: Molecular insights into evolving vertebrate physiology. *Biochemical Journal*, 474(13), 2219–2233. https://doi.org/10.1042/BCJ20170173

Lu, L., Li, J., Moussaoui, M., & Boix, E. (2018). Immune modulation by human secreted RNases at the extracellular space. Frontiers in Immunology, Vol. 9, p. 1. https://doi.org/10.3389/fimmu.2018.01012

Lizhnyak, P. N., Muldoon, P. P., Pilaka, P. P., Povlishock, J. T., & Ottens, A. K. (2019). Traumatic Brain Injury Temporal Proteome Guides KCC2-Targeted Therapy. *Journal of Neurotrauma*, *36*(22), 3092–3102. https://doi.org/10.1089/neu.2019.6415

Mammaro, A., Carrara, S., Cavaliere, A., Ermito, S., Dinatale, A., Pappalardo, E. M., … Cacciatore, A. (2009). Hypertensive Disorders in Pregnancy. Journal of Prenatal Medicine, 3(1), 1–5. https://doi.org/10.5005/jp/books/12492_29

Mazurek, S. (2011). Pyruvate kinase type M2: A key regulator of the metabolic budget system in tumor cells. *International Journal of Biochemistry and Cell Biology*, *43*(7), 969–980. https://doi.org/10.1016/j.biocel.2010.02.005

McDonnell, W. F., Stewart, P. W., Smith, M. V., Pan, W. K., & Pan, J. (1999). Ozone-induced respiratory symptoms: Exposure-response models and association with lung function. *European Respiratory Journal*, *14*(4), 845–853. https://doi.org/10.1034/j.1399-3003.1999.14d21.x

Miller, C. N., Dye, J. A., Ledbetter, A. D., Schladweiler, M. C., Richards, J. H., Snow, S. J., Wood, C. E., Henriquez, A. R., Thompson, L. C., Farraj, A. K., Hazari, M. S., & Kodavanti, U. P. (2017). Uterine Artery Flow and Offspring Growth in Long-Evans Rats following Maternal Exposure to Ozone during Implantation. *Environmental Health Perspectives*, *125*(12), 127005. https://doi.org/10.1289/EHP2019

Mirkin, S., Arslan, M., Churikov, D., Corica, A., Diaz, J. I., Williams, S., Bocca, S., & Oehninger, S. (n.d.). *In search of candidate genes critically expressed in the human endometrium during the window of implantation*. https://doi.org/10.1093/humrep/dei051

Mostovenko, E., Young, T., Muldoon, P. P., Bishop, L., Canal, C. G., Vucetic, A., Zeidler-Erdely, P. C., Erdely, A., Campen, M. J., & Ottens, A. K. (2019). Nanoparticle exposure driven circulating bioactive peptidome causes systemic inflammation and vascular dysfunction. *Particle and Fibre Toxicology*, *16*(1). https://doi.org/10.1186/s12989-019-0304-6

Mumaw, C. L., Levesque, S., McGraw, C., Robertson, S., Lucas, S., Stafflinger, J. E., Campen, M. J., Hall, P., Norenberg, J. P., Anderson, T., Lund, A. K., McDonald, J. D., Ottens, A. K., & Block, M. L. (2016). Microglial priming through the lung-brain axis: The role of air pollution-induced circulating factors. *FASEB Journal*, *30*(5), 1880–1891. https://doi.org/10.1096/fj.201500047

Mumby, S., Chung, K. F., & Adcock, I. M. (2019). Transcriptional effects of ozone and impact on airway inflammation. *Frontiers in Immunology, 10*(JULY), 1610. Frontiers Media S.A. https://doi.org/10.3389/fimmu.2019.01610

Nakanishi, T. (2007). The problem of species comparison of developmental toxicity: Can we extrapolate human developmental toxicity induced by environmental chemicals from the data of rodents? Yakugaku Zasshi, *127*(3), 491–500. https://doi.org/10.1248/yakushi.127.491

Neerhof, M. G., & Thaete, L. G. (2008). The Fetal Response to Chronic Placental Insufficiency. *Seminars in Perinatology*, *32*(3), 201–205. W.B. Saunders. https://doi.org/10.1053/j.semperi.2007.11.002

Obermeier, B., Daneman, R., & Ransohoff, R. M. (2013). Development, maintenance and disruption of the blood-brain barrier. *Nature Medicine,19*(12), 1584–1596. NIH Public Access. https://doi.org/10.1038/nm.3407

Olsson, D., Mogren, I., & Forsberg, B. (2013). Air pollution exposure in early pregnancy and adverse pregnancy outcomes: A register-based cohort study. *BMJ Open*, *3*(2). https://doi.org/10.1136/bmjopen-2012-001955

Oudin, A., Bråbäck, L., Åström, D. O., Strömgren, M., & Forsberg, B. (2016). Association between neighbourhood air pollution concentrations and dispensed medication for psychiatric disorders in a large longitudinal cohort of Swedish children and adolescents. *BMJ Open*, *6*(6), e010004. https://doi.org/10.1136/bmjopen-2015-010004

Park, H. W., & Shepard, T. H. (1994). Volume and glucose concentration of rat amniotic fluid: Effects on embryo nutrition and axis rotation. *Teratology, 49*(6), 465–469. https://doi.org/10.1002/tera.1420490606

Park, J. W., Taube, C., Joetham, A., Takeda, K., Kodama, T., Dakhama, A., McConville, G., Allen, C. B., Sfyroera, G., Shultz, L. D., Lambris, J. D., Giclas, P. C., Holers, V. M., & Gelfand, E. W. (2004). Complement Activation Is Critical to Airway Hyperresponsiveness after Acute Ozone Exposure. *American Journal of Respiratory and Critical Care Medicine, 169*(6), 726–732. https://doi.org/10.1164/rccm.200307-1042oc

Paffett, M. L., Zychowski, K. E., Sheppard, L., Robertson, S., Weaver, J. M., Lucas, S. N., & Campen, M. J. (2015). Ozone Inhalation Impairs Coronary Artery Dilation via Intracellular Oxidative Stress: Evidence for Serum-Borne Factors as Drivers of Systemic Toxicity. *Toxicological Sciences*, *146*(2), 244–253. https://doi.org/10.1093/TOXSCI

Paul, W. E., & Zhu, J. (2010). How are TH2-type immune responses initiated and amplified? In Nature Reviews Immunology (Vol. 10, Issue 4, pp. 225–235). NIH Public Access. https://doi.org/10.1038/nri2735

Pedersen, B., Holscher, T., Sato, Y., Pawlinski, R., & Mackman, N. (2005). A balance between tissue factor and tissue factor pathway inhibitor is required for embryonic development and hemostasis in adult mice. Blood, 105(7), 2777–2782. https://doi.org/10.1182/blood-2004-09-3724

Pepper, M. S., Rosnoblet, C., Di Sanza, C., & Kruithof, E. K. (2001). Synergistic induction of t-PA by vascular endothelial growth factor and basic fibroblast growth factor and localization of t-PA to Weibel-Palade bodies in bovine microvascular endothelial cells. *Thrombosis and haemostasis*, *86*(2), 702–709.

Père, M. C. (2003). Materno-foetal exchanges and utilisation of nutrients by the foetus: Comparison between species. *Reproduction Nutrition Development*, *43*(1), 1–15. EDP Sciences. https://doi.org/10.1051/rnd:2003002

Peretz, A., Sullivan, J. H., Leotta, D. F., Trenga, C. A., Sands, F. N., Allen, J., Carlsten, C., Wilkinson, C. W., Gill, E. A., & Kaufman, J. D. (2008). Diesel exhaust inhalation elicits acute vasoconstriction in vivo. *Environmental Health Perspectives*, *116*(7), 937–942. https://doi.org/10.1289/ehp.11027

Pierik, E., Prins, J. R., van Goor, H., Dekker, G. A., Daha, M. R., Seelen, M. A. J., & Scherjon, S. A. (2020). Dysregulation of Complement Activation and Placental Dysfunction: A Potential Target to Treat Preeclampsia? *Frontiers in Immunology, 10*, 3098. Frontiers Media S.A. https://doi.org/10.3389/fimmu.2019.03098

Pijnenborg, R., Robertson, W. B., Brosens, I., & Dixon, G. (1981). Review article: Trophoblast invasion and the establishment of haemochorial placentation in man and laboratory animals. *Placenta, 2*(1), 71–91. Placenta. https://doi.org/10.1016/S0143-4004(81)80042-2

Postlethwait, E. M., Langford, S. D., & Bidani, A. (1994). Determinants of inhaled ozone absorption in isolated rat lungs. *Toxicology and Applied Pharmacology*, *125*(1), 77–89. https://doi.org/10.1006/taap.1994.1051

Power, M. C., Weisskopf, M. G., Alexeeff, S. E., Coull, B. A., Avron, S., & Schwartz, J. (2011). Traffic-related air pollution and cognitive function in a cohort of older men. *Environmental Health Perspectives*, *119*(5), 682–687. https://doi.org/10.1289/ehp.1002767

Power, M. C., Weisskopf, M. G., Alexeeff, S. E., Wright, R. O., Coull, B. A., Spiro, A., & Schwartz, J. (2013). Modification by hemochromatosis gene polymorphisms of the association between traffic-related air pollution and cognition in older men: A cohort study. *Environmental Health: A Global Access Science Source*, *12*(1), 16. https://doi.org/10.1186/1476-069X-12-16

Pryor, W. A. (1992). How far does ozone penetrate into the pulmonary air/tissue boundary before it reacts? *Free Radical Biology and Medicine*, *12*(1), 83–88. https://doi.org/10.1016/0891-5849(92)90060-T

Pryor, W. A., Squadrito, G. L., & Friedman, M. (1995). A new mechanism for the toxicity of ozone. *Toxicology Letters*, *82–83*(C), 287–293. https://doi.org/10.1016/0378-4274(95)03563-X

Pustovrh, M. C., Jawerbaum, A., White, V., Capobianco, E., Higa, R., Martínez, N., López-Costa, J. J., & González, E. (2007). The role of nitric oxide on matrix metalloproteinase 2 (MMP2) and MMP9 in placenta and fetus from diabetic rats. *Reproduction*, *134*(4), 605–613. https://doi.org/10.1530/REP-06-0267

Ransohoff, R. M., & Engelhardt, B. (2012). The anatomical and cellular basis of immune surveillance in the central nervous system. *Nature Reviews Immunology*, *12*(9), 623–635. Nat Rev Immunol. https://doi.org/10.1038/nri3265

Regal, J. F., Gilbert, J. S., & Burwick, R. M. (2015). The complement system and adverse pregnancy outcomes. *Molecular Immunology, 67*(1), 56–70. Elsevier Ltd. https://doi.org/10.1016/j.molimm.2015.02.030

Regal, J. F., Burwick, R. M., & Fleming, S. D. (2017). The Complement System and Preeclampsia. *Current hypertension reports*, *19*(11), 87. https://doi.org/10.1007/s11906-017-0784-4

Reynolds, L. P., & Redmer, D. A. (1995). Utero-placental vascular development and placental function. *Journal of animal science*, *73*(6), 1839–1851. J Anim Sci. https://doi.org/10.2527/1995.7361839x

Rivas-Arancibia, S., Guevara-Guzmán, R., López-Vidal, Y., Rodríguez-Martínez, E., Zanardo-Gomes, M., Angoa-Pérez, M., & Raisman-Vozari, R. (2010). Oxidative Stress Caused by Ozone Exposure Induces Loss of Brain Repair in the Hippocampus of Adult Rats. *TOXICOLOGICAL SCIENCES*, *113*(1), 187–197. https://doi.org/10.1093/toxsci/kfp252

Roberts, A. L., Lyall, K., Hart, J. E., Laden, F., Just, A. C., Bobb, J. F., Koenen, K. C., Ascherio, A., & Weisskopf, M. G. (2013). Perinatal air pollutant exposures and autism spectrum disorder in the children of Nurses' Health Study II participants. *Environmental Health Perspectives*, *121*(8), 978–984. https://doi.org/10.1289/ehp.1206187

Roberts, J. M., & Cooper, D. W. (2001). Pathogenesis and genetics of pre-eclampsia. *Lancet*, *357*(9249), 53–56. Elsevier Limited. https://doi.org/10.1016/S0140-6736(00)03577-7

Robertson, S., Colombo, E. S., Lucas, S. N., Hall, P. R., Febbraio, M., Paffett, M. L., & Campen, M. J. (2013). CD36 Mediates Endothelial Dysfunction Downstream of Circulating Factors Induced by O3 Exposure. *Toxicological Sciences*, *134*(2), 304–311. https://doi.org/10.1093/TOXSCI

Rudziak, P., Ellis, C. G., & Kowalewska, P. M. (2019). Role and Molecular Mechanisms of Pericytes in Regulation of Leukocyte Diapedesis in Inflamed Tissues. *Mediators of inflammation*, *2019*, 4123605. https://doi.org/10.1155/2019/4123605

Saili, K. S., Zurlinden, T. J., Schwab, A. J., Silvin, A., Baker, N. C., Hunter, E. S., Ginhoux, F., & Knudsen, T. B. (2017). Blood-brain barrier development: Systems modeling and predictive toxicology. *Birth Defects Research*, *109*(20), 1680–1710. John Wiley and Sons Inc. https://doi.org/10.1002/bdr2.1180

Samet, J. M., Dominici, F., Curriero, F. C., Coursac, I., & Zeger, S. L. (2000). Fine Particulate Air Pollution and Mortality in 20 U.S. Cities, 1987–1994. *New England Journal of Medicine*, *343*(24), 1742–1749. https://doi.org/10.1056/NEJM200012143432401

Sasaki, T., Hirabayashi, J., Manya, H., Kasai, K., & Endo, T. (2004). Galectin-1 induces astrocyte differentiation, which leads to production of brain-derived neurotrophic factor. *Glycobiology, 14*(4), 357–363. https://doi.org/10.1093/GLYCOB

Say, L., Chou, D., Gemmill, A., Tunçalp, Ö., Moller, A. B., Daniels, J., Gülmezoglu, A. M., Temmerman, M., & Alkema, L. (2014). Global causes of maternal death: A WHO systematic analysis. *The Lancet Global Health*, *2*(6), e323–e333. https://doi.org/10.1016/S2214-109X(14)70227-X

Schreibelt, G., Kooij, G., Reijerkerk, A., Doorn, R., Gringhuis, S. I., Pol, S., Weksler, B. B., Romero, I. A., Couraud, P., Piontek, J., Blasig, I. E., Dijkstra, C. D., Ronken, E., & Vries, H. E. (2007). Reactive oxygen species alter brain endothelial tight junction dynamics via RhoA, PI3 kinase, and PKB signaling. *The FASEB Journal, 21*(13), 3666–3676. https://doi.org/10.1096/fj.07-8329com

Seo, J. H., Maki, T., Maeda, M., Miyamoto, N., Liang, A. C., Hayakawa, K., Pham, L. D. D., Suwa, F., Taguchi, A., Matsuyama, T., Ihara, M., Kim, K. W., Lo, E. H., & Arai, K. (2014). Oligodendrocyte precursor cells support blood-brain barrier integrity via TGF-β signaling. *PLoS ONE, 9*(7). https://doi.org/10.1371/journal.pone.0103174

Shan, L., Fan, Y., Li, H., Liu, W., Gu, H., Zhou, F., & Yuan, Z. (2012). Proteomic analysis of amniotic fluid of pregnant rats with spina bifida aperta. *Journal of Proteomics*, *75*(4), 1181–1189. https://doi.org/10.1016/j.jprot.2011.10.033

Shatrov, J. G., Birch, S. C. M., Lam, L. T., Quinlivan, J. A., McIntyre, S., & Mendz, G. L. (2010). Chorioamnionitis and cerebral palsy: A meta-analysis. *Obstetrics and Gynecology, 116*(2), 387–392. Obstet Gynecol. https://doi.org/10.1097/AOG.0b013e3181e90046

Shimonovitz, S., Hurwitz, A., Dushnik, M., Anteby, E., Geva-Eldar, T., & Yagel, S. (1994). Developmental regulation of the expression of 72 and 92 kd type IV collagenases in human trophoblasts: A possible mechanism for control of trophoblast invasion. *American Journal of Obstetrics & Gynecology*, *171*(3), 832–838. https://doi.org/10.5555/URI:PII:0002937894901074

Singh, J., Ahmed, A., & Girardi, G. (2011). Role of complement component C1q in the onset of preeclampsia in mice. Hypertension, 58(4), 716–724. https://doi.org/10.1161/HYPERTENSIONAHA.111.175919

Singh, U., & Jialal, I. (2006). Oxidative stress and atherosclerosis. In *Pathophysiology* (Vol. 13, Issue 3, pp. 129–142). Elsevier. https://doi.org/10.1016/j.pathophys.2006.05.002

Soares, M. J., Hunt, J. S., Ain, R., Konno, T., Canham, L. N., & Soares, M. J. (2006). Phenotypic Analysis of Rat Placenta. *Methods in Molecular Medicine*, *121*, 295–313.

Soares, M. J., Chakraborty, D., Rumi, M. A. K., Konno, T., & Renaud, S. J. (2011). Rat placentation: An experimental model for investigating the hemochorial maternal-fetal interface. *Placenta*, *33*(4), 233–244. https://doi.org/10.1016/j.placenta.2011.11.026

Sodek, J., Ganss, B., & McKee, M. D. (2000). Osteopontin. *Critical Reviews in Oral Biology and Medicine*, *11*(3), 279–303. https://doi.org/10.1177/10454411000110030101

Sohet, F., Lin, C., Munji, R. N., Lee, S. Y., Ruderisch, N., Soung, A., Arnold, T. D., Derugin, N., Vexler, Z. S., Yen, F. T., & Daneman, R. (2015). LSR/angulin-1 is a tricellular tight junction protein involved in blood-brain barrier formation. *Journal of Cell Biology*, *208*(6), 703–711. https://doi.org/10.1083/jcb.201410131

Solberg, H., Rinkenberger, J., Danø, K., Werb, Z., & Lund, L. R. (2003). A functional overlap of plasminogen and MMPs regulates vascularization during placental development. *Development, 130*(18), 4439–4450. https://doi.org/10.1242/dev.00642

State of the Air. (2019). Retrieved July 21, 2020, from American Heart Association website: http://www.stateoftheair.org/assets/sota-2019-full.pdf

Stamatovic, S. M., Johnson, A. M., Keep, R. F., & Andjelkovic, A. V. (2016). Junctional proteins of the blood-brain barrier: New insights into function and dysfunction. *Tissue Barriers, 4*,(1), Taylor and Francis Inc. https://doi.org/10.1080/21688370.2016.1154641

Starossom, S. C., Mascanfroni, I. D., Imitola, J., Cao, L., Raddassi, K., Hernandez, S. F., Bassil, R., Croci, D. O., Cerliani, J. P., Delacour, D., Wang, Y., Elyaman, W., Khoury, S. J., & Rabinovich, G. A. (2012). Galectin-1 Deactivates Classically Activated Microglia and Protects from Inflammation-Induced Neurodegeneration. *Immunity, 37*(2), 249–263. https://doi.org/10.1016/j.immuni.2012.05.023

Stedman, D. H. (2004). Photochemical Ozone Formation, Simplified. *Environmental Chemistry*, *1*, 65–66. https://doi.org/10.1071/EN04032

Steegers, E. A. P., Von Dadelszen, P., Duvekot, J. J., & Pijnenborg, R. (2010). Pre-eclampsia. *The Lancet*, *376*(9741), 631–644. https://doi.org/10.1016/S0140-6736(10)60279-6

Stenczer, B., Rigó, J., Jr, Prohászka, Z., Derzsy, Z., Lázár, L., Makó, V., Cervenak, L., Balogh, K., Mézes, M., Karádi, I., & Molvarec, A. (2010). Plasma osteopontin concentrations in preeclampsia - is there an association with endothelial injury?. *Clinical chemistry and laboratory medicine*, *48*(2), 181–187. https://doi.org/10.1515/CCLM.2010.042

Stetler-Stevenson, W. G., Liotta, L. A., & Kleiner, D. E. (1993). Extracellular matrix 6: Role of matrix metalloproteinases in tumor invasion and metastasis. *The FASEB Journal, 7*(15), 1434–1441. https://doi.org/10.1096/fasebj.7.15.8262328

Stone, O. A., El-Brolosy, M., Wilhelm, K., Liu, X., Romão, A. M., Grillo, E., Lai, J. K. H., Günther, S., Jeratsch, S., Kuenne, C., Lee, I. C., Braun, T., Santoro, M. M., Locasale, J. W., Potente, M., & Stainier, D. Y. R. (2018). Loss of pyruvate kinase M2 limits growth and triggers innate immune signaling in endothelial cells. *Nature Communications, 9*(1), 1–12. https://doi.org/10.1038/s41467-018-06406-8

Suzuki, H., Hasegawa, Y., Kanamaru, K., & Zhang, J. H. (2010). Mechanisms of osteopontin-induced stabilization of blood-brain barrier disruption after subarachnoid hemorrhage in rats. *Stroke*, *41*(8), 1783–1790. https://doi.org/10.1161/STROKEAHA.110.586537

Takata, K., Fujikura, K., Shin, B.-C., & Takata, K. (1997). Ultrastructure of the Rodent Placental Labyrinth: A Site of Barrier and Transport. In *Journal of Reproduction and Development* (Vol. 43, Issue 1).

Tamagawa, E., Bai, N., Morimoto, K., Gray, C., Mui, T., Yatera, K., Zhang, X., Xing, L., Li, Y., Laher, I., Sin, D. D., Man, S. F. P., & Van Eeden, S. F. (2008). Particulate matter exposure induces persistent lung inflammation and endothelial dysfunction. *American Journal of Physiology - Lung Cellular and Molecular Physiology*, *295*(1), L79. https://doi.org/10.1152/ajplung.00048.2007

Tarango, C. (2014). Disorders of Coagulation in the Neonate. In Pathobiology of Human Disease: A Dynamic Encyclopedia of Disease Mechanisms (pp. 1586–1594). Elsevier Inc. https://doi.org/10.1016/B978-0-12-386456-7.07912-0

Tayebjee, M., Karalis, I., Nadar, S., Beevers, D., Macfadyen, R., Lip, G. (2005). Circulating matrix metalloproteinase-9 and tissue inhibitors of metalloproteinases-1 and -2 levels in gestational hypertension. American Journal of Hypertension, 18(3), 325–329. https://doi.org/10.1016/j.amjhyper.2004.09.014

Tham, A., Lullo, D., Dalton, S., Zeng, S., van Koeverden, I., & Arjomandi, M. (2017). Modeling vascular inflammation and atherogenicity after inhalation of ambient levels of ozone: exploratory lessons from transcriptomics. *Inhalation Toxicology*, *29*(3), 96–105. https://doi.org/10.1080/08958378.2017.1310333

Than, N. G., Wildman, D. E., Erez, O., Edwin, S. S., Espinoza, J., Kim, C. J., … Romero, R. (2006). Trophoblast, Galectin-1 and pre-eclampsia. *American Journal of Obstetrics and Gynecology*, *195*(6), S138. https://doi.org/10.1016/j.ajog.2006.10.481

Than, N. G., Erez, O., Wildman, D. E., Tarca, A. L., Edwin, S. S., Abbas, A., Hotra, J., Kusanovic, J. P., Gotsch, F., Hassan, S. S., Espinoza, J., Papp, Z., & Romero, R. (2008). Severe preeclampsia is characterized by increased placental expression of galectin-1. *Journal of Maternal-Fetal and Neonatal Medicine*, *21*(7), 429–442. https://doi.org/10.1080/14767050802041961

Tian, L., Stefanidakis, M., Ning, L., Van Lint, P., Nyman-Huttunen, H., Libert, C., Itohara, S., Mishina, M., Rauvala, H., & Gahmberg, C. G. (2007). Activation of NMDA receptors promotes dendritic spine development through MMP-mediated ICAM-5 cleavage. *Journal of Cell Biology, 178*(4), 687–700. https://doi.org/10.1083/jcb.200612097

Tirado-González, I., Freitag, N., Barrientos, G., Shaikly, V., Nagaeva, O., Strand, M., Kjellberg, L., Klapp, B. F., Mincheva-Nilsson, L., Cohen, M., & Blois, S. M. (2013). Galectin-1 influences trophoblast immune evasion and emerges as a predictive factor for the outcome of pregnancy. *Molecular Human Reproduction*, *19*(1), 43–53. https://doi.org/10.1093/MOLEHR/GAS043

Tisi, D. K., Emard, J. J., & Koski, K. G. (2004). Total protein concentration in human amniotic fluid is negatively associated with infant birth weight. *The Journal of Nutrition*, *134*(7), 1754–1758. https://doi.org/10.1093/jn/134.7.1754

Tsangaris, G. T., Karamessinis, P., Kolialexi, A., Garbis, S. D., Antsaklis, A., Mavrou, A., & Fountoulakis, M. (2006). Proteomic analysis of amniotic fluid in pregnancies with Down syndrome. *PROTEOMICS*, *6*(15), 4410–4419. https://doi.org/10.1002/pmic.200600085

Tu, J., Tu, W., & Tedders, S. H. (2016). Spatial variations in the associations of term birth weight with ambient air pollution in Georgia, USA. *Environment International*, *92–93*, 146–156. https://doi.org/10.1016/j.envint.2016.04.005

Ulrich, R., Gerhauser, I., Seeliger, F., Baumgärtner, W., & Alldinger, S. (2005). Matrix Metalloproteinases and Their Inhibitors in the Developing Mouse Brain and Spinal Cord: A Reverse Transcription Quantitative Polymerase Chain Reaction Study. Developmental Neuroscience, 27(6), 408–418. https://doi.org/10.1159/000088455

Underwood, M. A., Gilbert, W. M., & Sherman, M. P. (2005). State of the Art Amniotic Fluid: Not Just Fetal Urine Anymore. *Journal of Perinatology*, *25*, 341–348. https://doi.org/10.1038/sj.jp.7211290

United Nations. (2018, May 16). *68% of the world population projected to live in urban areas by 2050, says UN | UN DESA | United Nations Department of Economic and Social Affairs*. United Nations: Department of Economic and Social Affairs. https://www.un.org/development/desa/en/news/population/2018-revision-of-world-urbanization-prospects.html

Valavanidis, A., Vlachogianni, T., Fiotakis, K., & Loridas, S. (2013). Pulmonary oxidative stress, inflammation and cancer: Respirable particulate matter, fibrous dusts and ozone as major causes of lung carcinogenesis through reactive oxygen species mechanisms. In *International Journal of Environmental Research and Public Health*, *10*(9), 3886–3907. Int J Environ Res Public Health. https://doi.org/10.3390/ijerph10093886

Volk, H. E., Hertz-Picciotto, I., Delwiche, L., Lurmann, F., & McConnell, R. (2011). Residential proximity to freeways and autism in the CHARGE study. *Environmental Health Perspectives*, *119*(6), 873–877. https://doi.org/10.1289/ehp.1002835

Volk, H. E., Lurmann, F., Penfold, B., Hertz-Picciotto, I., & McConnell, R. (2013). Traffic-related air pollution, particulate matter, and autism. *JAMA Psychiatry*, *70*(1), 71–77. https://doi.org/10.1001/jamapsychiatry.2013.266

Wai, P. Y., & Kuo, P. C. (2008). Osteopontin: Regulation in tumor metastasis. In *Cancer and Metastasis Reviews*, *27*(1), 103–118. Springer. https://doi.org/10.1007/s10555-007-9104-9

Wan, P. C., Bao, Z. J., Wu, Y., Yang, L., Hao, Z. D., Yang, Y. L., Shi, G. Q., Liu, Y., & Zeng, S. M. (2011). α vβ 3 Integrin may Participate in Conceptus Attachment by Regulating Morphologic Changes in the Endometrium during Peri-implantation in Ovine. *Reproduction in Domestic Animals, 46(*5), 840–847. https://doi.org/10.1111/j.1439-0531.2011.01752.x

Wang, C. C., Lo, H. F., Lin, S. Y., & Chen, H. (2013). RACK1 (receptor for activated C-kinase 1) interacts with FBW2 (F-box and WD-repeat domain-containing 2) to up-regulate GCM1 (glial cell missing 1) stability and placental cell migration and invasion. *The Biochemical journal*, *453*(2), 201–208. https://doi.org/10.1042/BJ20130175

Wang, Y., Cao, Y., Mangalam, A. K., Guo, Y., LaFrance-Corey, R. G., Gamez, J. D., Atanga, P. A., Clarkson, B. D., Zhang, Y., Wang, E., Angom, R. S., Dutta, K., Ji, B., Pirko, I., Lucchinetti, C. F., Howe, C. L., & Mukhopadhyay, D. (2016). Neuropilin-1 modulates interferon-γ-stimulated signaling in brain microvascular endothelial cells. *Journal of cell science*, *129*(20), 3911–3921. https://doi.org/10.1242/jcs.190702

Webb, A. H., Gao, B. T., Goldsmith, Z. K., Irvine, A. S., Saleh, N., Lee, R. P., Lendermon, J. B., Bheemreddy, R., Zhang, Q., Brennan, R. C., Johnson, D., Steinle, J. J., Wilson, M. W., & Morales-Tirado, V. M. (2017). Inhibition of MMP-2 and MMP-9 decreases cellular migration, and angiogenesis in in vitro models of retinoblastoma. *BMC cancer*, *17*(1), 434. https://doi.org/10.1186/s12885-017-3418-y

Weber, C. E., Li, N. Y., Wai, P. Y., & Kuo, P. C. (2012). Epithelial-Mesenchymal Transition, TGF-β, and Osteopontin in Wound Healing and Tissue Remodeling After Injury. *Journal of Burn Care & Research*, *33*(3), 311–318. https://doi.org/10.1097/BCR.0b013e318240541e

Wegmann, M., Fehrenbach, A., Heimann, S., Fehrenbach, H., Renz, H., Garn, H., & Herz, U. (2005). NO2-induced airway inflammation is associated with progressive airflow limitation and development of emphysema-like lesions in C57BL/6 mice. *Experimental and Toxicologic Pathology*, *56*(6), 341–350. https://doi.org/10.1016/j.etp.2004.12.004

Wellenius, G. A., Boyle, L. D., Coull, B. A., Milberg, W. P., Gryparis, A., Schwartz, J., Mittleman, M. A., & Lipsitz, L. A. (2012). Residential proximity to nearest major roadway and cognitive function in community-dwelling seniors: Results from the mobilize Boston study. *Journal of the American Geriatrics Society*, *60*(11), 2075–2080. https://doi.org/10.1111/j.1532-5415.2012.04195.x

White, F. J., Ross, J. W., Joyce, M. M., Geisert, R. D., Burghardt, R. C., & Johnson, G. A. (2005). Steroid Regulation of Cell Specific Secreted Phosphoprotein 1 (Osteopontin) Expression in the Pregnant Porcine Uterus1. *Biology of Reproduction*, *73*(6), 1294–1301. https://doi.org/10.1095/biolreprod.105.045153

Whitley, G. S. J., & Cartwright, J. E. (2010). Cellular and Molecular Regulation of Spiral Artery Remodelling: Lessons from the Cardiovascular Field. *Placenta*, *31*(6), 465–474. https://doi.org/10.1016/j.placenta.2010.03.002

Whiteside, C., & Hassan, H. M. (1988). Role of oxyradicals in the inactivation of catalase by ozone. *Free radical biology & medicine*, *5*(5-6), 305–312. https://doi.org/10.1016/0891-5849(88)90101-3

Wirth, D., Christians, E., Manaut, C., Dessy, C., Foidart, JM., & Gustin, P. (2002). Differential heat shock gene hsp70-1 response to toxicants revealed by in vivo study of lungs in transgenic mice. *Cell Stress & Chaperones*, 7(4). https://doi.org/10.1379/1466-1268(2002)007<0387:DHSGHR>2.0.CO;2

Wong, C. G., Bonakdar, M., Mautz, W. J., & Kleinman, M. T. (1996). Chronic inhalation exposure to ozone and nitric acid elevates stress-inducible heat shock protein 70 in the rat lung. *Toxicology, 107*(2), 111–119. https://doi.org/10.1016/0300-483X(95)03250-J

Wooding, P., & Burton, G. (2008). Haemochorial Placentation: Mouse, Rabbit, Man, Apes, Monkeys. In *Comparative Placentation*, 185–230. Springer Berlin Heidelberg. https://doi.org/10.1007/978-3-540-78797-6_8

Woodward, N. C., Haghani, A., Johnson, R. G., Hsu, T. M., Saffari, A., Sioutas, C., Kanoski, S. E., Finch, C. E., & Morgan, T. E. (2018). Prenatal and early life exposure to air pollution induced hippocampal vascular leakage and impaired neurogenesis in association with behavioral deficits. *Translational Psychiatry*, *8*, 261. https://doi.org/10.1038/s41398-018-0317-1

Woodworth, M. B., Custo Greig, L., Kriegstein, A. R., & MacKlis, J. D. (2012). Snapshot: Cortical development. *Cell*,*151*(4). Cell Press. https://doi.org/10.1016/j.cell.2012.10.004

Wu, G., Hu, X., Ding, J., & Yang, J. (2019). Abnormal expression of HSP70 may contribute to PCOS pathology. Journal of ovarian research, 12(1), 74. https://doi.org/10.1186/s13048-019-0548-7

Xia, J., & Liu, H. (2009). Implication of Expression of Osteopontin and Its Receptor Integrin αvβ3 in the Placenta in the Development of Preeclampsia. J Huazhong Univ Sci Technol,*Med Sci, 29*(6), 755–760. https://doi.org/10.1007/s11596-009-0617-z

Xu, B., Shanmugalingam, R., Chau, K., Makris, A., & Hennessy, A. (2020). Galectin-1–Related Modulation of Trophoblast Endothelial Interactions by Integrins α1 and β1. *Reproductive Sciences, 27*(5), 1097–1109. https://doi.org/10.1007/s43032-019-00046-z

Yang, Y., Schlepütz, C. M., Bellucci, F., Allen, M. W., Durbin, S. M., & Clarke, R. (2013). Structural investigation of ZnO O-polar (000 1^{-}) surfaces and Schottky interfaces. *Surface Science*, *610*, 22–26. https://doi.org/10.1016/j.susc.2012.12.018

Yoon, H. K., Cho, H. Y., & Kleeberger, S. R. (2007). Protective role of matrix metalloproteinase-9 in ozone-induced airway inflammation. Environmental Health Perspectives, 115(11), 1557–1563. https://doi.org/10.1289/ehp.10289

Zhang, R., Pan, X., Huang, Z., Weber, G. F., & Zhang, G. (2011). Osteopontin enhances the expression and activity of MMP-2 via the SDF-1/CXCR4 axis in hepatocellular carcinoma cell lines. *Plus One*, *6*(8). https://doi.org/10.1371/journal.pone.0023831

Zhang, J., Yang, G., Zhu, Y., Peng, X., Li, T., & Liu, L. (2018). Relationship of Cx43 regulation of vascular permeability to osteopontin-tight junction protein pathway after sepsis in rats. *American Journal of Physiology - Regulatory Integrative and Comparative Physiology*, *314*(1), R1–R11. https://doi.org/10.1152/ajpregu.00443.2016

Ye, Y., Vattai, A., Zhang, X., Zhu, J., Thaler, C. J., Mahner, S., Jeschke, U., & von Schönfeldt, V. (2017). Role of Plasminogen Activator Inhibitor Type 1 in Pathologies of Female Reproductive Diseases. *International journal of molecular sciences*, *18*(8), 1651. https://doi.org/10.3390/ijms18081651

Zhang, W., Ge, Y., Cheng, Q., Zhang, Q., Fang, L., & Zheng, J. (2018). Decorin is a pivotal effector in the extracellular matrix and tumour microenvironment. *Oncotarget*, Vol. 9, pp. 5480–5491. https://doi.org/10.18632/oncotarget.23869

Zhang, J. J., Wei, Y., & Fang, Z. (2019). Ozone pollution: A major health hazard worldwide. *Frontiers in Immunology*, Vol. 10, p. 2518. https://doi.org/10.3389/fimmu.2019.02518

Zhang, Z., Deng, X., Liu, Y., Liu, Y., Sun, L., & Chen, F. (2019). PKM2, function and expression and regulation. In Cell and Bioscience (Vol. 9, Issue 1, pp. 1–25). BioMed Central Ltd. https://doi.org/10.1186/s13578-019-0317-8

Zhu, Y., Zhang, C., Liu, D., Ha, S., Kim, S. S., Pollack, A., & Mendola, P. (2017). Ambient Air Pollution and Risk of Gestational Hypertension. *American Journal of Epidemiology*, *186*(3), 334–343. https://doi.org/10.1093/aje

Vita

Alexander I. Hamm was born on September 8, 1992, in York, Pennsylvania. He graduated from Dover Area High School in his hometown of Dover, Pa in 2014. He received a Bachelor's of Science from Susquehanna University, Selinsgrove, Pa.